2009

Optimal field coverage path planning on 2D and 3D surfaces

Jian Jin
Iowa State University

Optimal field coverage path planning on 2D and 3D surfaces

by

Jian Jin

A dissertation submitted to the graduate faculty

in partial fulfillment of the requirements for the degree of

DOCTOR OF PHILOSOPHY

Major: Agricultural Engineering

Program of Study Committee:
Lie Tang, Major Professor
Stuart Birrell
Matthew Helmers
Yan-Bin Jia
Brian Steward

Iowa State University

Ames, Iowa

2009

TABLE OF CONTENTS

LIST OF TABLES

LIST OF FIGURES

ABSTRACT

With the rapid adoption of automatic guidance systems, automated path planning has great potential to further optimize field operations. Field operations should be done in a manner that minimizes time, travel over field surfaces and is coordinated with specific field operations, machine characteristics and topographical features of arable lands. To reach this goal, intelligent coverage path planning algorithm is key. This dissertation documents our innovative research in optimal field coverage path planning on both 2D and 3D surfaces.

To determine the full coverage pattern of a given 2D planar field by using boustrophedon paths, it is necessary to know whether to and how to decompose a field into sub-regions and how to determine the travel direction within each sub-region. A geometric model was developed to represent this coverage path planning problem, and a path planning algorithm was developed based on this geometric model. The search mechanism of the algorithm was guided by a customized cost function resulting from the analysis of different headland turning types and implemented with a divide-and-conquer strategy. The complexity of the algorithm was analyzed, and methods for reducing the computational time were discussed. Field examples with complexity ranging from a simple convex shape to an irregular polygonal shape that has multiple obstacles within its interior were tested with this algorithm. The results were compared with other reported approaches or farmers' actual driving patterns. These results indicated the proposed algorithm was effective in producing optimal field decomposition and coverage path direction in each sub-region.

In real world, a great proportion of farms have rolling terrains, which have considerable influences to the design of coverage paths. Coverage path planning in 3D space has a great potential to further optimize field operations. To design optimal coverage paths on 3D terrain surfaces, there were five important steps: terrain modeling and representation, topography impacts analysis, terrain decomposition and classification, coverage cost analysis and the development of optimal path searching algorithm. Each of the topics was investigated in this dissertation research. The developed algorithms and methods were successfully implemented in software and tested with practical 3D terrain farm fields with various topographical features. Each field was decomposed into sub-regions based on terrain

features. An optimal “seed curve” was found for each sub-region and parallel coverage paths were generated by offsetting the “seed curve” sideways until the whole sub-region was completely covered. Compared with the 2D planning results, the experimental results of 3D coverage path planning showed its superiority in reducing both headland turning cost and soil erosion cost.

CHAPTER 1. GENERAL INTRODUCTION

1.1 Introduction

In 2004, in the United States, there were 2,107,925 farms of 990,724,750 acres in total (Economic Research Service/USDA, 2007) and 3,223,017 annual person equivalents of labor (6,446,034,000 hours of labor per year) spent on various in-field farming operations. With these operations, there were also huge consumptions of fuel, machine maintenance, chemicals and fertilizer. The development of technologies for improving the field efficiency is therefore of great significance. With the rapid adoption of automatic guidance systems in agriculture, automated path planning has potential to further optimize field operations. In the meantime, with the trend towards larger farms and corporate farming, the use of low-skilled or contracted labor is ever increasing, making automatic path planning practically valuable. Field operations should be done in a manner that minimizes time, travels over field surfaces and is coordinated with specific field operations, machine characteristics and topographical features of arable lands. In this way, the effective field efficiency of different field operations can be maximized. Current uses of automatically guided field equipment only enables the machine to follow parallel straight or contour paths that provide a complete field coverage, but little operational optimization has been taken into account, especially when irregularities of field boundaries and slopes are presented. To improve field efficiency and, in particular, to fully utilize the advantages provided by automatically guided farming equipment, an optimal coverage path planner is of great importance.

Former research on coverage path planning has been reported, but no complete solution under the context of arable farming has been provided. Fabret et al. (2001) approached the coverage path planning problem by formulating it as a Traveling Salesman Problem (TSP). A “steering edge” was used to provide the guiding direction for the successive swaths. Yang et al. (2004) applied neural networks for coverage path planning. The model was proposed for generating collision-free complete coverage robot paths. Coverage costs, such as the cost of turnings at the edges, were not investigated by this model, thus making it not necessarily applicable for farm field coverage planning.

For agricultural field operations, boustrophedon paths (straight parallel paths with alternate directions) represent the most straight forward approach since they can be easily followed by agricultural equipment. Given a field, once an optimal coverage direction is determined, the whole field can usually be covered by boustrophedon paths guided by this direction. Therefore, the most important component in coverage path planning is to determine the best direction of paths, so that the coverage cost can be minimized. The simplest method is to follow the longest edge of the field (Fabre et al., 2001), but it is only suitable for fields with simple convex shapes such as a rectangular field. To have a generic solution for coverage path planning, irregularities of field boundaries and slopes have to be considered. One attempt of incorporating field boundary irregularity in path planning was made by Oksanen et al. (2007) who used a search algorithm to find a field splitting direction between 0 and 180 degrees. This splitting direction was then adopted to guide the paths. However, optimized decomposition could not be guaranteed in their approach.

The searching mechanism for optimal paths must be driven by a coverage cost function. Among the various coverage costs for 2D planar fields, coverage efficiency is of the highest concern, which is inversely related to the total operational time in the field. While operating along those straight sections of the boustrophedon paths in the interior of a field, the speed and the total travelling distance (which can be closely approximated as the field area divided by the swath width) are almost constant. Therefore, the cost on the straight path sections in the interior of the field is almost constant and the total coverage cost is then primarily determined by the cost of headland turning part of the paths. In order to reduce the total turning cost, the number of turns needs to be minimized. Besides, those turns with relatively high operational costs need to be avoided. Fields of irregular shapes have inefficiencies related to headland turns when headlands are at an angle to machine travel (Hunt, 2001). For an angled turn, the total travel time in the headland can be dramatically longer compared with the case when the headland is orthogonal to the machine travel. These angled turns should be discouraged in order to save the costs of operator effort.

When designing an optimal coverage path planner that can cope with field boundary irregularities, field decomposition has a potential to further improve the field efficiency of farming equipment before determining the best path direction of a given field. Given a 2D

planar field boundary, the whole field can be decomposed into several sub-regions that can reduce the overall cost in terms of time required for a field equipment to fully cover the entire operational surfaces. This field decomposition process has to take place simultaneously with the path direction searching process. So far the only field decomposition method adopted in coverage path planning is the trapezoidal decomposition method. Trapezoidal decomposition is a popular method for subdividing a field (Berg et al., 2000). Choset et al. (1997) and Oksanen et al. (2007) adopted the trapezoidal decomposition method for coverage path planning. However, their work did not include detailed discussions of how to determine the direction of the trapezoidal decomposition lines, and there was little evidence that these parallel lines could provide the best decomposition of a given field with regard to minimizing the coverage costs. A new field decomposition method for the purpose of coverage cost minimization is needed.

The 2D coverage path planning algorithms assume that the fields are flat and ignore elevation changes, making them only proper for flat farm fields. A large proportion of farms have rolling terrains, which have considerable influences on the design of coverage paths: Only 47% of cropland in the United States is on less than 2% slopes; 48% of the cropland is on slopes between 2% and 10%. In Iowa, 9.5% of cropland has slopes in the 10-15% range (National Resources Inventory, USDA, 1992). Applying planimetric field models would cause problems on some of those terrain fields. For example, there would be skips and overlaps between adjacent furrows, which in turn would have economic impacts. Stombaugh et al. (2009) figured out that on higher slopes, the surface area difference between planimetric and topographic models becomes significant, so that skips and overlaps between furrows occur. Koostra et al. (2006) showed that the error between planimetric and topographic surface areas could be as much as 5% in some typical farm fields. Dillon et al. (2006) demonstrated the economic impact of the area discrepancies between planimetric and topographic models.

Soil erosion is another major concern when planning paths on terrain surfaces. Van Doren (1950) indicated that runoff from contoured fields was often less than that from fields tilled up and down the slope. Ignoring the slopes on the terrain and executing projected straight parallel paths on terrain fields would cause severe soil erosion problem. Wendt

(1997) found out that tillage and planting operations performed on the contour were very effective in reducing erosion from storms of low to moderate intensity. When tillage is oriented along the contour, the ridges or oriented roughness will partially or completely redirect the runoff, thereby modifying the flow pattern. High ridges from tillage on the contour cause runoff to flow around the hill slope rather than directly down slope, significantly reducing the grade along the flow path and reducing the flow's detachment and transport capacity. Developing an algorithm which plans the paths to be along the contour directions on the slope to the best extent would be effective in reducing soil erosion cost.

No former research on 3D terrain field coverage path planning was reported. However, research on 3D surface coverage path planning has been reported for other applications. Kim and Sarma (2003) used vector fields to generate coverage trajectories on a class of simple surfaces and discussed a possible formulation of surface segmentation based on a principle that minimized cycle time. Sheng et al. (2003) developed procedures that segmented the projection of a 3D surface on planar surface to optimize the process cycle time. Vincze et al. (2003) presented an approach to generating trajectories for automated spray painting. Elementary surface geometries were extracted from a surface and each region was then painted with a specific painting strategy related to the elementary geometry. Atkar et al. (2005) adopted a hierarchical procedure to segment a complex automotive surface into simple components for trajectory planning in automotive spray-painting. After the surface decomposition, Atkar generated trajectories by selecting a seed curve, determining a speed profile along each pass, and selecting the optimal spacing between successive passes. However, the objectives of the above applications are different from that of farm field coverage path planning. For instance the main objective of painting trajectory planning is to ensure uniform paint deposition on the surface, which is not a concern in farm field coverage. Besides, segmenting the surface into patches of simple shapes was not necessarily helpful for farm field coverage, which might cause over-dividing of the field and thus increase the headland turning costs. Thus, developing a new 3D terrain coverage path planning algorithm is desired to further optimize field operations on terrain field surfaces.

1.2 Research Objectives

The overall objective of this research was to better understand how an optimal coverage path planner could minimize the operational cost of agricultural field equipment to cover a field. The research project reported in this dissertation has two phases: 1) the optimal field coverage path planning for 2D planar farm fields; 2) the optimal field coverage path planning for 3D terrain farm fields. Both the 2D and 3D path planning research had the following specific objectives:

1) To formulate the coverage path planning problem as an optimization problem;
2) To investigate various costs of the field operations, thus to determine the cost function for the optimization problem;
3) To investigate a search algorithm for finding the optimal field decomposition and path pattern which minimizes the coverage cost;
4) To evaluate the effectiveness of the developed optimal coverage path planner.

1.3 Dissertation Overview

This dissertation contains two main parts: optimal 2D planar field coverage path planning (Chapter 2) and optimal 3D terrain field coverage path planning (Chapter 3). In Chapter 1, the general introduction to the research is presented. In Chapter 2, the 2D planning research is described. A geometric model is first introduced to represent this coverage path planning problem. Then based on the coverage cost analysis, the newly developed searching algorithm for the optimal field segmentation and optimal coverage path direction is described. The experimental results are listed at last. In Chapter 3, the 3D planning research is described. The various topography impacts to the coverage of 3D terrain field are analyzed first and the different coverage costs on 3D terrain surfaces are quantified. The method for terrain decomposition and the searching algorithm for optimal 3D coverage solution are described. The results of the 3D terrain field coverage path planning experiments are provided finally. In Chapter 4, the research work is concluded and recommendations for the future work are suggested.

1.4 References

Atkar, P. N., Greenfield, A., Conner, D. C., Choset, H. and Rizzi, A. A., 2005. Hierarchical Segmentation of Surfaces Embedded in R3 for Auto-Body Painting. In Proceedings of the 2005 IEEE International Conference on Robotics and Automation Barcelona, Spain, April 2005. Page: 574-579.

Berg, M. D., Kreveld, V. M., Overmars, M. and Schwarzkopf, O., 2000. Computational Geometry. 2nd ed. Springer.

Choset, H. and Pignon, P., 1997. Coverage Path Planning: The Boustrophedon Cellular Decomposition. Proceedings of International Conference on Field and Service Robotics, Canberra, Australia.

Dillon, C., Gandonou, M. J., Koostra, B., Stombaugh, T. and Mueller, T., 2006. Evaluating the Economic Impact of Field Area Measurements. Poster and abstract presented at the 8th International Conference on Precision Agriculture, July 23-26, Minneapolis, MN.

Economic Research Service/USDA. 2007. Structure and Finances of U.S. Farms: Family Farm Report, 2007 Edition / EIB-24.

Fabret, S., Soueres, P., Taix, M. and Cordessed, L., 2001. Farmwork Path Planning for Field Coverage with Minimum Overlapping. Proceedings of 2001 8th IEEE International Conference.

Hunt, D., 2001. Farm Power and Machinery Management. Ames, IA. Iowa State Press.

Kim, T. and Sarma, S., 2003. Optimal Sweeping Paths on a 2-Manifold: A New Class of Optimization Problems Defined by Path Structures. IEEE Transactions on Robotics and Automation, 19(4):613–636, August 2003.

Koostra, B.K., Stombaugh, T., Mueller, G. T. and Shearer, A. S., 2006. Evaluating the Effect of Terrain on Field Area Measurements. ASABE Paper No. 061045, St. Joseph, MI: ASABE.

Oksanen, T. and Visala, A., 2007. Path Planning Algorithms for Agricultural Machines. Agricultural Engineering International: the CIGR Ejournal. 4: Manuscript ATOE 07 009.

Sheng, W., Chen, H., Xi, N., Chen, Y. and Song, M., 2003. Surface Partitioning in Automated CAD-Guided Tool Planning for Additive Manufacturing. In IEEE/RSJ Int'l. Conf. on Intelligent Robots and Systems, volume 2, pages 2072–2077, Las Vegas,USA, 2003.

Stombaugh, T., Koostra, K. B., Dillon, R. C., Mueller, G. T. and Pike, C. A., 2009. Implications of Topography on Field Coverage When Using GPS-Based Guidance. University of Kentucky.

Van Doren, A. C., Stauffer, S. R. and Kidder, H. E, 1950. Effect of Contour Farming on Soil Loss and Runoff, Soil Sci. Soc. Am. Proc. 15 (1950), pp. 413–417.

Vincze, M., Pichler, A. and Biegelbauer, G., 2003. Detection of Classes of Features for Automated Robot Programming. In IEEE Int'l. Conf. on Robotics and Automation, volume 1, pages 151–156, Taipei, Taiwan, September 2003.

Wendt, G., 1998. Guidelines for the Use of the Revised Universal Soil Loss Equation (RUSLE) Version 1.06 on Mined Lands, Construction Sites, and Reclaimed Lands. Peabody Western Coal Company.

Yang, S. X. and Luo, C., 2004. A Neural Network Approach to Complete Coverage Path Planning. IEEE Transactions on Systems, Man, and Cybernetics—Part B: Cybernetics. 34(1): 718-725.

CHAPTER 2. OPTIMAL 2D PLANAR FIELD COVERAGE PATH PLANNING

2.1 Abstract

With the rapid adoption of automatic guidance systems, automated path planning has great potential to further optimize field operations. Field operations should be done in a manner that minimizes time, travel over field surfaces and is coordinated with specific field operations, machine characteristics and topographical features of arable lands. To reach this goal, intelligent coverage path planning algorithm is the key. To determine the full coverage pattern of a given field by using boustrophedon paths, it is necessary to know whether to and how to decompose a field into sub-regions and how to determine the travel direction within each sub-region. A geometric model was developed to represent this coverage path planning problem, and a path planning algorithm was developed based on this geometric model. The search mechanism of the algorithm was guided by a customized cost function resulting from the analysis of different headland turning types and implemented with a divide-and-conquer strategy. The complexity of the algorithm was analyzed, and methods for reducing the computational time were discussed. Field examples with complexity ranging from a simple convex shape to an irregular polygonal shape that has multiple obstacles within its interior were tested with this algorithm. The results were compared with other reported approaches or farmers' actual driving patterns. These results indicated the proposed algorithm was effective in producing optimal field decomposition and coverage path direction in each sub-region.

2.2 Introduction

In 2004, in the United States, there were 2,107,925 farms of 990,724,750 acres in total (Economic Research Service/USDA, 2007) and 3,223,017 annual person equivalents of labor (6,446,034,000 hours of labor per year) spent on various in-field farming operations. With these operations, there were also huge consumptions on fuel, machine maintenance, chemicals, fertilizer and so on. The development of technologies for improving the field efficiency is therefore of great significance. With the rapid adoption of automatic guidance systems in agriculture, automated path planning has potential to further optimize field operations. In the meantime, with the trend towards larger farms and corporate farming, the use of low-skilled or contracted labor is ever increasing, making automatic path planning

practically valuable. Field operations should be done in a manner that minimizes time, travels over field surfaces and is coordinated with specific field operations, machine characteristics and topographical features of arable lands. In this way, the effective field efficiency of different field operations can be maximized. Current uses of automatically guided field equipment only enables the machine to follow parallel straight or contour paths that provide a complete field coverage, but little operational optimization has been taken into account, especially when irregularities of field boundaries are presented. To improve field efficiency and in particular to fully utilize the advantages provided by the automatically guided farming equipment, an optimal coverage path planner is of great importance.

Some coverage path planning research has been reported, but there has been no complete solution under the context of arable farming. Fabret et al. (2001) approached the coverage path planning problem by formulating it as a Traveling Salesman Problem (TSP). In their approach, a “steering edge” of the field was chosen which provided the direction to guide the successive swaths. Then a series of “characteristic points” in the headland of the field was collected and an “associated graph” was constructed using a TSP solver to connect those points by the lines in the steering direction. Yang et al. (2004) applied neural networks for coverage path planning. The simulation results from their work showed that the proposed model was capable of planning collision-free complete coverage robot paths. However, the collision-free requirement is not a priority in coverage planning for arable farming. Coverage costs, such as the cost of turnings at the edges, were not investigated by this model, thus making it not necessarily applicable for farm field coverage planning.

When designing an optimal coverage path planner that can cope with field boundary irregularities, field decomposition has a potential to further improve the field efficiency of farming equipment before determining the best path direction of a given field. If the whole field can be decomposed into several sub-regions that can reduce the overall cost in terms of time required for a field equipment to fully cover the entire operational surfaces, then a proper field decomposition process has to take place simultaneously with the path direction searching process. So far the only field decomposition method adopted in coverage path planning is the trapezoidal decomposition method. Trapezoidal decomposition is a popular method for subdividing a field (Berg et al., 2000). During the decomposition process, a

direction was chosen, and a set of parallel lines in this direction through all the vertices of the field boundary was drawn. The field was then divided by these lines into a trapezoidal map. Choset et al. (1997) and Oksanen et al. (2007) adopted the trapezoidal decomposition method for coverage path planning. However, their work did not include detailed discussions of how to determine the direction of the trapezoidal decomposition lines; and there was little evidence that these parallel lines could provide the best decomposition of a given field with regard to minimizing the coverage costs.

The most important component in coverage path planning is to determine the best direction of paths. For agricultural field operations, boustrophedon paths (straight parallel paths with alternate directions) represent the most straight forward approach since they can be easily followed by agricultural equipment. Given a field, once an optimal coverage direction is determined, the whole field can usually be covered by boustrophedon paths guided by this direction. There have been several choices for finding the optimal path direction. The simplest method is to follow the longest edge of the field (Fabre et al., 2001), but following the longest edge direction is only suitable for fields with simple convex shapes such as a rectangular field. To have a generic solution for coverage path planning, irregularities of field boundaries have to be considered. One such attempt was first made by Oksanen et al. (2007) who used a search algorithm to find an optimal trapezoidal splitting direction (same as the path direction) between 0 and 180 degrees according to an unspecified cost function. In each round of the algorithm, the field was first split into trapezoids based on the chosen direction, and the trapezoids were merged into larger blocks. Then the largest or most efficient driving block of the field was selected using certain criteria including the area and the route length of the block and driving efficiency. Once the trapezoidal block was selected, it was covered along the splitting direction and removed from the original field. The same algorithm was then applied iteratively for the rest of the field until the paths of the whole field path were computed. However, the optimized decomposition could not be guaranteed in this approach, leading to a splitting direction that was not necessarily the most efficient path direction. For the purpose of searching for an optimal coverage path planning solution, the decomposition and direction search algorithm for minimizing headland turning cost based on an accurate computational model is desired.

The overall objective of this research was to better understand how a 2D optimal coverage path planner could minimize the operational time of an agricultural field equipment to cover a field. This research had the following specific objectives: 1) To formulate the coverage path planning problem as an optimization problem and to investigate a search algorithm for finding the optimal field decomposition and path directions; 2) To evaluate the effectiveness of the developed optimal coverage path planner. The following parts of this chapter describe the details of the developed 2D optimal coverage path planning methods. In 2.3.1, a geometric model was developed to represent this coverage path planning problem. Section 2.3.2 describes a field boundary simplification algorithm which reduces the boundary data without undermining the planning algorithm while maintaining an acceptable resemblance to the actual field shape. The coverage cost analysis is provided in 2.3.3, including the cost analysis of different headland turning types as well as the method of selecting the optimal headland turning type. Section 2.3.4 discusses the searching algorithm for the optimal field segmentation method. Section 2.3.5 describes the recursive searching algorithm of 2D optimal coverage path planning. Section 2.3.6 discusses the possible transition between neighboring sub-regions which may further reduce the coverage cost. The time complexity of the algorithm is analyzed in 2.3.7. Methods for reducing the complexity are provided too. The experimental results are listed in 2.4.

2.3 Methods

The algorithm developed for optimal coverage path planning for arable farming on 2D surfaces contained several steps. First, a geometric representation of the field shape was adopted for the formulation of the 2D path planning problem. Second, the optimal path direction and the optimal field decomposition were searched to solve the problem. To search for the optimal path direction, the cost function of the angled turns was defined. Multiple headland turning types might be available and the turning cost depended on the adopted headland turning type at each field edge. The costs of several most commonly used headland turning types were analyzed and the method for selecting the most suitable turning type was developed. To search for the optimal decomposition, a topological undirected graph was

built for finding all possible dividing lines. The details of these steps are described below and the general algorithm is summarized.

2.3.1 Problem Modeling

To develop an optimal coverage path planner, a geometric model for defining the inputs and outputs of the planning algorithm needed to be developed. A field had only one outside boundary which commonly contained straight edges. If a field boundary contained curves, they could always be approximated by chains of line segments connecting the sampled points on the curves. The more points were sampled, the more accurate the curve was approximated. Therefore, the outside contour of a field could always be represented as a polygon. There might also be obstacles within the field from which farming equipment was prohibited, such as ponds, trees and water ways. Similarly, these obstacles could be represented by polygonal holes within the polygonal outside boundary of a field. As a result, a farm field could be represented as one outside boundary polygon and probably a number of smaller inside polygons that represented obstacles. For a 2D field, this was a planar subdivision that could be represented by a data structure called Doubly-Connected Edge List (DCEL) (Muller et al., 1977).

For farm field coverage path planning, it was critical to find out the best way to decompose a field into multiple sub-regions and the corresponding best path direction for each region, such that the total cost of covering these regions with boustrophedon paths could be minimized. To summarize, the input of a farm field coverage path planning problem was a planar subdivision representing the field as well as some other parameters such as the operation width, vehicle's minimum turning radius and headland width, while the output was a list of planar subdivisions with each representing a divided sub-region that was also marked with the best path direction.

2.3.2 Field Boundary Simplification

The field boundary information was the main input to the 2D planar field coverage path planning algorithm. Mostly the boundary information was obtained from in-field data collection with GPS equipped vehicles. As a result, the boundary information was composed of a collection of points on the boundary in the form of polylines. The obtained boundary

polylines often had too high resolution, especially at those smoother boundary sections, where a large set of points were densely distributed along smooth lines. This would result in an unnecessarily complicated field model, which would greatly increase the computational complexity for the path planning algorithm. Therefore, it's necessary to reduce the number of vertices on the polylines to only the essential ones that suffice the resolution of the coverage planning application.

The objective here was to develop an adaptive filtering algorithm for field boundaries such that the boundary data was reduced without undermining the planning algorithm while maintaining an acceptable resemblance to the actual field shape. Former methods had been reported and utilized for field boundary simplification, such as Vertex Reduction, Perpendicular Distance Algorithm, Douglas Peucker Algorithm, Harris Corner Detection and other corner detection methods. Vertex reduction is the brute-force algorithm for polyline simplification. Successive vertices that are clustered too closely are reduced to a single vertex. Perpendicular Distance Algorithm, reported by Jenks (1989), calculates the perpendicular distance from a line connecting two points to an intermediate point. The intermediate point is retained only if the length of this perpendicular is greater than the tolerance. Given a curve composed of line segments, the Douglas Peucker algorithm (Douglas et al., 1973) finds a similar curve with fewer points: It works from the top down by starting with a crude initial guess at a simplified polyline, namely the single edge joining the first and last vertices of the original polyline. The algorithm then recursively divides the line with the point farthest from each edge, and this process continues for each edge of the current guess until all vertices on the original polyline are within displacement tolerance of the simplification. Since the vertices at the corners on the boundary are often characteristic points of the shape, they can be detected and adopted for the simplified boundary. Harris Corner Detection algorithm (Harris et al., 1988) calculates two convolution matrices with the input image and the derivative masks in both x and y directions, creating the image derivatives with the same dimension as the input image. The output image is created using the "Harris" measure, with the locations of the corners indicated as blurred dots on the image. Thresholding this image yields all the corners in the image. There are many other corner detectors such as Rosenfeld and Johnston RJ73, Rosenfeld and Weszka RW75,

Freeman and Davis FD77 and Beus and Tiu BT87 (Liu et al., 1990). There are two common main steps for all these algorithms: First, a measure of corner strength (`cornerity') is assigned to each point; Second, the corner points are selected based on this measure.

Among the former boundary simplification methods introduced above, Vertex Reduction is the fastest and least complicated algorithm, but gives the coarsest result. The objective of Douglas Peucker algorithm is to obtain a “Least Set” of vertices which 1) meet the “distance threshold” requirement; and 2) the requirement will not be met if any vertex is removed from the set. For most of the cases, given a curve composed of line segments, there would be multiple such “Least Sets” existing. The resulting Least Set is determined by the sequence of adding points, which in turn is determined by the algorithm. The Douglas Peucker algorithm has a short running time (it is proven as one of the fastest searching algorithm for such a Least Set), but it does not guarantee to find the “best” Least Set. For example, for some of the Least Sets, the remaining points often do not include the points at the boundary corners, resulted in minor shape distortions. Another drawback of Douglas Peucker is that it only has the control over the “distance error”, while for the field boundary representation, there may be other criteria such as the “edge direction error.” There are also limitations with the corner detection algorithms. All corner detection algorithms focus only on the local curvature in order to detect the corner points. This may lead to the missing of the global shape characteristics. Consider the boundary of a big circle as an example, no corner points will be detected by these algorithms. For the field boundary simplification, a “global view” is critical when deciding which points are to be reserved.

For the 2D coverage path planning application, a new algorithm for field boundary simplification was developed. The algorithm was composed of three steps:

Step 1, Wavelet low-pass filter for de-noising purpose.

This was an optional step. It’s particularly useful when the collected boundary data contained much noise. Since wavelet analysis was able to break down a signal into different resolution levels, it’s particularly suitable for the de-noising of field boundaries. The X-coordinates and Y-coordinates of the points went through the wavelet low-pass filter (filter

"haar", level 4, soft thresholding, using the heuristic variant of Stein's Unbiased Risk as the threshold selection rule) separately.

Step 2, Thresholds for "integrated direction error" and "integrated distance error" were defined. The algorithm checked through the points with a window containing n consecutive points. The window moved forward by one point each time. The last point in the window was retained if either of the two integrals was about to exceed the threshold.

The coverage path planning project required the accurate representation of both boundary positions and boundary directions. Therefore, instead of only focusing on the distance error, the algorithm checked both distance and direction errors. Besides, instead of checking the errors of one single point, the algorithm checked the integrated error of a sequence of points by using a moving window. This equipped the algorithm with a "global view" when simplifying the boundaries.

Step 3, Each retained point was selected at the best position (such as at the turning corners with the maximum local curvature, and so on), which was not necessarily the last point when a threshold was broken.

The third step was a modification to the second step, but was of key effect. The advantages of the "preference to the points with higher curvature value" are shown in the test results (section 2.4.1) in comparison with the results of Douglas Peucker algorithm.

2.3.3 Coverage Cost Analysis

2.3.3.1 General Description of the Cost Function

For coverage path planning, coverage efficiency was of the highest concern. Coverage efficiency was inversely related to the total operational time. While operating along those straight sections of the boustrophedon paths in the interior of a field, with 2D coverage path planning, the speed and the total travelling distance (which was almost the field area divided by the swath width) were almost constant. Therefore, the cost on the straight path sections in the interior of the field was almost constant and the total coverage cost was then primarily determined by the cost of headland turning part of the paths. In this application, the cost function was defined as the sum of the headland turning cost, and the

turning cost was calculated as the time required for accomplishing the turnings. There were other costs such as the headland open-up cost and the cost of using high yield areas as headland. The analysis of these costs was not included in this application and remained as future work.

In order to reduce the total turning cost, the number of turns needed to be minimized. Besides, those turns with relatively high operational costs needed to be avoided. Fields of irregular shapes had inefficiencies related to headland turns when headlands were at an angle to machine travel (Hunt, 2001). For an angled turn as shown in fig. 2.1, the total travel distance in the headland was dramatically increased compared with the case when the headland was orthogonal to the machine travel. This extra travel distance caused losses in time and operator effort.

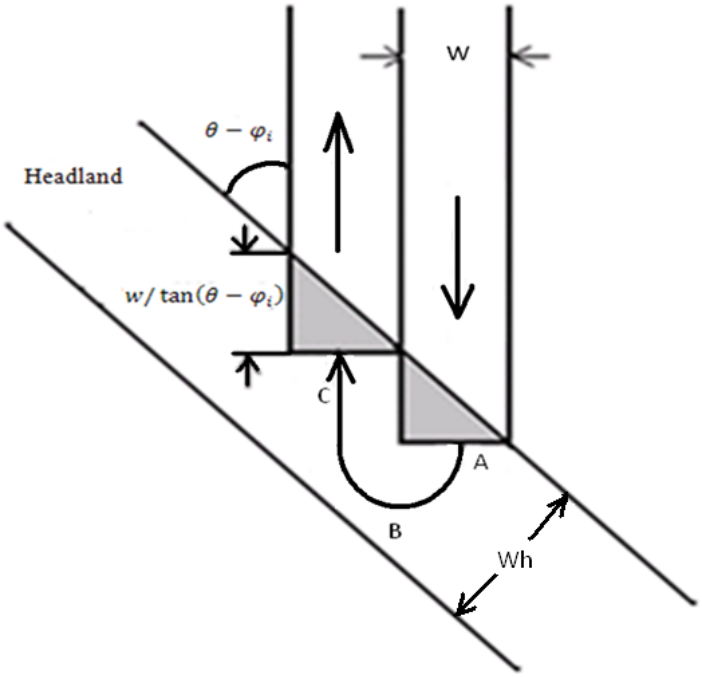

Figure 2.1. Illustration of an angled turn. w was the swath width; θ was the swath direction and φ_i was the edge direction.

The number of turns, Ni, on the i^{th} edge depended on the length of the edge and the angle between the edge and the machine travel direction. N_i was calculated as:

$$N_i = L_i|\sin(\theta - \varphi_i)|/2w \quad (2.1)$$

where L_i was the length of the edge; w was the swath width; θ was the swath direction and φ_i was the edge direction.

Assuming the turning cost in fig. 2.1 could be estimated as C_{turn} , except for the situation where the path and the edge were parallel or nearly parallel, the cost on the i^{th} edge was

$$C_i = C_{turn} \cdot N_i \quad (2.2)$$

The total turning cost of covering a field with boustrophedon path along direction θ was thus the sum of costs on all edges, including the edges of the internal obstacles in the field. The total cost was then computed as:

$$C = \sum_{i=1}^{p} C_i \quad (2.3)$$

where p was the number of field edges.

The objective of optimization was to minimize C by choosing a value of θ for $\theta \in [0, 180°)$.

The following sub-section is the detailed analysis of the turning cost "C_{turn}" for different headland turning types.

2.3.3.2 Cost Analysis of Different Headland Turning Types

As described above, the criterion was to have an accurate estimation of C_{turn}. In fig. 2.1, it was assumed that a "U" turn (the trajectory A-B-C) could be made. However, due to restricted minimum turning radius of field equipment, predefined row width and limited headland space, "U" turn might not be applicable in some situations. Sometimes even when "U" turn was applicable, it was however not the most cost-effective turn. Instead, other headland turning types such as "flat" turns, "bulb (keyhole)" turns, "hook (asymmetric bulb)"

turns and “fishtail” turns were more efficient. In the following, different headland turning types were investigated and compared.

Case 1: “Flat” Turn

When the vehicle and implement turning radius was smaller than half the swath width ($r < w/2$), a “flat” turn could be made instead of a conventional “U” turn with a larger turning radius (as the dashed curve in fig. 2.2). When the center point of the implement reached point “A”, part of the implement started to exit the interior of the field. However in order to completely finish the coverage of the current swath, the vehicle needed to keep moving straight ahead until point “B” was reached. The vehicle then made the “flat” turn from “B” to “C”, and started to re-enter the field from “D”, until the entire width of the implement was inside the field from point “E”. This headland turning type would save headland space and reduce the length of the total turning trajectory, thus reduce the time cost of turning.

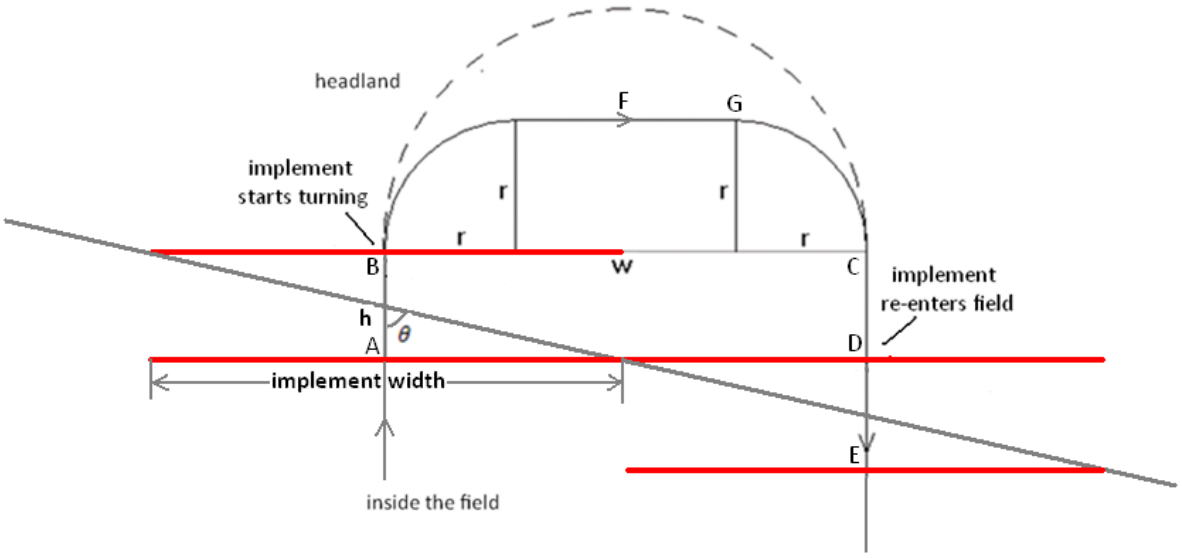

Figure 2.2. The “flat” turn made in headland when $r < w/2$. The dashed curve was a “U” turn to be compared.

Assuming v was the turning speed, the time cost on this turn (from “B” to “D”) was

$$C_{turn} = \frac{w(1+\cot\theta)+r(\pi-2)}{v} \quad (2.4)$$

This same turning speed v was also assumed for other headland turning cases.

Case 2: "U" Turn

"U" turn happened at the critical state of the "flat" turn when $r = w/2$ (fig. 2.3). Similarly, the time cost on a "U" turn was

$$C_{turn} = \frac{(\pi+2\cot\theta)w}{2v} \quad (2.5)$$

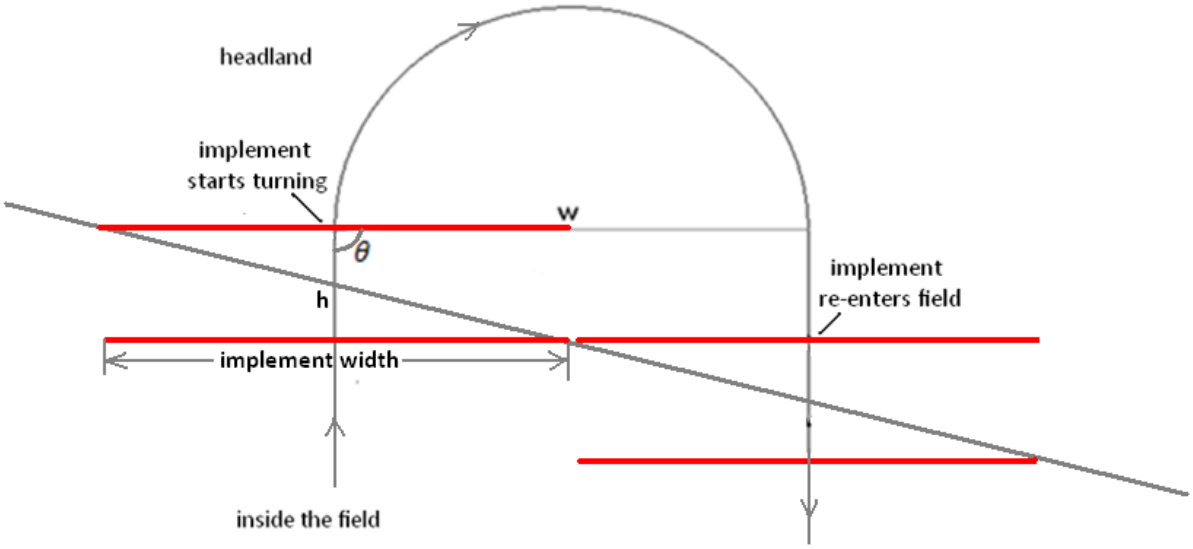

Figure 2.3. The "U" turn made in headland when $r = w/2$.

Case 3: "Bulb" Turn

When $r > w/2$, there was not enough space for the vehicle to make a "flat" turn or "U" turn, and a "bulb" turn was needed. To make a "bulb" turn, the vehicle started by turning away to the opposite direction first to make enough turning space (E-F), then turned back (F-G), and finally reversed the turning direction again (G-H) to enter the next swath (fig. 2.4).

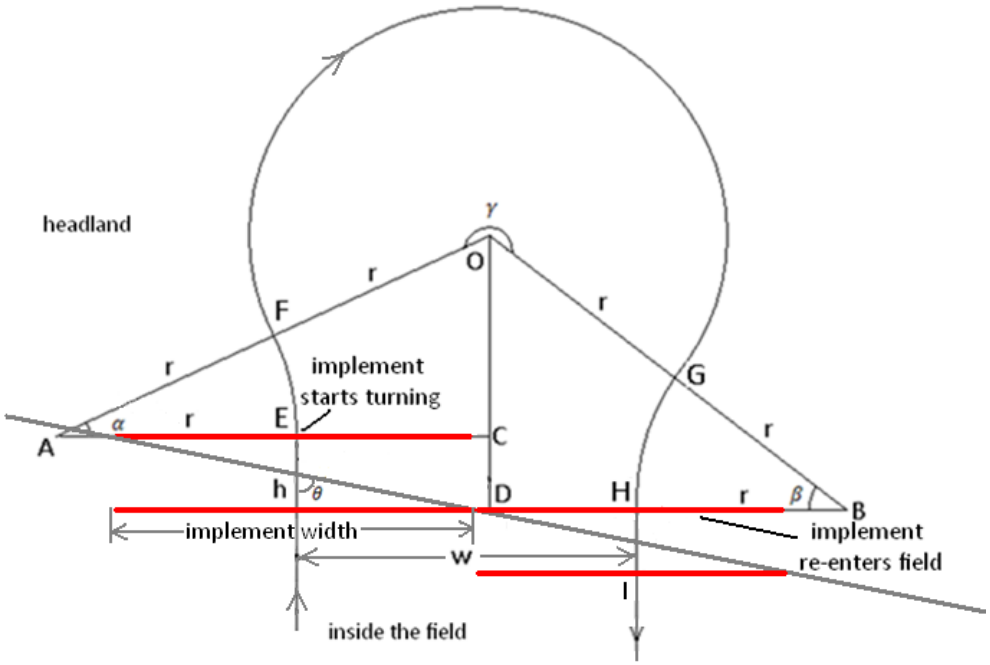

Figure 2.4. The "bulb" turn made in headland when $r > w/2$.

In the case of "bulb" turn described in fig. 2.4, the vehicle started from the field exit point E, when the vehicle was still travelling in alignment with the swath direction. The curve ended when the vehicle re-entered the field at point H, where the vehicle must be heading along the direction of the swath again. Theoretically, to ultimately save headland space and reduce the turning distance, the vehicle should always be turning with its minimum turning radius, r.

The headland width also imposed limitation to "bulb" turns. The headland provided enough space for a "bulb" turn only if:

$$W_h > r(1 + 2\sin\theta\sin\alpha + 2\cos\theta\cos\alpha - \cos\theta) + \frac{w}{2} \quad (2.6)$$

where W_h was the headland width; r was the vehicle's minimum turning radius; α was the radius of section EF in fig. 2.4, θ was the angle between swath direction and the edge and w was the operation width.

From geometric analysis of fig. 2.4, the following equations were derived:

$$h = w/\tan\theta \quad (2.7)$$

$$\alpha + \beta = \text{acos}\left(\frac{w}{2r} + \frac{h^2+w^2}{8r^2} - \frac{1}{2}\right) \quad (2.8)$$

Hence, the time cost on this "bulb" turn was: $C_{turn} = r(\alpha + \beta + \gamma)/v \quad (2.9)$

Since $\gamma = \pi + \alpha + \beta$, from equations (2.7), (2.8) and (2.9), the cost function of the bulb turn was obtained as:

$$C_{turn} = r(\pi + 2\text{acos}(\frac{w}{2r} + \frac{w^2(1+\tan^2\theta)}{8r^2\tan^2\theta} - 1/2)\,)/v \quad (2.10)$$

Case 4: "Hook" Turn (Asymmetric "Bulb" Turn)

When $r > w/2$, another headland turning type called "hook" turn could be applied instead of the "bulb" turn. Rather than starting by turning away toward the opposite direction as the "bulb" turn did, "hook" turn started like a "U" turn. When reaching point F, it reversed the turning direction and adjusted to the next adjacent swath (fig. 2.5).

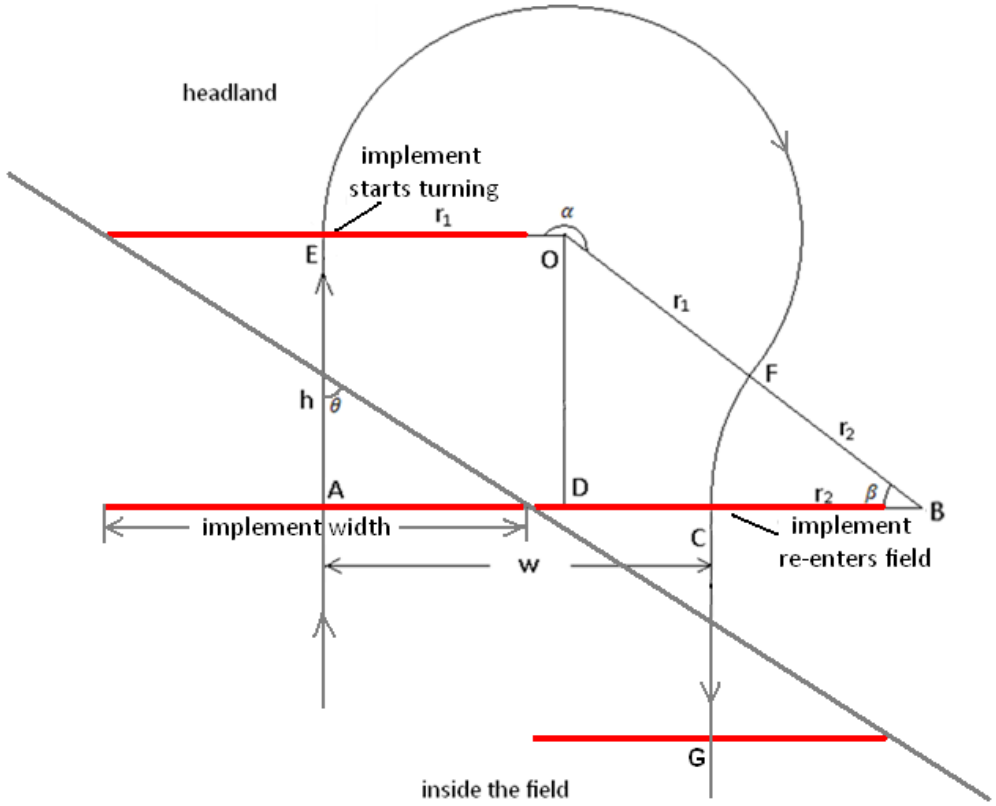

Figure 2.5. The "hook" turn made in headland when $r > w/2$.

The turning trajectory of a “hook” turn in the headland consisted of two sections: EF and FC (fig. 2.5). Again, as in the case of “bulb” turn, theoretically the vehicle should be turning with its minimum turning radius for section EF to maximally save headland space and reduce the turning distance. While for section FC, the turning radius needed to be chosen so that the vehicle would fit the next adjacent row when reaching point C, resulting in the following equations:

$$r_1 = r \quad (2.11)$$

where r was the minimum turning radius of the vehicle, and

$$r_2 > r_1 \quad (2.12)$$

From geometric analysis of fig. 2.5, we could further derive the following:

$$r_2 = \frac{w^2 \cot^2\theta + w^2 - 2wr}{4r - 2w} \quad (2.13)$$

$$\beta = \sin^{-1}\frac{4rw\cot\theta - 2w^2\cot\theta}{4r^2 - 4wr + w^2\cot^2\theta + w^2} \quad (2.14)$$

Combining equations (2.12) and (2.13), the “hook” turn could be a feasible solution only when

$$4r^2 \leq h^2 + w^2 \quad (2.15)$$

or equivalently

$$r \leq \frac{w}{2\sin\theta} \quad (2.16)$$

In fig. 2.5, equation 2.16 actually means EC needed to be longer than 2r for a “hook” turn to be feasible. This situation tended to happen when θ was larger. Besides, as in the case of “bulb” turn, “hook” turn could face the problem of limited headland width too. A “hook” turn required less turning space than a “bulb” turn and the headland provided enough space for a “hook” turn only when:

$$W_h > r(1 + \cos\theta) + \frac{w}{2} \quad (2.17)$$

The time cost on this turn was:

$$C_{turn} = (r_1\alpha + r_2\beta)/v \quad (2.18)$$

Since $\alpha = \beta + \pi$, from equations (2.13), (2.14) and (2.18), the cost function of the "hook" turn was:

$$C_{turn} = (r\pi + \frac{4r^2 - 4wr + w^2\cot^2\theta + w^2}{4r - 2w}\sin^{-1}\frac{4rw\cot\theta - 2w^2\cot\theta}{4r^2 - 4wr + w^2\cot^2\theta + w^2})/v \quad (2.19)$$

Case 5: Headland Turning Types with Limited Headland Width

When headland width was smaller than the critical case shown in fig. 2.6, none of the above headland turning types could be applied. The critical situation is expected when

$$W_h = r(1 + \cos\theta) + \frac{w}{2}(1 + \sin\theta\cos\theta) \quad (2.20)$$

When $W_h < r(1 + \cos\theta) + \frac{w}{2}$, the space of headland was too limited for the normal headland turning types, and other types incorporating reversing were needed. For example, "fishtail" turn (or switch-back turn) has been used in practice. Kise et al. (2002) created switch-back turning paths by applying third-order Spline function based on the constraints including minimum turning radius and maximum steering speed. However, the different angled turns were not considered and the discussion was only based on the assumption when the path direction was orthogonal to the field edge. Besides, other constraints such as the limited headland width were not included. The turning cost of those reverse types of turnings depended largely on the vehicle's motion characteristics, which could hardly be described with a universal cost function as in the cases of other turning types. The analysis of fish-tail turning cost remained as future work. Nevertheless, it can be expected that the cost of turning of reversed turns in limited headland space would be higher than that of other headland turning types when $W_h \geq r(1 + \cos\theta) + \frac{w}{2}(1 + \sin\theta\cos\theta)$.

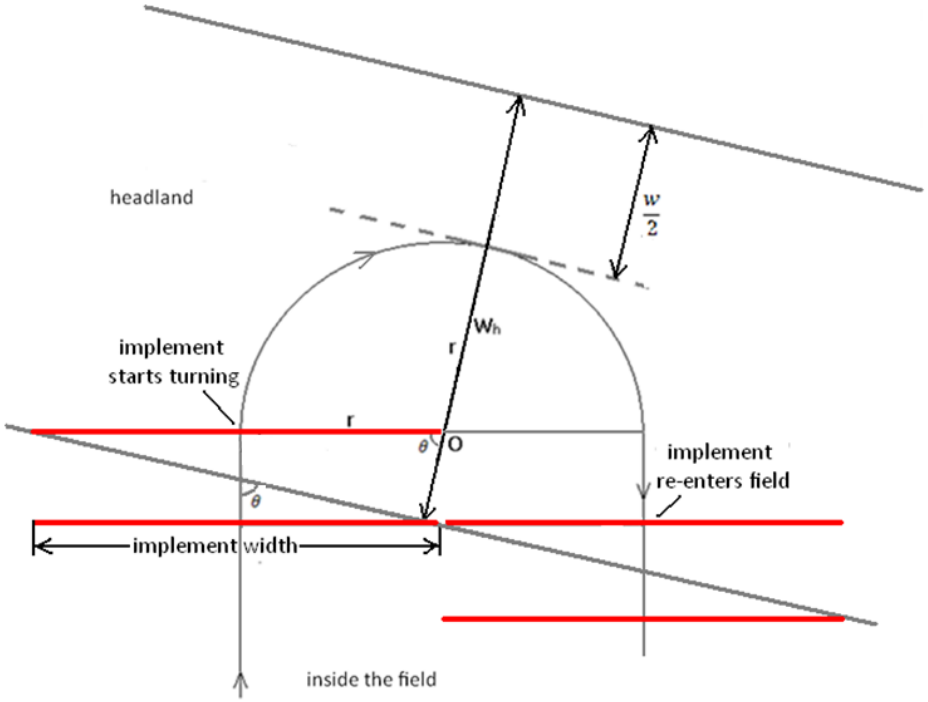

Figure 2.6. The minimum headland width for all the turning types in case 1 through case 4.

2.3.3.3 Selection of Headland Turning Types

When $W_h > r(1 + 2\sin\theta\sin\alpha + 2\cos\theta\cos\alpha - \cos\theta) + \frac{w}{2}$ (equation 2.6) and $r \leq \frac{w}{2\sin\theta}$ (equation 2.16), both "bulb" turn and "hook" turn were applicable. The operational costs of these two types of turns needed to be compared to make the choice. The ratio of turning cost of a "bulb" turn to a "hook" turn was calculated as a function of r, w and θ (fig. 2.7). The upper-right flat "zero" area in fig. 2.7 is an invalid area since $r > \frac{w}{2\sin\theta}$ for those points. For those valid points, the ratios were always less than 1, which means "bulb" turns always have shorter turning distances than "hook" turns. However, "hook" turns had their advantages too. First, "hook" turns required less headland width. It could be verified mathematically that equation 6 was a more restricted condition than equation (2.17). Second, since the turning radius of the FC section in fig. 2.5 was larger, it was easier for the vehicle to adjust to the next adjacent swath before entering the field again. So the choice between a "bulb" turn and a "hook" turn could still depend on farmers' preference.

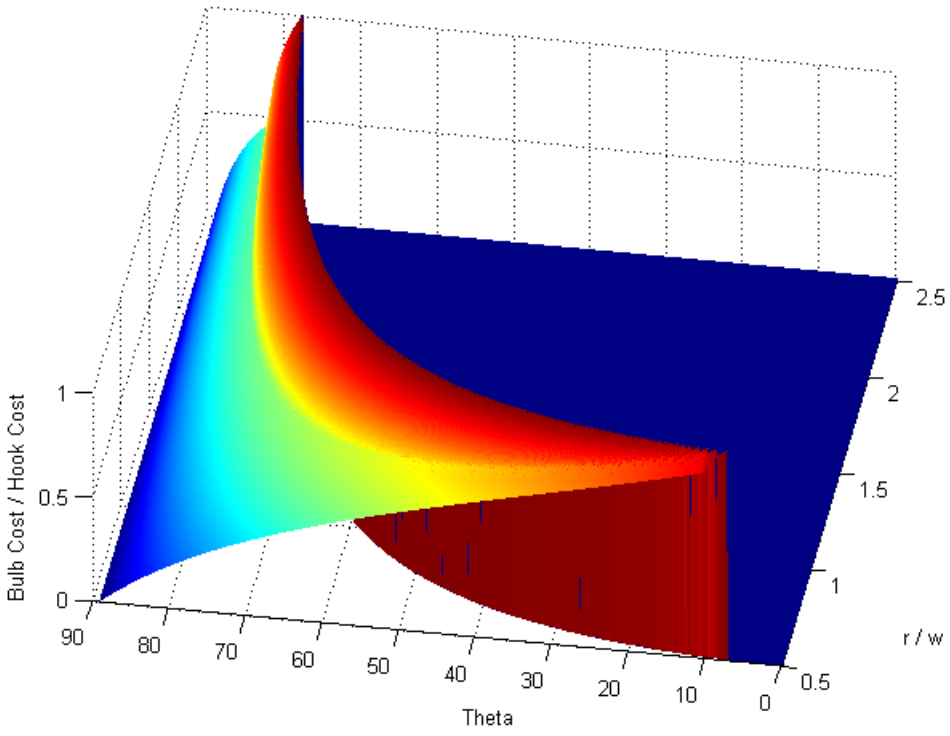

Figure 2.7. The ratio of turning cost of a “bulb” turn to a “hook” turn as a function of swath width (w), minimum turning radius (r), and angle between swath and edge (theta). The upper-right flat “zero” area is an invalid area where neither of the two headland turning types is feasible.

Similar to the choice between “Bulb” turn and “Hook” turn, the choice among all the five headland turning types above depended on the swath width, headland width, minimum turning radius and the angle between swath and edge. The restrictions and conditions for each headland turning type were summarized in a decision tree below (Fig. 2.8).

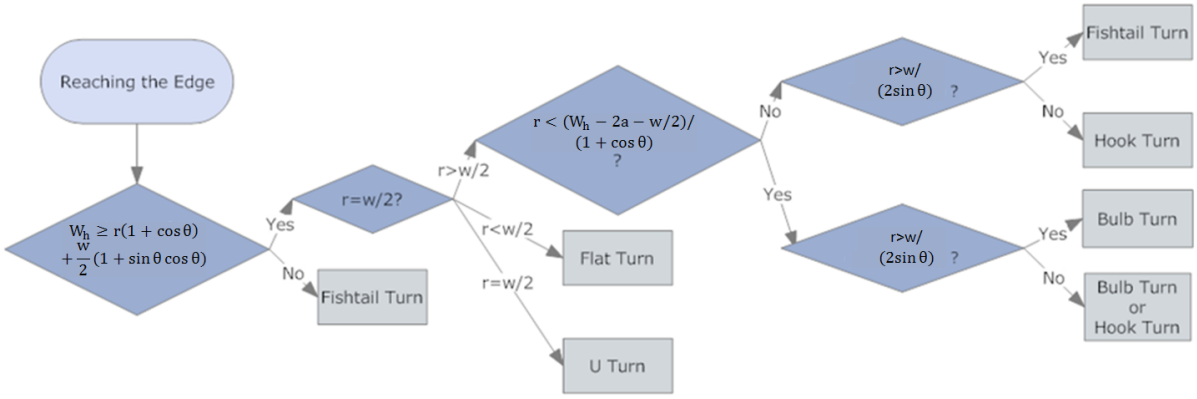

Figure 2.8. The decision tree for determining the most feasible headland turning type, where r was the minimum turning radius of the vehicle; θ was the angle between the swath and headland boundary; w was swath width; Wh was the width of headland; $a = r(\sin\theta\sin\alpha + \cos\theta\cos\alpha - \cos\theta)$ while α was the angle of arch EF in fig. 2.4 which was a function of r, θ, and w.

2.3.4 Field Segmentation

Since the goal of this optimal path planning application was to output a list of planar subdivisions that were also marked with the best path directions, all subdividing schemes needed to be found and evaluated. In this case, a topological undirected graph was constructed as the tool for the searching task. The undirected graph was first generated from the planar subdivision representation of the field, which was the input of the algorithm. New points and edges were then added to the graph: all the diagonals were added, and from each vertex (including the vertices on the internal holes), rays were drawn into the internal area of the field (fig. 2.9). Each ray must intersect with an edge of the original polygons. The step size for drawing the rays (the angle between two neighboring rays) determined how precisely the optimal decomposition scheme could be constructed. The new undirected graph was built subsequently, where the vertices in the planar subdivision and the new intersection points corresponded to the vertices in the graph, while the edges in the planar subdivision and the newly drawn line segments corresponded to the edges in the graph.

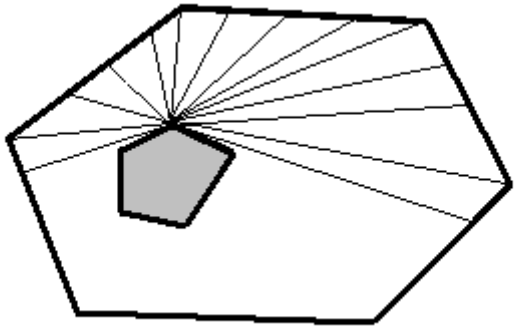

Figure 2.9. Drawing rays from a vertex.

Once the graph was constructed, a depth-first search was conducted in the graph. Each time it started by searching from a vertex on the outside boundary. Whenever the search reached another vertex on the outside boundary or itself, a new dividing line was formed, which was actually a chain of edges in the graph. Fig. 2.10 shows such a dividing line. It could be proved that by the depth-first search, all such dividing lines would be found.

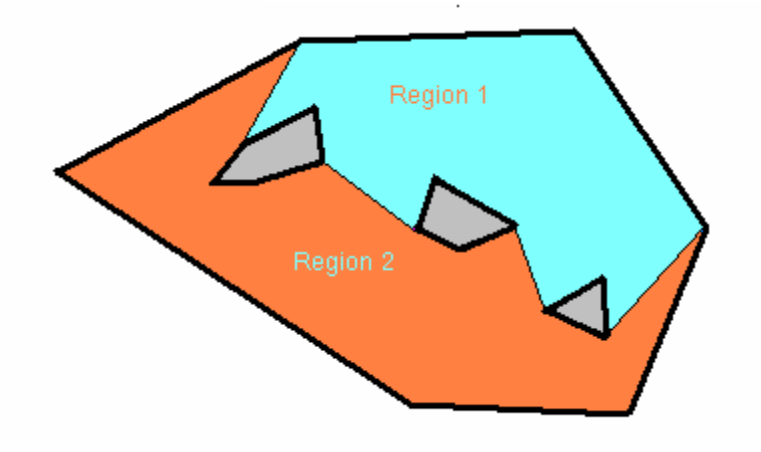

Figure 2.10. An example of a dividing line between two regions.

2.3.5 Recursive Searching Algorithm

To design this optimal coverage path planning algorithm, a divide and conquer strategy was adopted. Specifically, for a given field f, the algorithm first searched for the optimal path direction d without any decomposition. The cost of this coverage was recorded as C. Then, instead of covering f as a whole, the algorithm tried all possible ways of decomposing f into two sub-regions. For each trial of decomposition, the coverage cost was then calculated for the two sub-regions by recursively applying the algorithm to each of them. The sum of the two costs was recorded for the decomposition. This decomposition process was carried out in a recursive fashion so that all possible solutions were exhaustively investigated. If a summed cost of any decomposition was lower than the original cost C, the decomposition with the lowest summed cost was returned. Otherwise, if no decomposition could provide a lower summed cost than covering the entire field as a whole, the original results of d and C were returned as the output.

This Optimal Path Planning (OPP) algorithm is outlined as:

Algorithm *OPP(f, w, r, W_h)*
Input: *f (planar subdivision of the field with boundary length and direction information), w (operation width), r (vehicle's minimum turning radius), W_h (headland width).*
Output: *A list of planar subdivisions representing the sub-regions, a coverage path direction for each region and the total coverage cost.*
Step 1: Find the optimal covering path direction and determine the most suitable headland turning type at each edge for the whole field f based on the turning cost function, where
d = the path direction
C = the cost of covering f with a boustrophedon path along direction d
Step 2: Search for a collection of all possible ways of decomposing f into two regions
Step 3: For each trial decomposition, say f1, f2 are the two regions, apply OPP algorithm recursively to f1 and f2 with returned coverage costs of C1 and C2, respectively. If C1 + C2 < C, this decomposition case is recorded.
Step 4: If there is no more valid decomposition, return the results of the Step 1, or else, return the case having the minimum C1+C2.
End of algorithm

2.3.6 Transition between Neighboring Sub-regions

In the 2D coverage path planning algorithm described above, the output is "A list of planar subdivisions (sub-regions), with a coverage direction for each region and the total coverage cost." Consequently, the whole region is divided into several sub-regions, and each sub-region is covered with boustrophedon paths along one single direction. The next region is not covered until the coverage of the current region is completed.

However, in some situations it may cost less for a vehicle to cover two or even more regions in a continuous fashion that utilizes smooth transitions between sub-regions. In the example shown in figure 2.11, the region is divided into two sub-regions. The red line is the dividing boundary of the sub-regions. In the original planning (fig. 2.11a), the two regions are covered one after another. Each time a vehicle reaches the dividing edge, it turns 180 degrees back into the region again. This can be improved by adopting the planning shown in fig. 2.11b. Instead of making the 180 degrees U-turn back, the vehicle can make a smooth turn and enter the neighboring region, which essentially removed the dividing boundary between two adjacent regions. In this example, the turning cost at the dividing edge can be reduced by this change, and the headland area can be saved too.

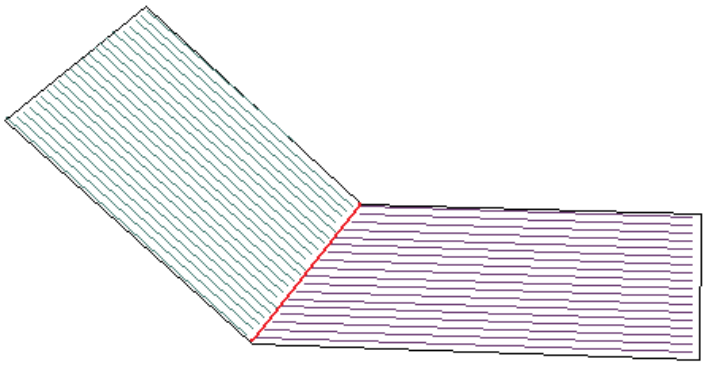

(a)

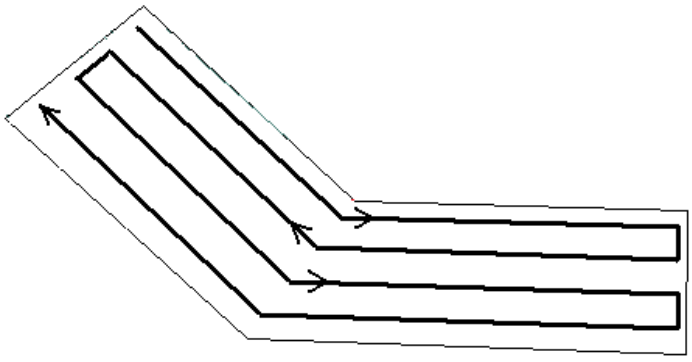

(b)

Figure 2.11. An example of region transition: (a) An example of covering sub-regions one-by-one; (b) Transition between sub-regions can save turning cost and head land area.

Following is a general description of a conceptual algorithm for combining those adjacent sub-regions for reducing turning cost during region transition.

In the original algorithm output, the edges of the boundaries of the sub-regions are either the edges from the original outside field boundary or the newly added dividing edges. The first step of the algorithm is to find out all the newly added dividing edges which are shared by two sub-regions.

Second, for each dividing edge shared by two sub-regions, it's checked if the total coverage cost can be reduced by combining the two regions. The decision of whether to recombine the two sub-regions is made by checking the sign of the following cost function:

$$F_t(\theta_1, \theta_2, L_i, \varphi_i) - C_i - \varepsilon * CH_i \quad (2.21)$$

where F_t is the new smooth turning cost during the transition between sub-regions. It's a function of several parameters: $\theta_1$and θ_2 are the path directions in the two regions seperately; L_i is the length of the dividing edge and φ_i is the direction of the dividing edge. C_i is the original turning costs; CH_i is the saved area of the headland and ε is the cost coefficient. If (2.21) has a negative value, the dividing edge should be removed and the regions should be combined.

The turning cost for the vehicle to transfer from one region to another can be evaluated as the time for the vehicle to change its direction by $|\theta_1 - \theta_2|$, as shown in figure 2.12. Assuming a constant turning speed d, the time for each turn is $|\theta_1 - \theta_2|r/d$, where r is the turning radius. The number of turnings can be calculated as

$$\min(L_i|\cos(\theta_1 - \varphi_i)|/2w, L_i|\cos(\theta_2 - \varphi_i)|/2w) \quad (2.22)$$

since the number of paths on the two sides of the dividing boundary may be different (more details are discussed below).

As a result, $F_t(\theta_1, \theta_2, L_i, \varphi_i)$ can be calculated as

$$F_t(\theta_1, \theta_2, L_i, \varphi_i) = |\theta_1 - \theta_2| r \cdot \min(L_i|\cos(\theta_1 - \varphi_i)|/2w, L_i|\cos(\theta_2 - \varphi_i)|/2wd) \quad (2.23)$$

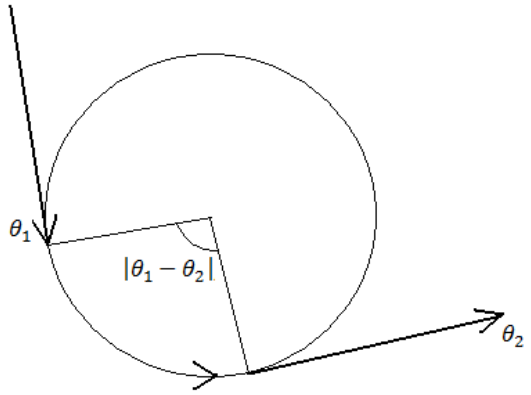

Figure 2.12. The smooth turning during transition.

Some modification to the cost function needs to be made based on the observation that the numbers of rows on the two sides of the dividing edge may not be equal. Actually in most of the cases these two numbers are un-equal unless the two path directions are with the same angle to the dividing edge. Taking fig. 2.13 as an example, the right region has eight rows but the left region has only six rows.

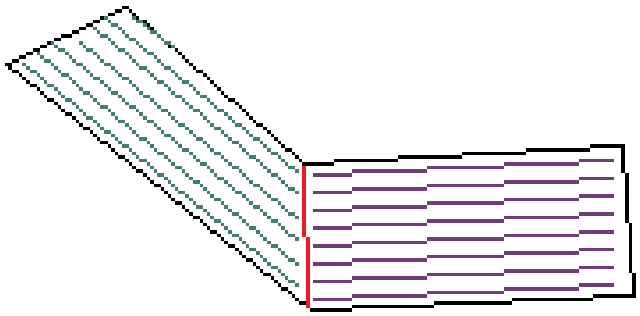

Figure 2.13. One case with unequal numbers of rows on the two sides of the dividing line.

One simple way to solve this “unequal numbers of rows problem” is to plan the sequence of covering these rows. The vehicle can simply go back and force in the first region, not entering the second region until the progress in the first region is leading at least one row width ahead of that in the second region (fig. 2.14). However, the rows on the two

sides are not exactly matched. There would always be some lateral offsets between the two rows (such as the offset for the transition from row 7 to row 8 in fig. 2.14). An "S" shape curve can be adopted to accomplish this minor lateral transition (fig. 2.15). The average lateral transition distance is half the path width and $F_t(\theta_1, \theta_2, L_i, \varphi_i)$ is modified as:

$$F_t(\theta_1, \theta_2, L_i, \varphi_i) = \pi w \cdot \min(L_i|\cos(\theta_1 - \varphi_i)|/2w, L_i|\cos(\theta_2 - \varphi_i)|/2w)/4d \quad (2.24)$$

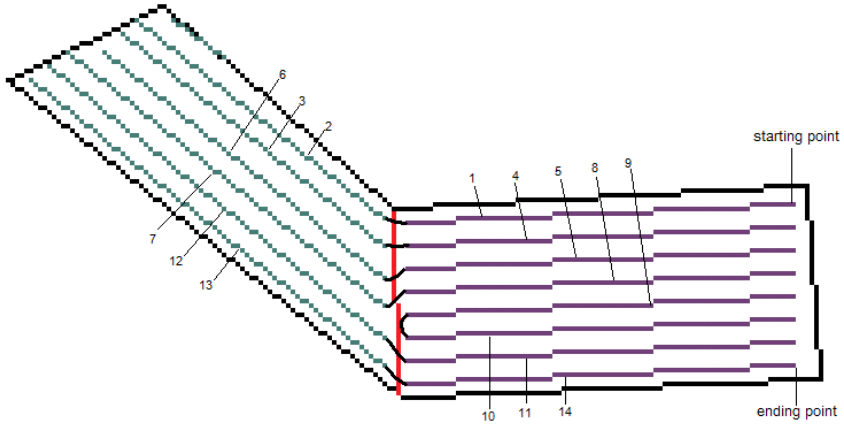

Figure 2.14. Planning the sequence of paths. The paths are labeled by the sequence of being covered.

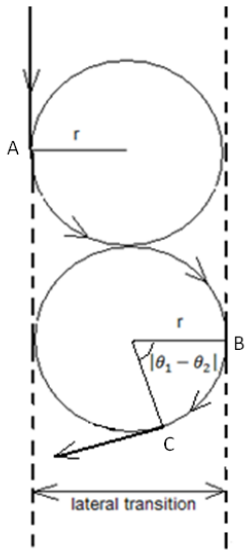

Figure 2.15. Adjusting for the lateral offset between the two rows. The "S" curve from A to B is adopted to accomplish the lateral transition. The vehicle then turns from B to C and enters the next region.

However, the “S” curves in fig. 2.15 bring higher cost. Besides, gaps and overlaps near the dividing boundaries are expected. Another option for solving this “unequal numbers of rows problem” is illustrated in fig. 2.16. Instead of turning at the dividing boundary, the vehicle keeps on moving into the next sub-region straight ahead, and makes the turning when meeting the next matched swath in the other sub-region. There would be some “unpaired” swaths in the regions with more swaths (paths 1and 4 in fig. 2.16a and paths 11and 14 in fig. 2.16b). For those swaths, U turns are adopted when they hit the boundary as before. In this way, the expensive “S” turns are replaced with easier turns.

There are two options for connecting the swaths in the two sub-regions. They can be paired either starting from the outside corner (fig. 2.16a) or starting from the inside corner (fig. 2.16b). In this project, the second approach was adopted because of potential problems of paring paths from outside. In fig. 2.16a, when the vehicle turns from path 13 to path 14, to eliminate uncovered area, the vehicle would follow path13 as far as possible, and then turn to path 14 with its minimum turning radius. However, when the vehicle transit from path 11 to path 12, an even smaller turning radius is needed since this turning is in the inner side of the turning from path 13 to 14, which is impossible to implement, or skipped areas between the swaths will occur. This problem is common when generating side-by-side parallel curved paths: while the most outside path is fixed, each subsequent path based on the outside path will suffer from sharper turnings and the turning space is more and more seriously limited.

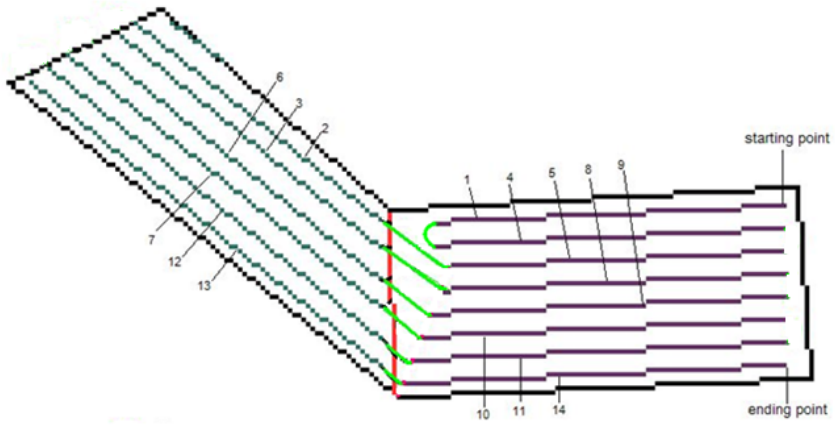

(a)

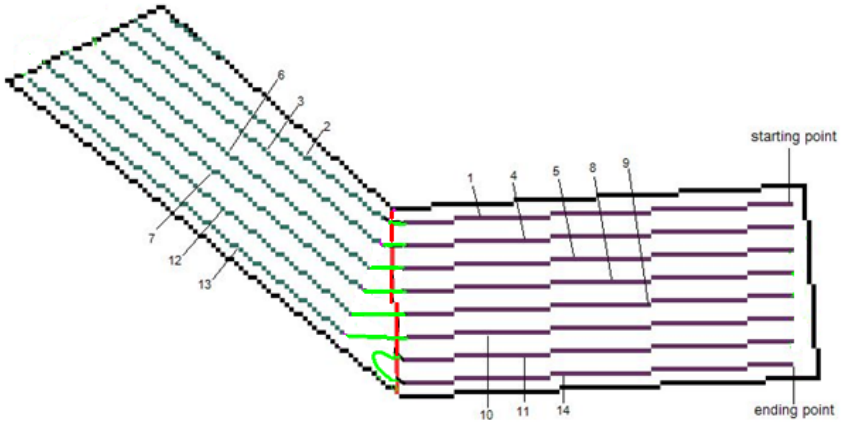

(b)

Figure 2.16. Turning when meeting the next matched swath in the other sub-region: (a) pair the swaths from outside corner; (b) pair the swaths from inside corner. The connection routes are highlighted with light-green lines to indicate the difference from the solution in fig. 2.14.

Based on the analysis above, concentric curves are adopted for the transition between the paired paths in fig. 2.16b. This method easily meets the vehicle's minimum turning radius limitations and eliminates gaps and overlaps between the adjacent swaths.

The cost function F_t is then modified as

$$F_t(\theta_1, \theta_2, L_i, \varphi_i) = |\theta_1 - \theta_2|(r + \frac{wN}{2})N + C_i' \quad (2.25)$$

where $N = \min\left(\frac{L_i|\cos(\theta_1-\varphi_i)|}{2w}, \frac{L_i|\cos(\theta_2-\varphi_i)|}{2w}\right)$, C_i' is the U turn costs between those unpaired paths, such as paths 11 and 14 in fig. 2.16b, which can be calculated as for the headland turnings.

There may be more than one dividing edges shared by two regions (fig. 2.17), and it's possible some of them are removed for region combination and some of them are kept, since the edges' directions can be different. In this situation, the two sub-regions are still combined as a new region.

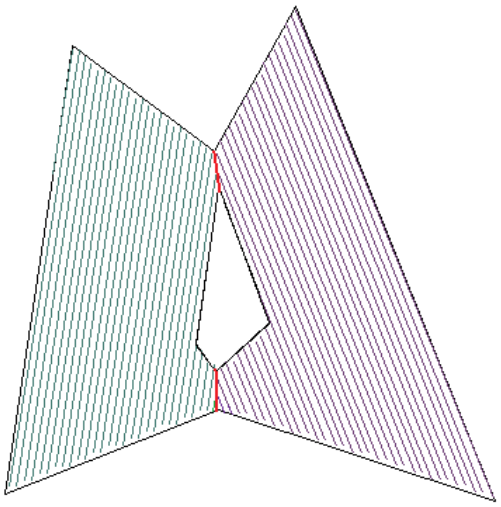

Figure 2.17. Regions sharing more than one dividing edges.

The region transition between neighboring sub-regions has been implemented and incorporated into the whole 2D planning algorithm. The updated Optimal Path Planning (OPP) algorithm can be summarized as follows:

Algorithm *OPP(f, w, r, W_h)*
Input: *f (planar subdivision of the field with boundary length and direction information), w (operation width), r (vehicle's minimum turning radius), W_h (headland width).*
Output: *A list of planar subdivisions representing the sub-regions, a coverage path direction for each region and the total coverage cost.*
Step 1: Find the optimal covering path direction and determine the most suitable headland turning type at each edge for the whole field f based on the turning cost function, where
d = the path direction
C = the cost of covering f with a boustrophedon path along direction d
Step 2: Search for a collection of all possible ways of decomposing f into two regions
Step 3: For each trial decomposition, say f_1, f_2 are the two regions, apply OPP algorithm recursively to f_1 and f_2 with returned coverage costs of C_1 and C_2, respectively. If $C_1 + C_2 < C$, this decomposition case is recorded.
Step 4: If there is no more valid decomposition, keep the results of the Step 1, or else, keep the case having the minimum C_1+C_2.
Step 5, Find out the dividing lines which can be removed to further reduce the turning costs by checking the sign of cost function $F_t(\theta_1, \theta_2, L_i, \varphi_i) - C_i - \varepsilon * CH_i$.
Step 6, Modify the result in step 4 according to the result in step 5.
End of algorithm.

2.3.7 Time Complexity Analysis and Running Time Reduction Methods

Except step 3 of the OPP algorithm described above, the time spent on searching for the decompositions dominated the required computational time for the algorithm. For a field

with totally n edges, the time spent on the depth first search was $T_d = O(n^3)$. In step 3, the OPP algorithm was called recursively on the two sub-regions, which assumably had a total of n_1 and n_2 edges. There were two restrictions for these parameters: $n_1 + n_2 <= n + 2m + 2$, where m was the number of obstacles of the original field, and $n >= 3(m+1)$ since there were at least three edges for each polygon. The total running time of the OPP algorithm was then computed as:

$$T_{opp} = O(n^3 \log(n)) \quad (2.26)$$

Modifications to the optimization algorithm were made to reduce the computational time. First, when constructing the undirected graph for the searching of the dividing lines, instead of drawing rays through each vertex to all directions, only the rays leading to new edges belonging to one of the following three categories were drawn, namely diagonals, line segments through the vertex and parallel to an edge, and line segments through the vertex and vertical to an edge. Adopting other dividing lines out of these three categories would mostly incur more angled turns and thus increase the total turning cost. This improvement not only reduced the computational time but also eliminated the errors caused by using big step size when drawing the rays.

The existence of obstacles significantly increased the running time. Sometimes for smaller obstacles, it was nearly unlikely for them to influence the decomposition scheme and the general direction of paths. It was also almost unlikely for the optimal dividing lines to go through any vertex of small obstacles. Therefore a group of internal obstacles with trivial influence on the general coverage planning were filtered out. The obstacles in this “trivial” group would not be considered in the algorithm when searching for the dividing lines.

None of these improvements above can change the form of asymptotic complexity given in (2. 26). However, they could reduce the expected running time substantially.

2.3.8 Performance Evaluation

The OPP algorithm was first implemented in Java J2SE 5.0 (Sun Microsystems, Santa Clara, CA) and later transferred to Visual C++ 2005 (Microsoft, Redmond, WA). The programs were tested on a computer with a 3.20GHz Pentium(R) 4 CPU and 1.50 GB of

RAM. The programs were used to find the optimal decomposition and straight parallel coverage path directions for planar fields with various shapes. Some of the outputs were compared with both former researchers' results and farmers' actual driving patterns. For most of the tests it was assumed by default that the equipment turning radius was 15 feet (John Deere 7030 tractor), the swath width was 40 feet (16 rows of corn plants) and the headland width was 80 feet (exactly two times of the swath width). Other settings were also assumed and adopted which are specified in this document. These settings can easily be changed when real data is available.

2.4 Results

2.4.1 Field Boundary Simplification Results

The newly developed field boundary simplification algorithm has been tested on practical farm fields. The test results on an example farm field with a complicated boundary shape are shown below. The original field boundary was composed of 5930 vertices, which were collected by GPS. In the first step, the wavelet low-pass filter was applied to the boundary. This resulted in a new boundary with only 505 vertices left. An overview of wavelet filtered field boundary and a zoom-in portion of it are given in the figures below. The original boundary is drawn in blue and the filtered boundary is drawn in red.

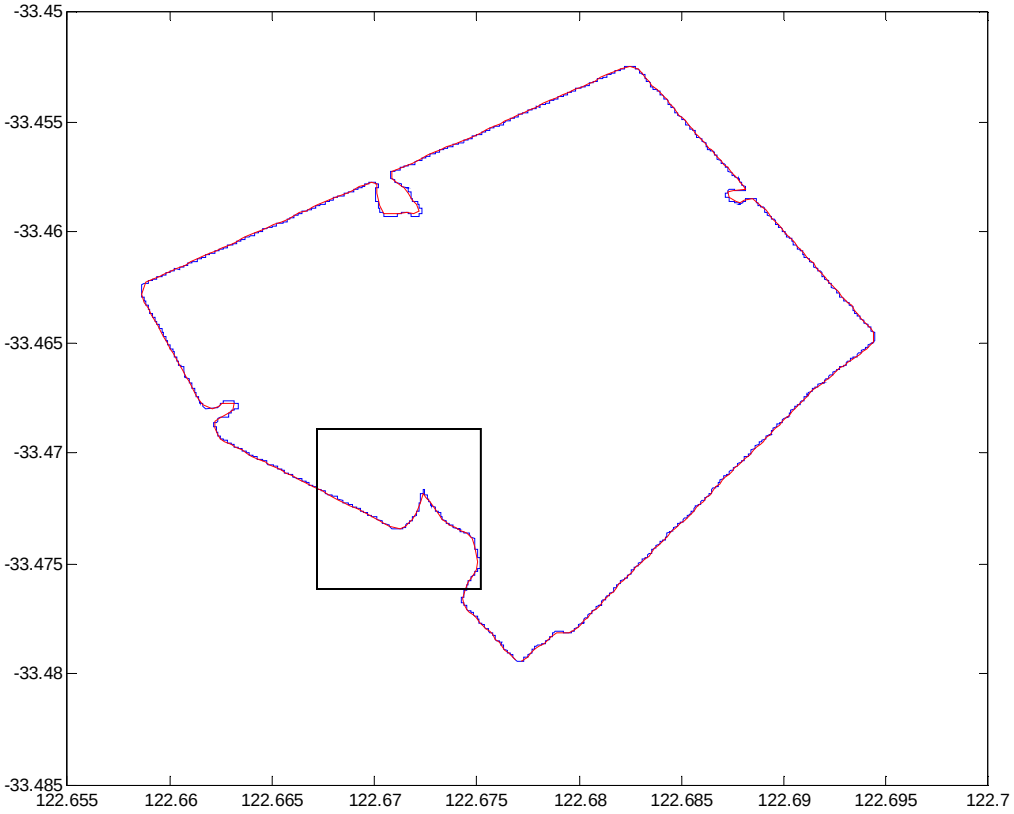
-33.45
-33.455
-33.46
-33.465
-33.47
-33.475
-33.48
-33.485
122.655
122.66
122.665
122.67
122.675
122.68
122.685
122.69
122.695
122.7

(a)

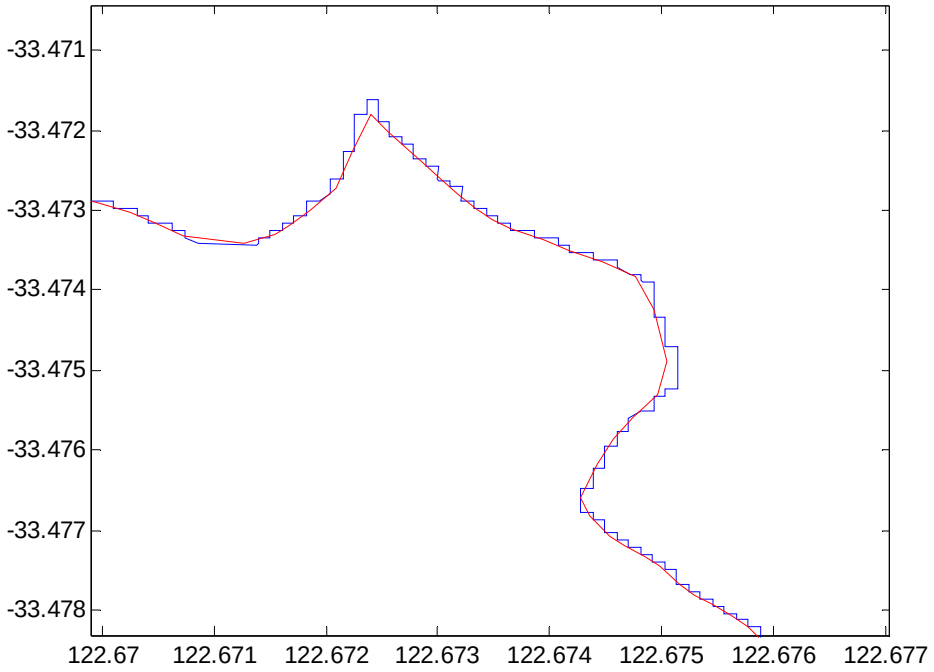

(b)

Figure 2.18. An overview of wavelet filtered field boundary: (a) Entire Boundary; (b) Enlarged image of a rectangular region in (a). The original boundary is drawn in blue and smoothed boundary is drawn in red. The X and Y axis labels are longitudes and latitudes in angles.

The smoothed boundary in fig. 2.18 was further simplified by applying step two and step three of the new simplification algorithm. To be compared with the new algorithm's result, Douglas Peucker's simplification was applied to the same boundary. For a fair comparison, the thresholds of both algorithms were set so that their results have nearly the same number of points (42 points for the new algorithm and 41 points for Douglas Peucker algorithm).

The two algorithms performed nearly the same at the smoother boundary sections. However they had different performances at the turning corners and those locally concave and convex sections, which were of primary concerns in path planning applications. For

example, in the following figure the point pointed by "→" represents the sharp turning point on the original boundary. The new algorithm accurately located this point and included it in the result, while Douglas Peucker algorithm skipped it.

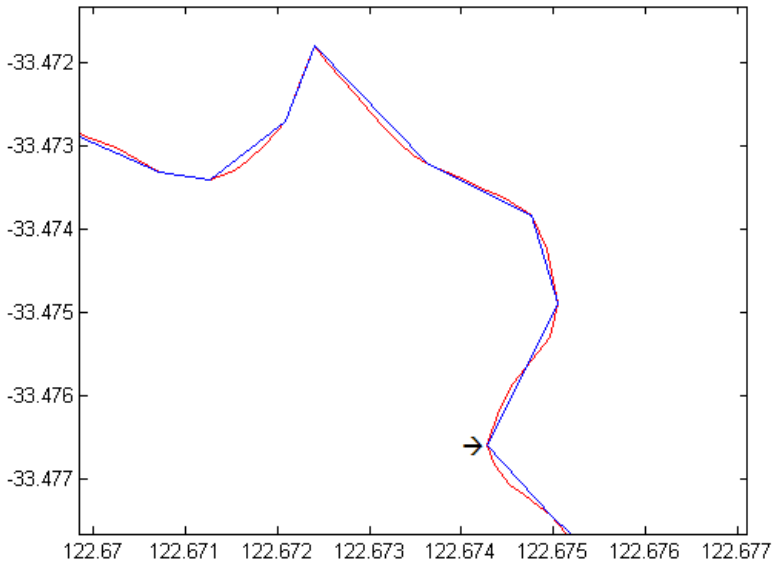

(a)

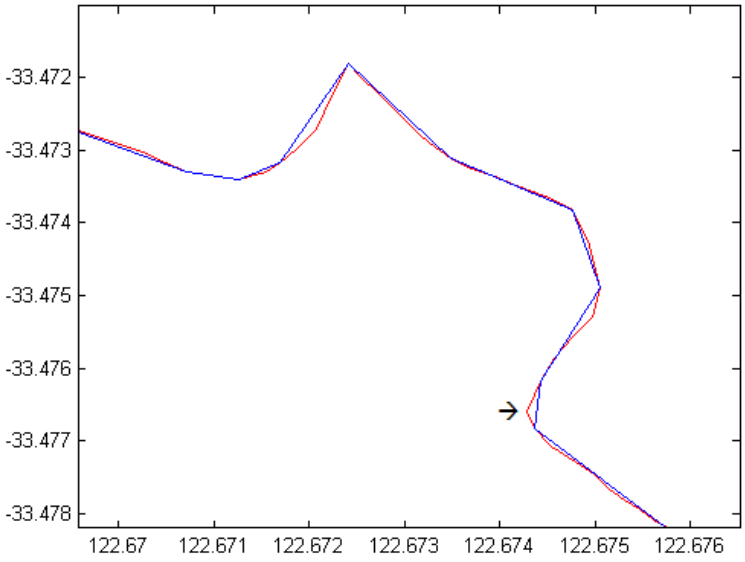

(b)

Figure 2.19. Comparison of ISU algorithm and Douglas Peucker algorithm (example 1): (a) result of ISU algorithm; (b) result of Douglas Peucker algorithm. In both cases, the red boundary is the original data and the blue boundary is the simplification result.

Similarly, in the following example part, the new algorithm located the turning corner correctly, while Douglas Peucker algorithm turned “too early” before reaching the turning point.

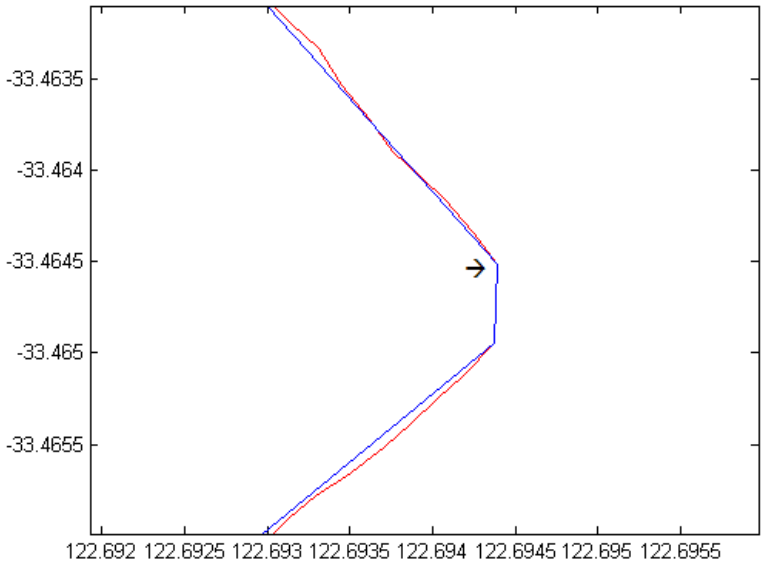

(a)

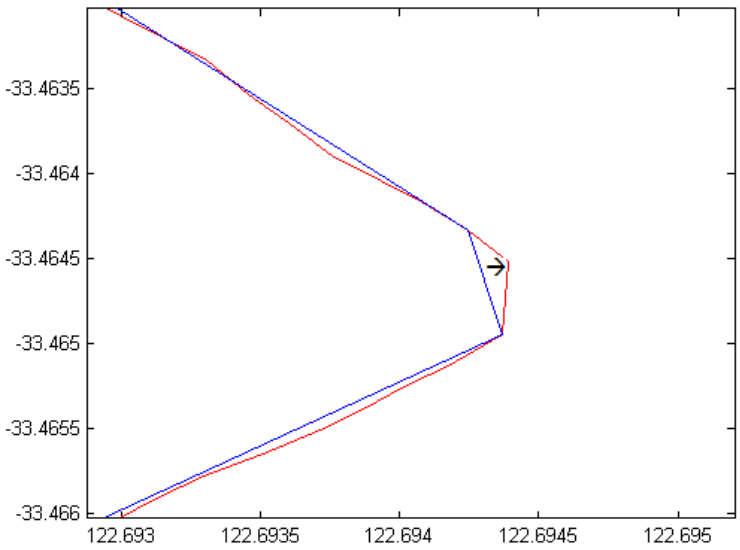

(b)

Figure 2.20. Comparison of ISU algorithm and Douglas Peucker algorithm (example 2): (a) result of ISU algorithm; (b) result of Douglas Peucker algorithm. In both cases, the red boundary is the original data and the blue boundary is the simplification result.

The same situation happened in another boundary section in fig. 2.21.

In fig. 2.22, both the new algorithm and Douglas Peucker algorithm used 6 points to represent the concave boundary section. However, the summed distance error of the new algorithm's result was only 37.9% of the Douglas Peucker's result, while the summed direction error of the new algorithm were only 31.0% of the Douglas Peucker's result.

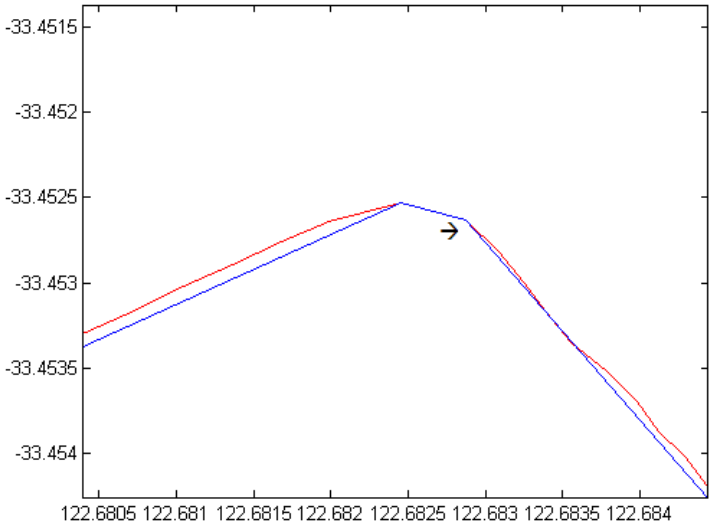

(a)

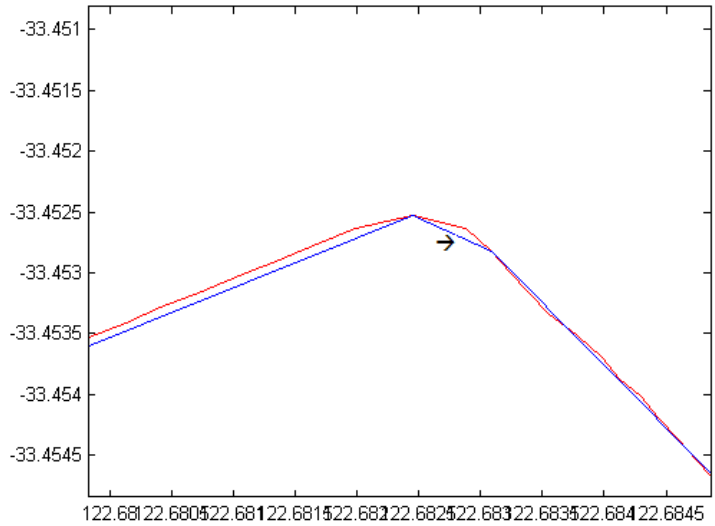

(b)

Figure 2.21. Comparison of ISU algorithm and Douglas Peucker algorithm (example 3): (a) result of ISU algorithm; (b) result of Douglas Peucker algorithm. In both cases, the red boundary is the original data and the blue boundary is the simplification result.

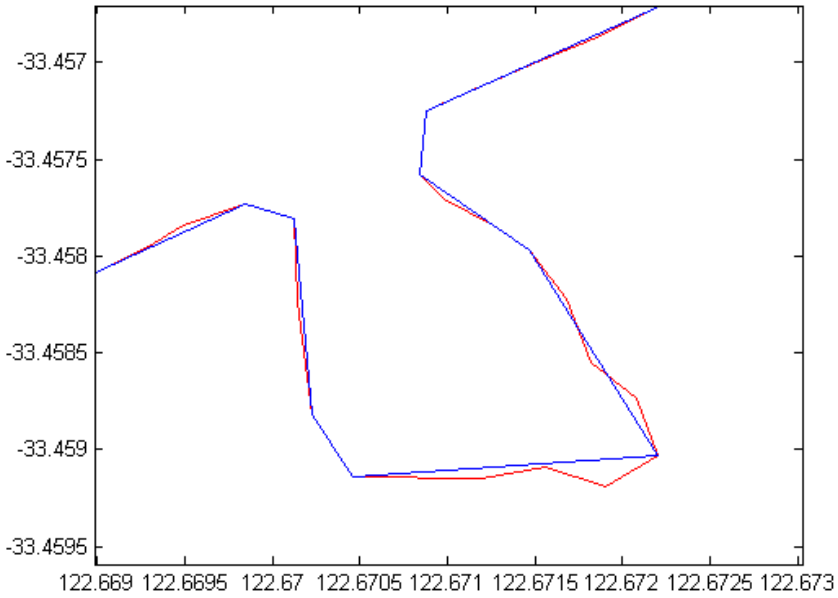

(a)

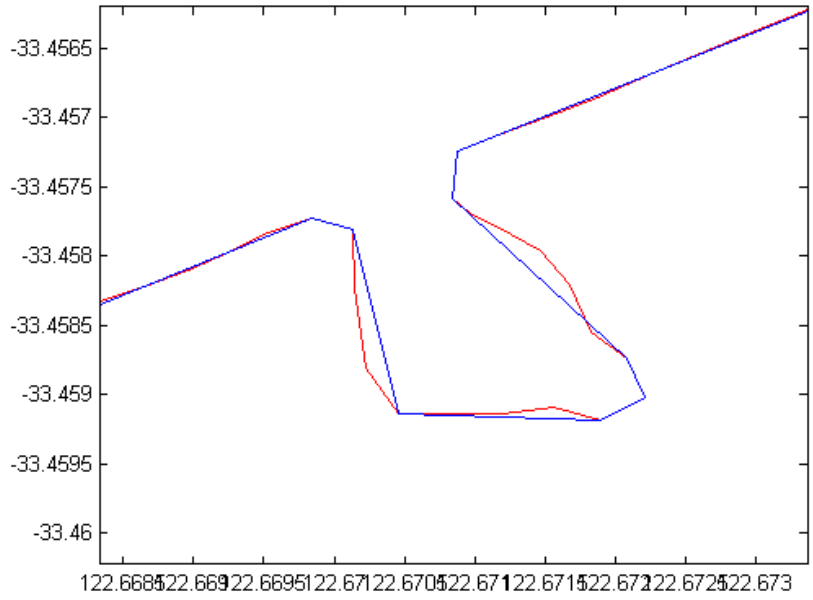

(b)

Figure 2.22. Comparison of ISU algorithm and Douglas Peucker algorithm (example 4): (a) result of ISU algorithm; (b) result of Douglas Peucker algorithm. In both cases, the red boundary is the original data and the blue boundary is the simplification result.

2.4.2 Optimal Field Coverage Path Planning Results

For all tested fields with no more than 20 vertices and 5 interior obstacles, the optimal solutions were found by OPP software within 60 seconds. Unless specified, it was assumed the default settings described in 2.3.8 were adopted for the equipment turning radius, the headland width and the swath width. According to the turning type decision tree (fig. 2.8), under this default assumption, “flat” turns should be adopted in most of the cases. Therefore in the following displayed examples the selected turning types are not specified unless any turning types other than “flat” turns were adopted.

In fig. 2.23, for the L-shape, the best solution returned by the algorithm was to decompose it into two rectangular shapes with coverage path directions along the longer edges.

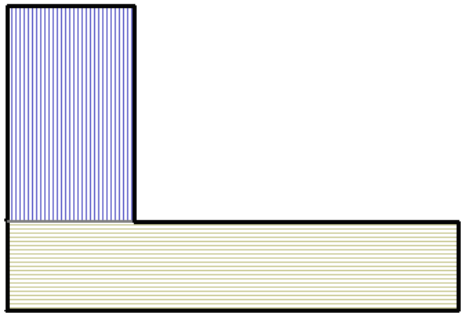

Figure 2.23. Field decomposition and path planning for an L-shape field.

Donnell Hunt (2001) pointed out that because of the higher costs of angled turns, when covering a right-angled triangle field, it’s better for the coverage pattern to be parallel to a perpendicular side rather than to the angled side. This was confirmed by OPP’s result shown in fig. 2.24. Fig. 2.24(a) shows the result when the default assumptions of the equipment turning radius, headland width and swath width were adopted. All turnings were of “flat” type in this result. Fig. 2.24(b) shows the result when the swath width was changed to 20 feet (8 rows of corn plants). “Bulb” turns (or sometimes “hook turns”, as discussed in 2.3.3.3) were adopted in this result because of the limited turning space.

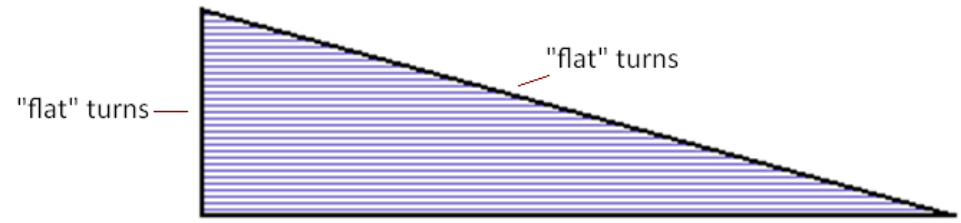

(a)

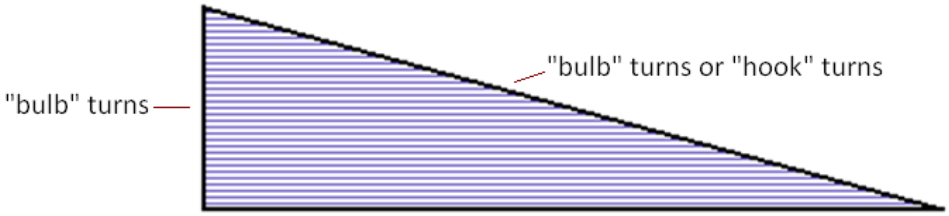

(b)

Figure 2.24. Path planning for a right-angled triangular field: (a) the result when the assumptions of the equipment turning radius (15 feet), headland width (80 feet) and swath width (40 feet) were adopted; (b) the result when the swath width was changed to 20 feet.

Farmers tend to choose the longest edge direction as the coverage path direction (fig. 2.25a). However, sometimes there exist better solutions than travelling along the longest edge direction. In the following example (fig. 2.25b), OPP made good use of the parallel relationship among three edges. According to the cost function described before, when compared with the solution in fig. 2.25a, solution in fig 2.25b saved 5% on the number of turns and 6% on the cost on the edges.

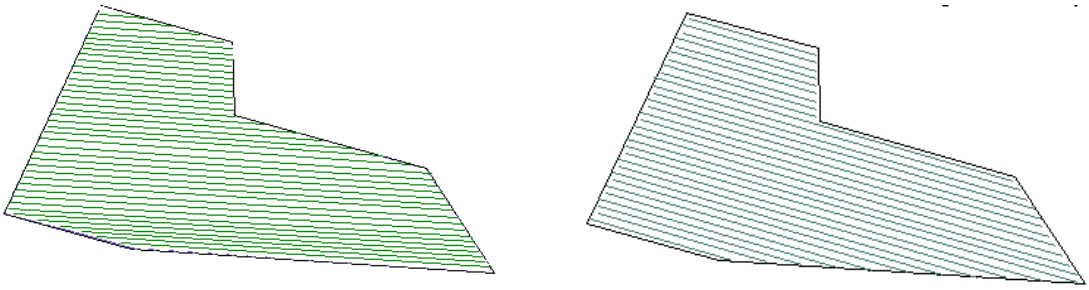

(a) (b)

Figure 2.25. Comparison of OPP with conventional approach: (a) conventional approach of covering along the longest edge; (b) OPP output.

The results from the OPP algorithm were compared with the solutions generated by some previous researchers. Fig. 2.26a is an example given by Oksanen et al. (2005). There were lots of angled turns in their solution. The solution generated by the OPP algorithm (fig. 2.26b) produced 4% more number of turns, but the cost of the angled turns was reduced, resulting in a 15% reduction of turning cost on the edges.

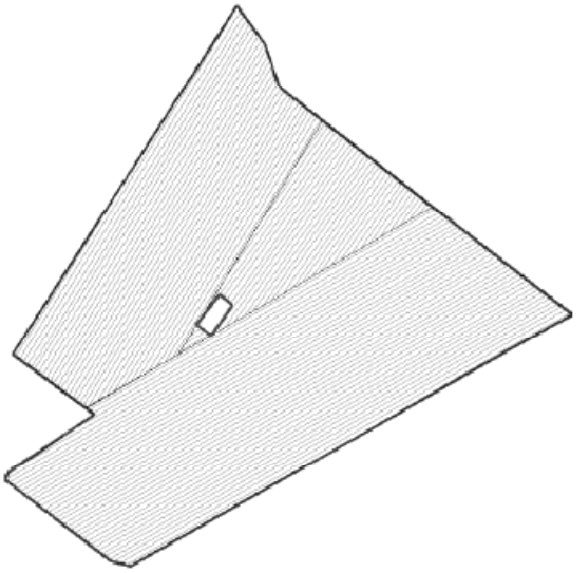

(a)

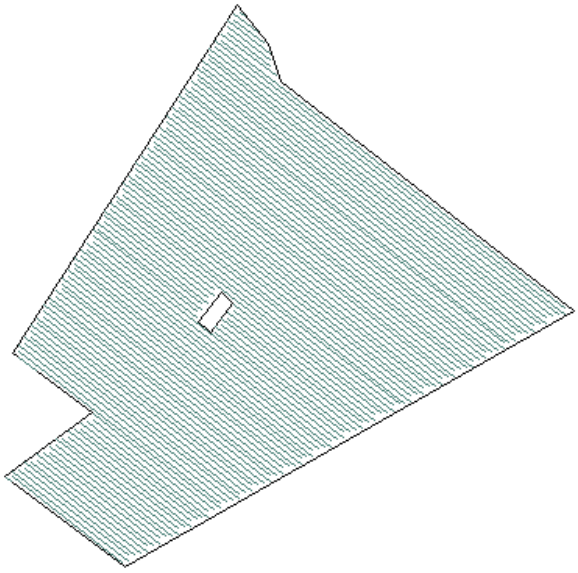

(b)

Figure 2.26. Comparison of OPP with others' approach: (a) approach of Oksanen et al.; (b) OPP output.

Fig. 2.27a is an example given by Fabret et al. (2001). Fig. 2.27b shows the result of OPP when the default assumptions of the equipment turning radius, headland width and swath width were adopted. All turnings were in "flat" type in this result. According to the cost function described before, the result in fig. 2.27b saved16% on the number of turns and 12% on the turning cost on the edges. Fig. 2.27c shows the result when the swath width was changed to 20 feet (8 rows of corn plants). Instead of being limited by using only diagonals as separation boundaries, OPP found a better dividing line that started at one vertex and was parallel to the bottom edge. "Bulb" turns (or sometimes "hook turns", as discussed in 2.3.3.3) were adopted in this result because of the limited turning space. The result in fig. 2.27c saved 9% on the number of turns and 14% on the turning cost on the edges compared with Fabret's result in fig. 2.27(a).

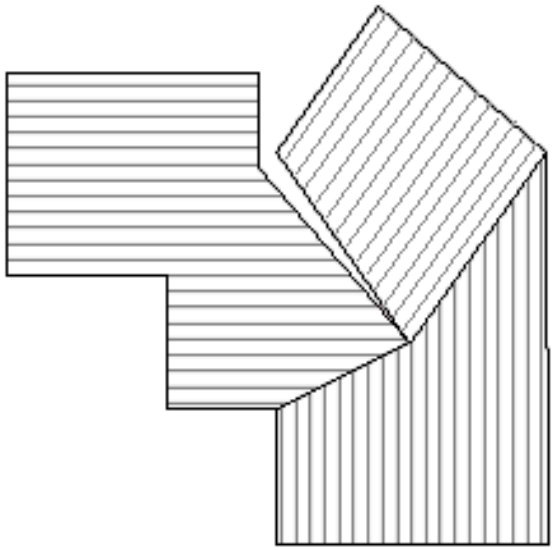

(a)

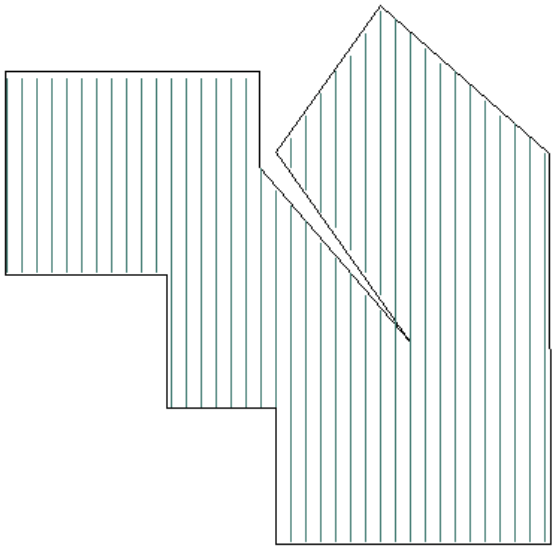

(b)

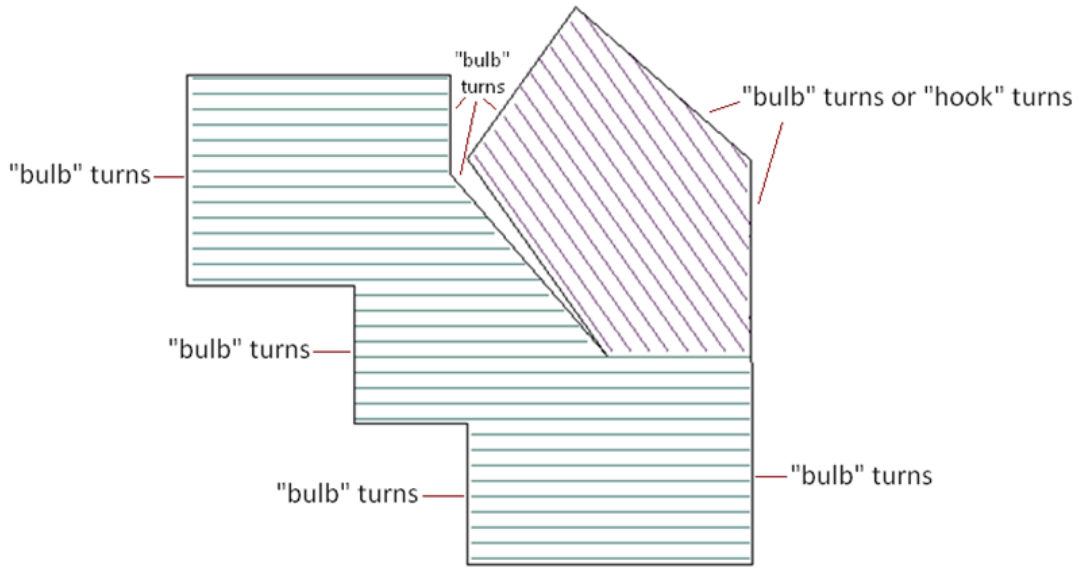

(c)

Figure 2.27. Comparison of OPP with others' approach: (a) approach of Fabret et al.; (b) OPP output when the assumptions of the equipment turning radius (15 feet), headland width (80 feet) and swath width (40 feet) were adopted. All turnings were in "flat" type in this result; (c) OPP output when the swath width was changed to 20 feet.

The example given by Fabret et al. (2001) was studied further by adding two obstacles into the field. The result is shown in fig. 2.28. If the former cover pattern in fig. 2.27c was not changed, the result would look as in fig. 2.28a. The OPP responded to the addition of the obstacles and obtained a new solution of fig. 2.28b. The decomposition was gone. Since the new obstacles brought some vertical edges into the field, it was reasonable to cover the field by the vertical paths. According to the cost function described before, compared with the solution in fig. 2.28a, saving from OPP on the number of turns was 4% and saving from OPP on the cost on the edges was 4%.

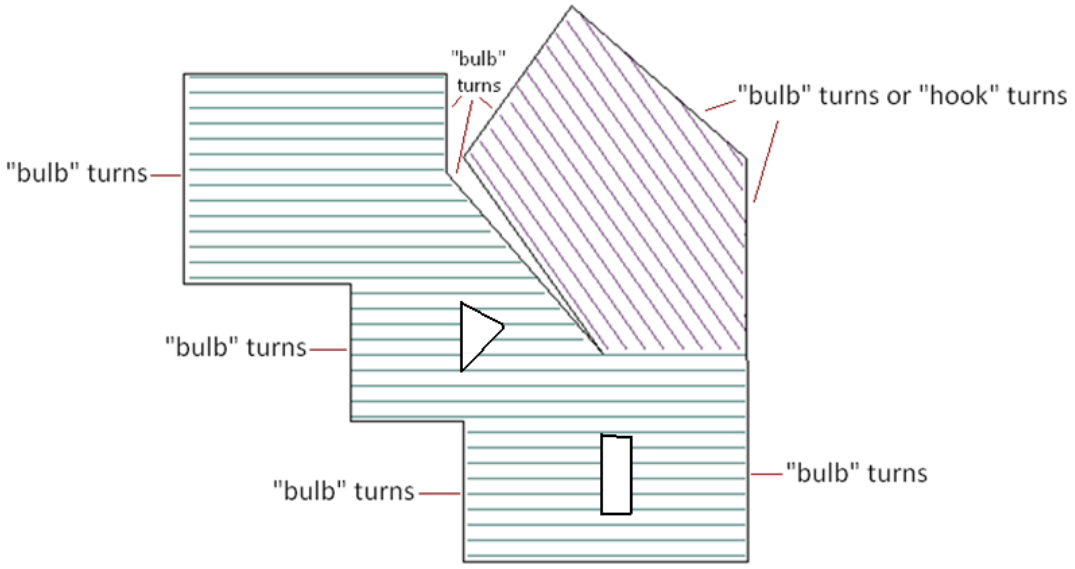

(a)

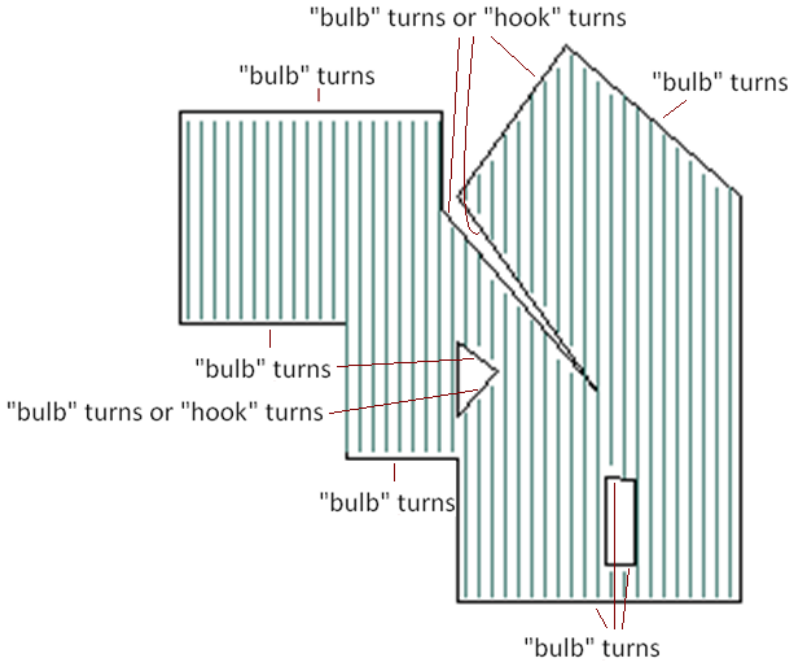

(b)

Figure 2.28. Adding two obstacles to the example field of Fabret et al.: (a) unchanged approach of fig. 2.27(c); (b) new OPP output.

An example of a complex field is shown in fig. 2.29. The three dividing lines were, separately, a diagonal, the extension of one edge (at the same time a diagonal too) and a line segment ending at one vertex and parallel to another edge.

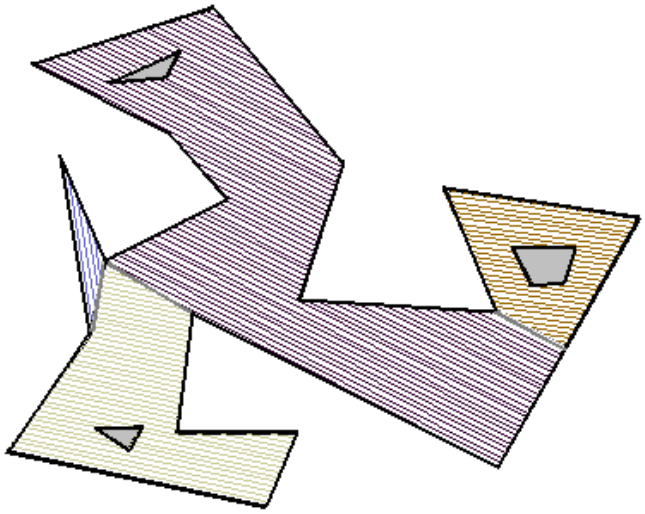

Figure 2.29. Field decomposition and path planning for a complex field.

The algorithm for transition between neighboring sub-regions has been implemented and incorporated into the whole 2D planning algorithm. Fig. 2.30 is one example field test result, in which concentric curves were adopted for the transition between the paired paths. The new solution's cost at the dividing boundary calculated by (2.25) was 44% lower than the turning cost at the dividing boundary in the original solution (fig. 2.30a).

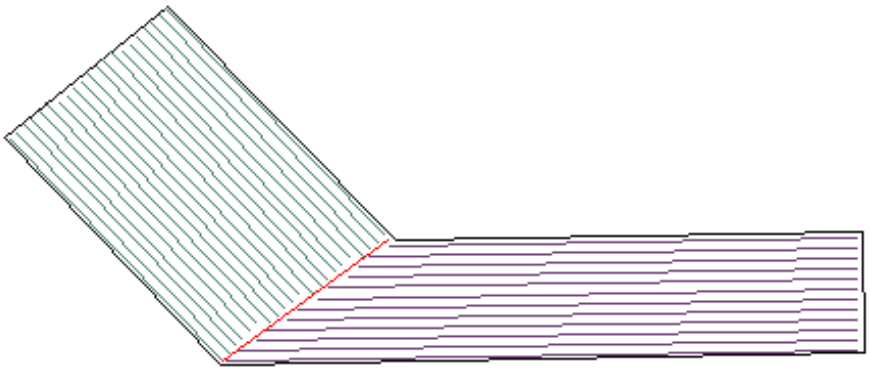

(a)

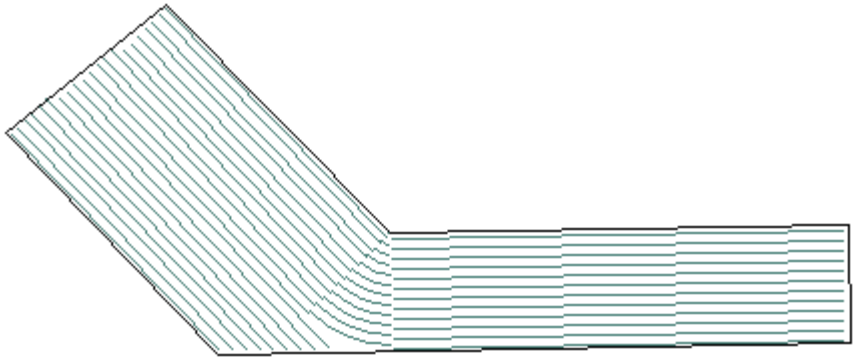

(b)

Figure 2.30. Transitions between neighboring sub-regions: (a) original OPP result without regional transition. The red line is the dividing boundary; (b) new OPP result with regional transition.

Figure 2.31 shows an example in which OPP gave the same output as the farmer's choice. The paths were not along the longest edge. Instead, the direction of another shorter edge was adopted to reduce angled turn costs.

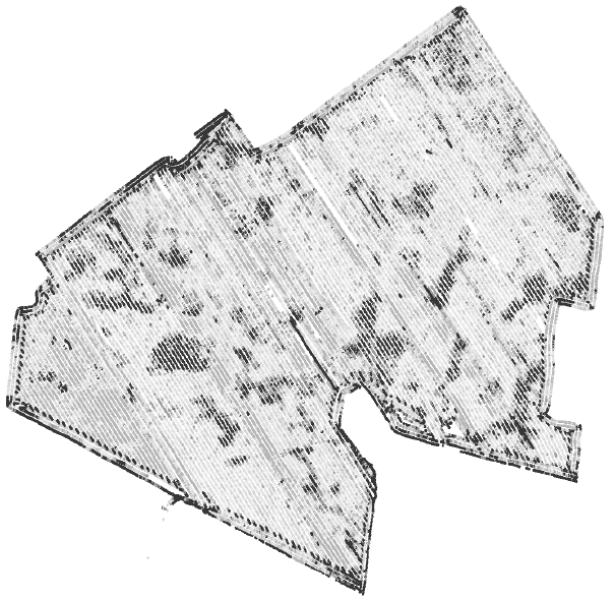

(a)

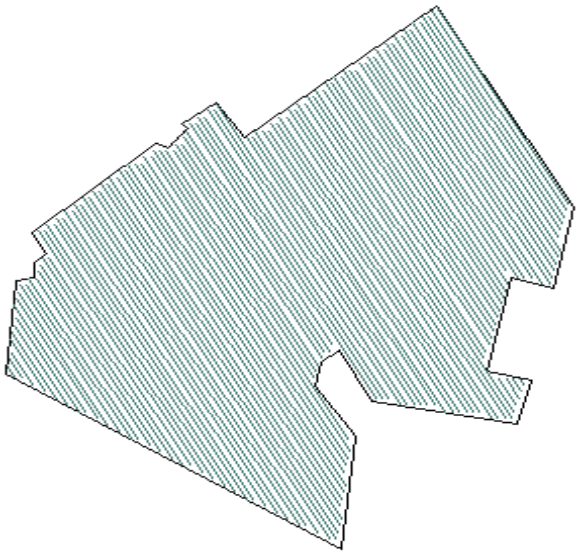

(b)

Figure 2.31. Comparison of OPP with farmer's approach: (a) Harvesting operation trajectory on the yield map of a farm field 1 in Ohio; (b) OPP output.

Figure 2.32 shows an example in which OPP gave a different solution from the farmer's. Compared with the farmer's actual driving pattern, OPP's solution had less number of turns but more angled turns. According to the cost function, overall the saving from OPP on the number of turns was 9% and the saving from OPP on the turning cost on the edges was 4%.

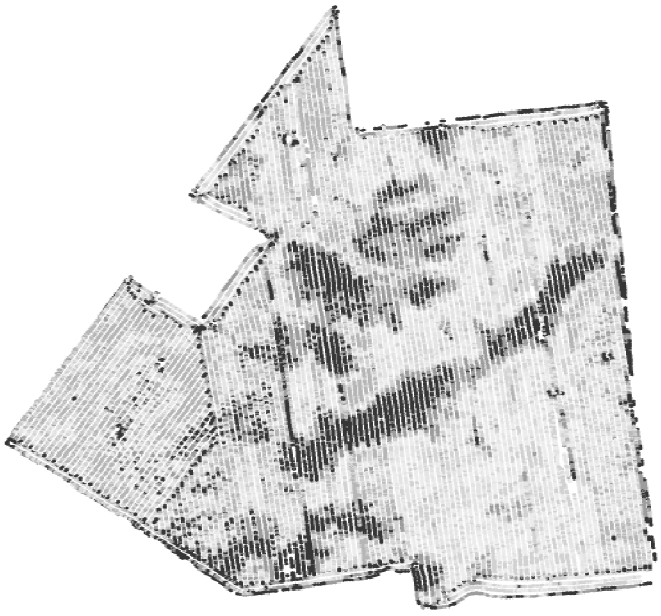

(a)

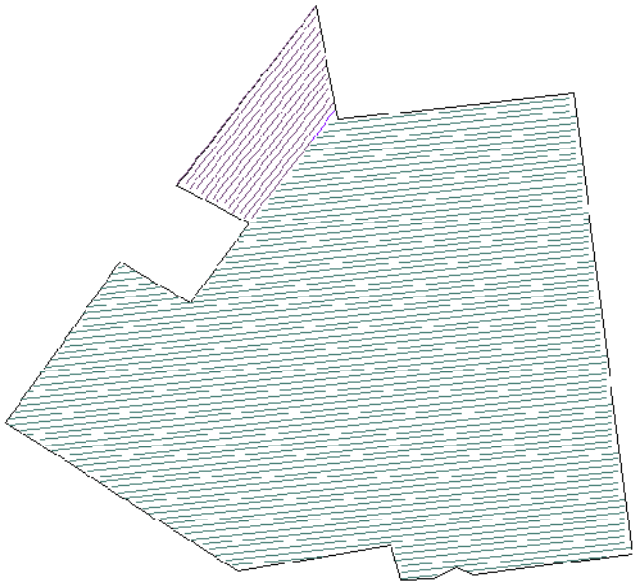

(b)

Figure 2.32. Comparison of OPP with farmer's approach: (a) Harvesting operation trajectory on the yield map of farm field 2 in Ohio; (b) OPP output.

Fig. 2.33 shows another practical example in which OPP gave the same output as the farmer's. The field was divided into two sub-regions in both solutions.

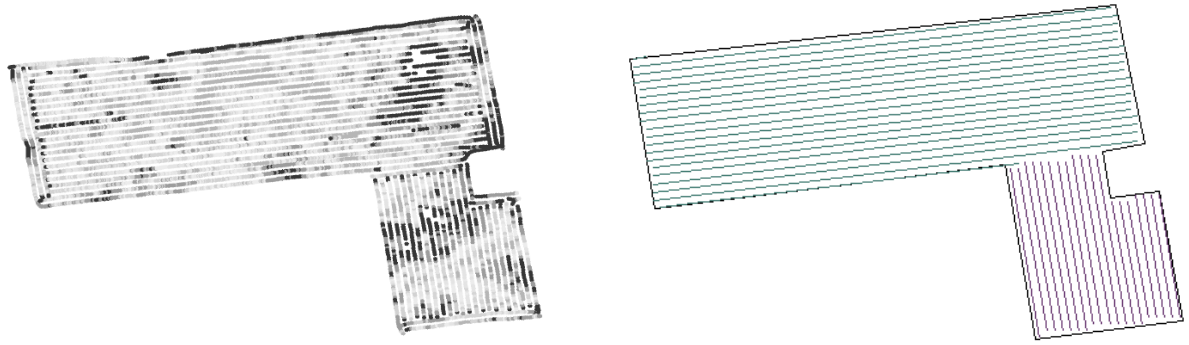

(a) (b)

Figure 2.33. Comparison of OPP with farmer's approach: (a) Harvesting operation trajectory on the yield map of farm field 3 in Ohio; (b) OPP output.

Fig. 2.34 shows a complicated practical example in which the outside boundary was composed of curves and there were multiple obstacles within the field. In the farmer's actual driving pattern, parallel curved paths along curved boundary sections were adopted. OPP found a direction for straight parallel paths for most of the field area, except for the left corner. The cost function could not be used here to compare the two solutions, since curved paths were involved in the farmer's driving pattern. However, OPP's solution generated more turns in this case, but the curved paths in the farmer's solution were with higher costs due to the higher operational control requirements (the cost from curved paths is discussed in more details in Chapter 3). Incorporating curve paths into the 2D path planning algorithm will be investigated as future work.

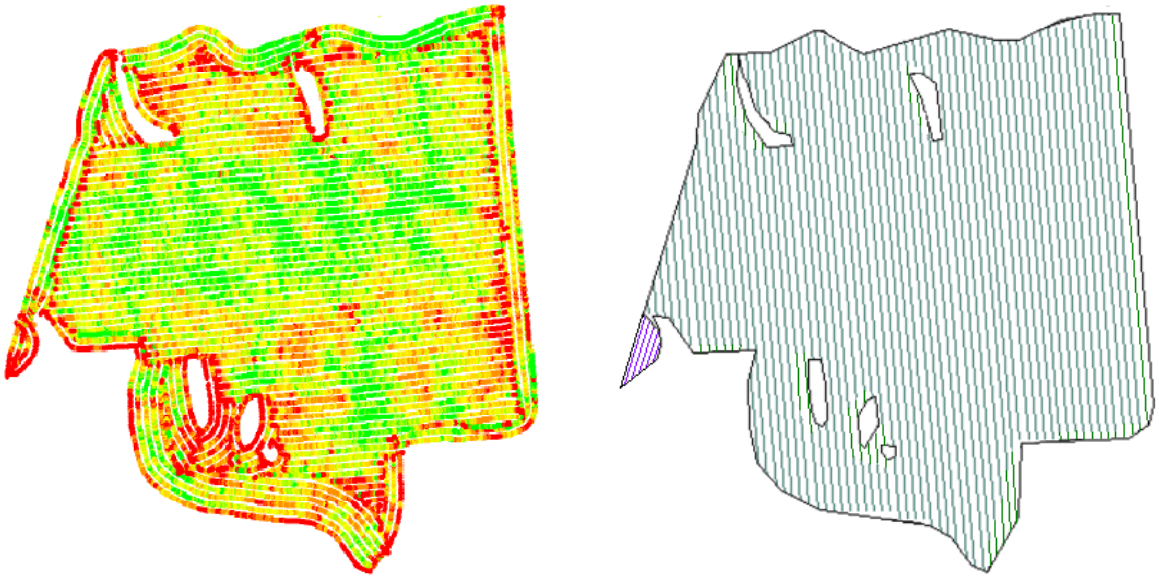

(a) (b)

Figure 2.34. Comparison of OPP with farmer's approach: (a) Harvesting operation trajectory on the yield map of farm field 4 in Ohio; (b) OPP output.

The comparison between OPP's results and other solutions in the examples above is summarized in table 2.1.

Table 2.1. Comparison between OPP's results and other solutions.

Field Name	OPP's Save on Number of Turns	OPP's Save on Headland Turning Cost
Designed Field (fig.2.25)	5%	6%
Oksanen's Field (fig. 2.26)	-4%	15%
Fabret's Field 1 with Default Assumption(fig. 2.27)	16%	12%
Fabret's Field 1 with Adjusted Assumption(fig. 2.27)	9%	14%
Fabret's Field 2 (fig. 2.28)	4%	4%
Ohio Field 1 (fig. 2.31)	0%	0%
Ohio Field 2 (fig. 2.32)	9%	4%
Ohio Field 3 (fig. 2.33)	0%	0%

2.5 Conclusions

The field boundary simplification algorithm has been developed. The reduction of boundary segments will substantially decrease the computational time for the optimal 2D field coverage path planning. As demonstrated in the results, the newly developed boundary simplification algorithm showed superior performance in delineating the original field boundaries when compared with other popular simplification algorithms such as Douglas Peucker. In particular, the new simplification algorithm could accurately locate the turning corners on the boundary. Besides, the new algorithm's result had not only lower distance error, but also lower direction error than former algorithm's result. This is important for optimal coverage path planning, since the cost function can be greatly influenced by the direction of the boundaries. The OPP algorithm was developed to find the optimal solution for decomposing the field into sub-regions and determining the coverage direction within each sub-region. The search mechanism of the algorithm was guided by a customized cost function that was concerned with the cost of different types of angled turns in the headland. The complexity of the algorithm was $O(n^3 \log(n))$ for a field with n edges in total. Methods for reducing the computational time have been investigated. Field examples with complexity

ranging from a simple convex shape to an irregular polygonal shape that has multiple obstacles within its interior were tested with the OPP algorithm. For all tested fields with no more than 20 vertices and 5 interior obstacles, the program found optimal coverage solutions within 60 seconds on a computer with a 3.20GHz Pentium(R) 4 CPU and 1.50 GB of RAM. The OPP's results were compared with the results of former researchers or farmers' actual driving patterns. The results have depicted that in the most extreme cases, OPP saved up to 16% in number of turns and 15% in headland turning cost. There were no cases where OPP outputted worse solutions than farmers' solutions in terms of headland turning cost. These results indicated that the OPP algorithm was effective in improving the field equipment efficiency on planar fields by producing optimal field decomposition and coverage path direction in each sub-region.

There are multiple ways the OPP algorithm can be further improved. In the current solutions of the OPP algorithm the paths are all in the form of straight lines. For some fields with curved boundaries, adopting curved paths may further improve the operation efficiency. In the United States, a great proportion of farms are with rolling terrains, and path planning on 3D terrains has a great potential to further optimize field operations. For 3D path planning, besides the headland turning cost, costs like soil erosion, speed control on slopes, topography impacts on the paths and so on need to be carefully analyzed. The 3D terrain optimal coverage path planning is discussed in Chapter 3. There can be various other problems, such as how to incorporate the loading and unloading locations into the algorithm and how to coordinate between the vehicles when there are multiple vehicles in the field. Solving these problems remains as the future work.

2.6 References

Berg, M. D., Kreveld, V. M., Overmars, M. and Schwarzkopf, O., 2000. Computational Geometry. 2nd ed. Springer.

Choset, H. and Pignon, P., 1997. Coverage Path Planning: The Boustrophedon Cellular Decomposition. Proceedings of International Conference on Field and Service Robotics, Canberra, Australia.

Douglas, D. and Peucker, T., 1973. Algorithms for the Reduction of the Number of Points Required to Represent a Digitized Line or Its Caricature. The Canadian Cartographer 10(2), 112-122.

Fabret, S., Soueres, P., Taix, M. and Cordessed, L., 2001. Farmwork Path Planning for Field Coverage with Minimum Overlapping. Proceedings of 2001 8th IEEE International Conference.

Harris, C. and Stephens, M., 1988. A Combined Corner and Edge Detector. Proceedings of the 4th Alvey Vision Conference. pp. 147--151.

Hunt, D., 2001. Farm Power and Machinery Management. Ames, IA. Iowa State Press.

Irving C., 1969. Introduction to Logic. 3rd ed. Macmillan Company, New York.

Jenks, G.F., 1989. Geographic Logic in Line Generalization. Cartographica, Vol. 26, No. 1, pp. 27-42.

Kise, M., Noguchi, N., Ishii, K. and Terao, H., 2002. Enhancement of Turning Accuracy by Path Planning for Robot Tractor. Proceedings of the 2002 Automation Technology for Off-Road Equipment Conference (Chicago, Illinois, USA). pp. 398-404.

Liu, C. H. and Srinath, D. M., 1990. Corner Detection from Chain-Code. Pattern Recognition, 23:51-68.

Muller, D. E. and Preparata, P. F., 1978. Finding the Intersection of Two Convex Polyhedral. Theoretical Computer Science. 7: 217-236.

Oksanen, T. and Visala, A., 2004. Optimal Control of Tractor-Trailer System in Headlands. ASAE International Conference on Automation Technology for Off-road Equipment, Kyoto. Japan: 255-263.

Oksanen, T. and Visala, A., 2007. Path Planning Algorithms for Agricultural Machines. Agricultural Engineering International: the CIGR Ejournal. 4: Manuscript ATOE 07 009.

Oksanen, T. and Visala, A., 2009. Coverage Path planning Algorithms for Agricultural Field Machines. Journal of Field Robotics, Vol. 26(8): 651-668.

Ryerson A. E. F. and Zhang, Q., 2007. Vehicle Path Planning for Complete Field Coverage Using Genetic Algorithms. Agricultural Engineering International: the CIGR Ejournal. 4: Manuscript ATOE 07 014.

USDA, 2007. Structure and Finances of U.S. Farms: Family Farm Report, Economic Research Service, 2007 Edition / EIB-24.

Yang, S. X. and Luo, C., 2004. A Neural Network Approach to Complete Coverage Path Planning. IEEE Transactions on Systems, Man, and Cybernetics—Part B: Cybernetics. 34(1): 718-725.

CHAPTER 3. OPTIMAL 3D TERRAIN FIELD COVERAGE PATH PLANNING

3.1 Abstract

Automated path planning is important for the optimization of field operations. Field operations should be done in a manner that minimizes time, travels over the field surface and are coordinated with specific field operations and topographic land features. Intelligent algorithms are desired for both 2D and 3D terrain field coverage path planning.

The full coverage pattern for a given 2D planar field by using boustrophedon paths has been investigated before. The 2D algorithm was developed to find the optimal solution for decomposing the field into sub-regions and determining the coverage direction within each sub-region. However, in real world, a great proportion of farms have rolling terrains, which have a considerable influence to the design of coverage paths. Coverage path planning in 3D space has a great potential to further optimize field operations. The following five research tasks are among those which are critical to accomplish the goal: terrain modeling and representation, topography impacts analysis, terrain decomposition and classification, coverage cost analysis and the development of optimal path searching algorithm. Each of the topics has been investigated in this work. The developed algorithms and methods have been successfully implemented in software and tested with practical 3D terrain farm fields with various topography features. Each field was decomposed into sub-regions based on terrain features. The optimal “seed curve” was found for each sub-region and the parallel coverage paths were generated by offsetting the “seed curve” sideways until the whole region was completely covered. Compared with the 2D planning results, the experimental results of 3D coverage path planning showed its superiority in reducing both headland turning cost and soil erosion cost.

3.2 Introduction

Automated path planning is important for the optimization of field operations. Currently, most coverage path planning algorithms are only capable of dealing with 2D planar fields. In chapter 2, a core optimization algorithm was developed that optimally decomposed a given planar field and planned an optimized operational pattern with

boustrophedon pathways for each sub-region. Based on the test results, the algorithm demonstrated a promising capability of finding a globally optimal field decomposition and coverage travel direction.

However, a great proportion of farms have rolling terrains, which have considerable influences on the design of coverage paths: Only 47% of cropland in the United States is on less than 2% slopes; 48% of the cropland is on slopes between 2% and 10%. In Iowa, 9.5% of cropland has slopes in the 10-15% range (National Resources Inventory, USDA, 1992). Therefore, coverage path planning for 3D terrain fields has a great potential to further optimize field operations.

For some of the 3D terrain surfaces, there could be problems to apply 2D coverage path planning algorithms, which assume that the fields are flat and ignore elevation changes. First, it may cause skips and overlaps between furrows, which in turn would have economic impacts. Stombaugh et al. (2009) pointed out that most GPS-based devices determine locations using only horizontal GPS coordinates (latitude and longitude). But on higher slopes, the surface area difference between planimetric and topographic models becomes significant, causing skips and overlaps between furrows. Koostra et al. (2006) showed that the error between planimetric and topographic surface areas could be as much as 5% in some typical farm fields. Dillon et al. (2006) demonstrated the economic impact of the area discrepancies between planimetric and topographic models. In Dillon's work, the differences of the two models were compared for thirteen agricultural fields in Kentucky with varying size and terrain. A production function of crop yield response to nutrient application served as a comparative focus. This allowed assessment of the magnitude of net returns differences in economically optimal nutrient application rates versus the less accurate but actually used planimetric technique. This study resulted in a mean loss of $0.24/ha ($0.10 per acre) among the thirteen fields, ranging from $0.01/ha (less than $0.01/ac) to $1.79/ha ($0.73/ac).

Another major problem of applying 2D path planning algorithm on 3D terrain is soil erosion. Van Doren (1950) indicated that soil runoff from contoured fields is often less than that from fields tilled up-and-down the slope. Ignoring the slopes on the terrain and executing projected straight parallel paths on terrain fields would cause severe soil erosion problems.

Wendt (1997) reported that tillage and planting operations performed on the contour are very effective in reducing erosion from storms of low to moderate intensity that are common in many areas of the United States. When tillage is oriented along the contour, the ridges or oriented roughness will partially or completely redirect the runoff, thereby modifying the flow pattern. When tillage leaves high ridges, runoff stays within the furrows between the ridges, and the flow direction is controlled by the tillage pattern. High ridges from tillage on the contour cause runoff to flow around the hillslope rather than directly downslope, significantly reducing the grade along the flow path and reducing the flow's detachment and transport capacity. As a result, developing an algorithm which plans the paths to be along the contour directions on the slope to the best extent would be effective in reducing soil erosion cost.

No former research on 3D terrain field coverage path planning was reported. However, research on 3D surface coverage path planning has been reported for other applications. Kim and Sarma (2003) used vector fields to generate coverage trajectories on a class of simple surfaces and discussed a possible formulation of surface segmentation based on a principle that minimized cycle time. However, they did not pursue the details of surface segmentation techniques. Sheng et al. (2003) developed procedures that segmented the projection of a 3D surface on planar surface to optimize the process cycle time. However, each segmented patch was stilled treated as 2D, and the costs were only roughly measured. For instance, the minimum altitude of a sub-polygon was simply used for the estimation of the number of turnings a tool had to make. Such rough measurements made it difficult for the method to achieve globally optimal coverage solutions. Vincze et al. (2003) presented an approach to generate trajectories for automated spray painting. Cavities (regions with negative curvature), ribs (parallel narrow regions with high curvature), and elementary surface geometries such as planes or cylinders were extracted from the surface. Each region was then painted with generated trajectories using pre-defined strategies. Their procedure was limited to surfaces that could be segmented into pre-defined parts. Besides, the lowest painting cost could not be guaranteed by using only pre-defined trajectory patterns. Atkar et al. (2005) adopted a hierarchical procedure to segment a complex automotive surface into geometrically as well as topologically simple components. The purpose of this segmentation

was to automate trajectory planning for spray-painting in automotive industry. After the surface decomposition, Atkar generated trajectories by selecting a seed curve, determining a speed profile along each pass, and selecting the optimal spacing between successive passes. However, the main objective of this application was to insure uniform paint deposition on the surface, which was not a concern in farm field coverage. Besides, segmenting the surface into geometrically and topologically simple patches was not necessarily helpful for farm field coverage, which might cause over-dividing of the field and thus increase the headland turning cost.

To accomplish the goal of optimal 3D terrain field coverage planning, multiple steps of different tasks were needed. Terrain modeling was the first step toward 3D path planning. Elevations of discrete points are used to represent the surfaces, namely the Digital Elevation Models (DEMs). Interpolating methods such as Kriging have been applied to estimate the elevation of any point based on the data points in DEMs (Aziz et al., 2006). However, interpolation could only provide elevation information at specified points. Instead, analytical models were derived from DEM to better describe the topographic surfaces in 3D space. This facilitated the task of terrain characterization as well as slope and curvature calculation, which would be essential in the cost calculation for different 3D surface coverage patterns. For the second step, quantitative analysis comparing between planimetric and topographic surface models was investigated too. The topography impacts to projected 2D planning on 3D terrain must be quantified in order to decide whether 3D coverage path planning algorithm was needed instead of the 2D planning algorithm. Third, terrain classification was another important step before the coverage paths could be designed on the terrain. Since the topography of a terrain field might have high variance from an area to another, it's often difficult to find one single coverage pattern for the whole field, and the divide-and-conquer strategy was needed. The terrain field could be classified and decomposed into sub-regions. By applying different coverage planning patterns to the sub-regions, the coverage cost could be further reduced. The fourth step was cost analysis for the coverage of 3D terrain surfaces. As in 2D coverage path planning, headland turning cost was still one of the major costs. However, there were some new costs for 3D coverage planning, such as the soil erosion cost and cost from the curvature of the curved path. Each category of cost was carefully analyzed

and calculated, and the goal of 3D coverage path planning was to find the optimal path in order to minimize these costs. Finally, the searching algorithm for the optimal path was developed. Since curved paths might be involved in 3D coverage path planning, the searching space of the optimal path could be much larger than in the 2D planning cases. Therefore the searching algorithm must be able to find out the optimal coverage solution, while keeping the computational complexity acceptable to modern computers.

The next part of this chapter addresses each of the five main steps above. In 3.3.1, the B-Splines 3D terrain modeling with discrete elevation points is introduced. In 3.3.2, the topography impacts to the coverage of 3D terrain field are analyzed. In 3.3.3, the method for terrain decomposition and classification is introduced. In 3.3.4, quantitative analysis of different coverage costs on 3D terrain surfaces is provided. In 3.3.5, the "Seed Curve" searching algorithm for optimal 3D coverage solution is provided. The results of the studies are provided in 3.4.

3.3 Methods

3.3.1 3D Terrain Modeling with Discrete Elevation Points

Terrain modeling was the first step toward 3D coverage path planning. Elevation of discrete points was measured to represent the surface, namely the Digital Elevation Models (DEMs). Interpolating methods such as Kriging were applied to estimate the elevation of any point based on the data points in DEMs (Aziz et al., 2006). However, interpolation can only provide elevation information at specified points. Instead, analytical models can be derived from discrete elevation model (DEM) to better describe the topographic surfaces in 3D space. This facilitates the task of terrain characterization as well as slope and curvature calculation, which are essential in the cost calculation for different decomposition and coverage patterns. There are some other advantages of analytical representation of the terrain surface: 1) The field terrain surface can be described with a smaller number of coefficients, compared with an m-by-n grid representation; 2) Some noisy data in the DEM model can be neglected by the analytical model and the analytical model always tend to provide a smooth description of the surface; 3) It is easier to calculate the relative position of any point to the described surface; 4) It is faster to calculate the distance from this point to the surface to check if the data set in

DEM is well fit by the analytical model. Substantial amount of former research work can be found in 3D surface modeling. Keren et al. (1994) stated that the advantages of using implicit polynomial for fitting curves and surfaces were its simplicity, the possibility to compute algebraic invariants, and the ease of containment computations. Jia et al. (2006) introduced a polynomial fitting method that constructs a surface patch by sampling along three concurrent curves on the surface. Besides using polynomials, Forsey et al. (1995) considered the fitting of tensor-product parametric spline surfaces to gridded data. However, all the former research was in other application fields such as pattern analysis or computer graphics. None of them was designated for farm field terrain modeling. Research particularly targeted at the farm field terrain modeling for coverage path planning purpose is still needed.

To have a good representing model of the terrain field, selection of the model is the key. Polynomials are the approximating functions of choice when a smooth function is to be approximated locally. Polynomials have been recommended for curve or surface fitting for several reasons. First, they are simple and do not require an excessive number of coefficients to describe. Second, they are mathematically easier to manipulate than other models. Third, the algorithm used for polynomial fitting is very robust to noise. Fourth, polynomials can fill in missing data easily. However, if a function is to be approximated on a larger interval, the degree of the approximating polynomial may have to be unacceptably large. Bezout's theorem (Fulton, 1974) can help to decide whether an Nth-degree polynomial can describe a given curve in 2D: “If Cm and Cn are zero sets of polynomials of degree m and n which do not share a common component, they can intersect at most m*n points.” Suppose there is a curve F, and observe that a line intersects F at five points. Because a line can be described by a polynomial of degree one, the theorem implies that F can be described by a polynomial of at least degree five. For a wave-like curve, it can intersect with a line at many points. High degree polynomials are needed to fit such curves. Therefore for 3D terrain, a field with many ridges and valleys requires higher degree polynomial models. On the other hand, low degree polynomials are needed to avoid over-fitting. Runge’s phenomenon (Berrut et al., 2004) states that between the interpolated points, the error between the real function and the interpolating polynomial gets worse for higher order polynomials. Runge’s phenomenon also

states that high-degree polynomial interpolation at equidistant points can be very dangerous. Unfortunately, the DEM data sets are often equidistant points.

To avoid these problems of polynomial models, spline models can be used, which are special functions defined piecewise by polynomials. Spline interpolation is often preferred to polynomial interpolation because it yields similar results, even when using lower degrees, while avoiding Runge's phenomenon for higher degrees. The pp-form and the B-form are two commonly used ways to represent a spline. The B-form has become the standard way to represent a spline, since the B-form makes it easy to build in smoothness requirements across breaks. The smoothness of a B-form spline is controllable based on the rule "knot multiplicity + condition multiplicity = order". Therefore, by adjusting the knot sequence and spline order, not only the precision of fitting, but also the smoothness can be easily controlled for the B-form spline. More details of the B-Splines fitting method can be found in the work of Cheng et al. (1989) and Forsey et al. (1995).

For the fitting of DEM data with B-form splines, the interpolation to gridded DEM data was implemented by tensor product splines:

$$f(x,y) = \sum_{i=1}^{m}\sum_{j=1}^{n} B(x|s_i,\dots,s_{i+h})B(y|t_j,\dots,t_{j+k})\,a_{ij} \quad (3.1)$$

where s and t were the knot sequences and a_{ij} was the corresponding coefficient array.

The gridded data (bivariate) were fitted with one variable at a time, taking advantage of the fact that a univariate least-squares fit depended linearly on the values being fitted.

3.3.2 Topography Impacts to Projected 2D Planning on 3D Terrain

Some new problems came up with 3D terrain coverage path planning, which didn't exist in 2D planning. Quantitative analysis comparing between planimetric and topographic surface models was needed. The topography impacts to projected 2D planning results on 3D terrain surfaces must be quantified in order to decide whether 3D coverage path planning algorithm was needed instead of the 2D planning algorithm. Following is the discussion of two such impacts: the soil erosion impact and the skips between projected 2D planning results on 3D terrain.

3.3.2.1 Soil Erosion Impact

Soil erosion is one of the mostly concerned problems in 3D terrain field coverage. Ignoring the slopes on the terrain and projecting straight parallel paths on terrain fields would cause severe soil erosion problem. Tillage and planting operations performed on the contour are very effective in reducing erosion. As a result, in order to reduce soil erosion cost, the paths need to be along or nearly along the contour directions on the slopes. The details of the method for quantifying the effect of a particular coverage path pattern on soil erosion are described in 3.3.4.1.

3.3.2.2 Skips between Paths when Projecting 2D Planning Results on 3D Terrain

2D coverage planning assumes that the field is flat and ignores elevation changes. While this assumption is valid in many flat agricultural fields, there is a significant portion of agricultural production areas where topography has impacts on operational patterns. When projecting 2D planning result to 3D terrain, the actual distance between paths on the topographic surface increases, and there will be skips between adjacent paths on the slopes (fig. 3.1). Former researchers figured out that this area discrepancy between planimetric and topographic models might result in economic impacts.

Stombaugh et al. (2009) calculated the width of the skip (or overlap) area between two adjacent paths by:

$$E = w - \frac{W_{e_1} + W_{e_2}}{2} + T_2 - T_1 \quad (3.2)$$

where E was the width of the skipped area; w was the machine width; W_{e_1} and W_{e_2} were the effective implement widths; T_1 and T_2 were the lateral translations of implement.

In (3.2), the lateral translation of implements T_1 and T_2 were another effect of machine roll on the slope. As the machine rolls, if there was no measurement and compensation of roll in the GPS position, the guidance system would attempt to keep the antenna on the desired path instead of the centerline of the machine. This would cause the machine implement to actually be translated to the side of the desired path. In this application, the skipped area caused by this lateral translation was neglected, since this translation can now be compensated for by current GPS guidance systems.

As a result, (3.2) was be simplified as

$$E = w - \frac{w_{e_1} + w_{e_2}}{2} \qquad (3.3)$$

The effective implement width was actually the implement width projected on the horizontal plane (fig. 3.1):

$$w_e = w \cdot \cos(r) \quad (3.4)$$

where r was the roll angel of the vehicle, which could be calculated as:

$$r = s \cdot \sin(\emptyset - \theta) \quad (3.5)$$

where s was the vehicle slope (same as the terrain slope) defined as the sin of the slope angle; $\emptyset$ was the vehicle heading; θ was the slope aspect. For both $\emptyset$ and θ, the reference direction was north.

From (3.3), (3.4) and (3.5), the width of skipped area could be calculated as:

$$E = w - \frac{w\cos(s_1\sin(\emptyset_1 - \theta_1)) + w\cos(s_2\sin(\emptyset_2 - \theta_2))}{2} \qquad (3.6)$$

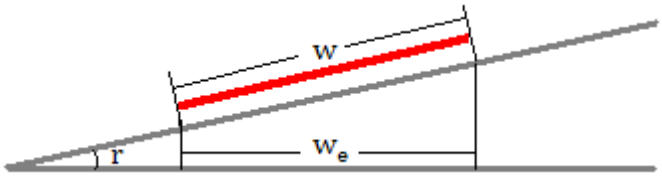

Figure 3.1. The actual distance between paths on the topographic surface increases when projecting 2D planning result to 3D terrain.

For one 3D terrain field covered with N straight parallel paths, the total skipped area could be integrated as:

$$\text{skipped area} = \sum_{i=1}^{N-1} \int_0^{L_i} E(x)dx \qquad (3.7)$$

where L_i was the length of the ith path; E(x) was the skip width at position x of path i, which could be calculated by (3.6).

3.3.3 Terrain Decomposition

The elevation data of a terrain field may have high variance from area to area. It's often difficult to find a single optimized coverage pattern for the whole field. As in the 2D coverage path planning, the divide-and-conquer strategy should be applied for 3D terrain fields.

Before the coverage paths can be designed, terrain decomposition and classification are needed (fig. 3.2). A field should be decomposed into sub-regions based on field attributes such as terrain features (elevation variance, surface slope, etc.), ground roughness, soil conditions and so on. Besides consideration of the field attributes, in order to eliminate increased turning costs, the field should be subdivided into sub-regions with comparatively smooth boundaries. Sometimes, recombination of some adjacent sub-regions with complementary shapes is needed so that coverage cost can be further reduced. After the decomposition, the partitioned sub-regions are classified based on the terrain type, vehicle attributes, user's opinions and so on. The most appropriate path planning strategy (such as 2D planning or 3D planning algorithms) should be applied to each region so as to achieve the minimum coverage cost.

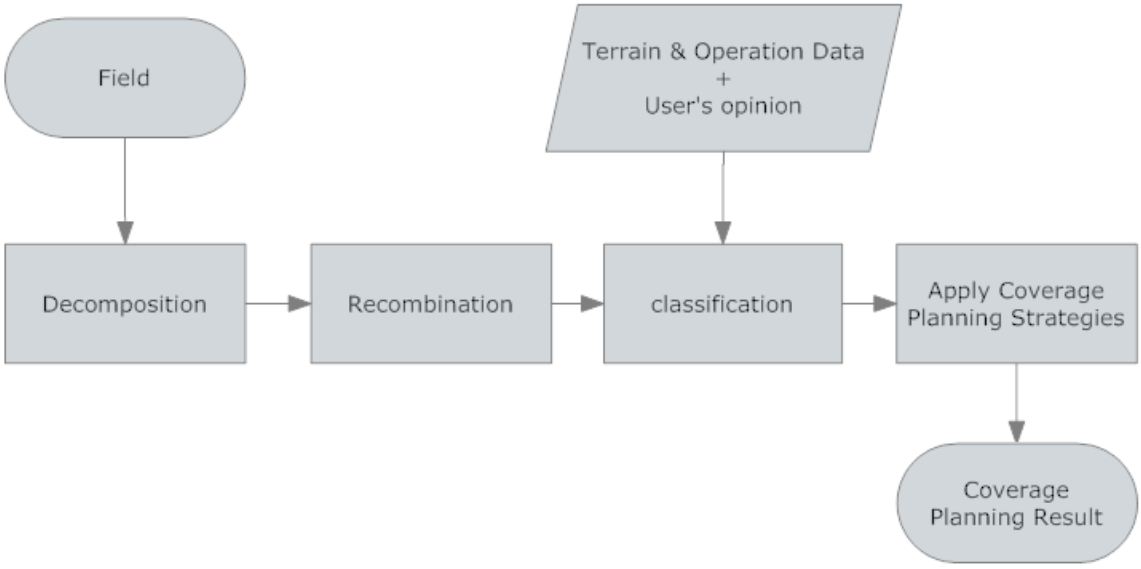

Figure 3.2. Process steps of terrain coverage planning.

As described above, the field decomposition should be based on multiple criteria. These criteria include (but not limited to): slope steepness (SS), local elevation variance

(EV), slope length (SL), curvature of terrain surface (K), ground roughness (GR), soil erodibility (SE) and so on. Among them, only the concerned criteria should be applied during decomposition. It is not desired that the field is decomposed into too many small cells because of any trivial terrain feature criterion, since over-subdivision will create new boundaries and thus increase the coverage cost. For instance, slope length, ground roughness and soil erodibility are all for the measurement of soil erosion. For those fields the owner does not have much concern about the impact of operation to soil erosion rate, it's not necessary to adopt these criteria in terrain decomposition. The selection of adopted criteria should be up to the operator.

The terrain decomposition should be made according to those adopted criteria with different weights. When there are more than one criteria adopted, they need to be checked one by one for the decomposition. During each round, thresholds are set up by the operator and each divided region of the field is further partitioned based on the current criterion. The weight of each criterion is reflected by how fine the thresholds are defined.

After decomposition, recombination of some adjacent sub-regions is needed. Since there is no control of area and shape of the sub-regions in the former decomposition step, recombination is a necessary step to eliminate over-subdivision. Combining sub-regions with small area with its adjacent regions can often reduce the complexity of coverage planning. Some regions should also be combined to eliminate isolated "holes" or "islands" in the region. For instance, those small hill top areas are always with low slopes and they should be combined with its surrounding high slope areas instead of being separated as a planar sub-region, unless the area is large or there are other special reasons. As a summary, there are two circumstances when recombination takes place: First, those regions with small areas should be combined with the neighboring regions. Second, holes and concave shapes should be eliminated, since dividing the field into geometrically simple and convex patches is helpful in reducing the coverage cost.

The general terrain decomposition algorithm is given bellow, assuming there are n ($n \geq 1$) field attributes adopted as decomposition criteria.

Algorithm TERRAINDECOMPOSITION (f)
Input: Planar subdivision f representing a field.

Output: A list of planar subdivisions, L, representing the sub-regions.
1. initialize L as containing f as the only item;
2. **for** i ← 1 to n
3. **for** each item R in L
4. **if** (R should be divided according to the ith criterion)
5. **then** remove R from L, and add the newly divided sub-regions into L;
6. **end if**
7. **end for**
8. **end for**
9. search for all pairs of adjacent sub-regions
10. **for** each pair of adjacent sub-regions, R1 and R2
11. **if** (combining the pair reduce the coverage cost)
12. **then** remove R1 and R2 from L, and add the newly combined sub-region into L;
13. **else** go to line 10 to start over again;
14. **end if**
15. **end for**
16. **return** L;

End of algorithm

After the decomposition and recombination, a coverage strategy needs to be selected for each sub-region. The sub-regions should be treated as either planar surface, for which 2D coverage planning algorithms is applied, or terrain surface, for which 3D coverage planning algorithms must be applied to eliminate coverage costs caused by the topography impacts. The decision on the adopted path planning strategy largely depends on the operator's concerns. For instance, for the same terrain field, different farmers may have different emphasis on operating efficiency or soil erosion prevention. However, by collecting field and related operation data, the operator should be able to get recommendations and suggestions for deciding on the best coverage strategy. The data may include: slope stiffness, curvature of terrain surface, operation type, crop type, slope length, vehicle width, height of vehicle's center of gravity, annual rain storm intensity, soil erodibility factor, ground roughness and so on. After processing the data, the computer could provide the operator with information such as the severity of soil erosion estimated by the RUSLE equation, different cost of headland turnings from different coverage strategies, and so on. These results would help the user to decide if the contours should be followed or not, and if 2D or 3D planning should be applied.

3.3.4 Coverage Cost Analysis

There are multiple categories of coverage costs in 3D terrain path planning. Among them, headland turning cost, soil erosion cost and cost from the curvature of the paths are three mostly concerned categories. The headland turning cost has been carefully analyzed in

2D coverage path planning (Chapter 2), which is still valid in 3D planning. The analysis of the erosion and curving costs is given in this part. The method for the integration of the different cost categories is also discussed.

3.3.4.1 Soil Erosion Cost

In consideration of soil and water conservation, contours should be followed on slope surfaces to eliminate soil erosion. The objective of the following discussion is to quantify the soil erosion from any practical tillage practice.

The Revised Universal Soil Loss Equation (RUSLE) is an erosion model designed to predict the longtime average annual soil loss carried by runoff from specific field slopes in specified cropping and management systems as well as from rangeland (Renard, 1997). RUSLE is in the form of:

$$A=R*K*L*S*C*P \quad (3.8)$$

where A is the estimated average soil loss in tons per acre per year, and R, K, L, S, C and P are the erosion factors: R is the rainfall-runoff erosivity factor; K is the soil erodibility factor; L is the slope length factor; S is the slope steepness factor; C is the cover-management factor; P is the support practice factor.

Among the six factors, the “support practice factor” P is the ratio of soil loss with contouring and/or strip-cropping to that with straight row farming up-and-down slope. This factor is of interest for coverage planning on 3D terrains, because it calculates the effect on soil erosion amount from the coverage path patterns. “The relative effectiveness of contouring for controlling erosion on various slopes is shown by the conservation practice factor P” (Schwab et al., 1993). Since the coverage path pattern doesn’t influence the other erosion factors in RUSLE except P, the P value can be used to indicate the soil erosion cost brought by a particular coverage pattern for a particular field.

Wendt (1998) provided that the P factor values for contour furrowing on a slope with a 10% gradient with high ridge heights can be as low as 0.35, which means the soil erosion of exact on-grade contouring farming is only 35% of that when straight furrows up and down the slope are adopted. However, in most of the field cases, the furrow direction is neither

exactly on-grade nor exactly following the slope, but with varying angles from the contour direction. This is the so called “off-grade contouring”. Following is the introduction of a method for calculating the P factor when a particular set of parallel paths (straight or curved) is adopted for the coverage of a terrain field so that off-grade contouring is formed on the slopes.

Experimental data showed that there was a rapid loss of effectiveness of contouring as grade along the furrows increased. Renard (1997) provided the following equation in USDA Agriculture Handbook to estimate P-factor values for off-grade contouring:

$$P_g = P_o + (1 - P_o)(\frac{S_f}{S_l})^{\frac{1}{2}} \qquad (3.9)$$

where P_g is the P factor for off-grade contouring; P_o is the P factor for on-grade contouring; S_f is the grade along the furrow (path) direction; S_l is the local steepness of the land.

If a set of parallel paths (either straight or curved) is applied to cover a terrain field, P_g would have different values when calculated at different locations, as P_o, S_f and S_l vary along the paths. In this project, the incurred soil erosion is estimated by averaging P_g throughout the whole terrain surface:

$$P_{off-grade} = \frac{\iint_D P_g \sqrt{1 + \left(\frac{dz}{dx}\right)^2 + \left(\frac{dz}{dy}\right)^2}\, dx\, dy}{\iint_D \sqrt{1 + \left(\frac{dz}{dx}\right)^2 + \left(\frac{dz}{dy}\right)^2}\, dx\, dy} \qquad (3.10)$$

where $P_{off-grade}$ is the estimated P factor of the particular off-grade contouring coverage pattern; D is the range of the field.

While the estimation of S_f and S_l in different locations is straight forward, the value of P_o depends on the terrain features such as slope steepness and so on. In this project, we adopted Renard (1997)’s equations for estimating the P_o value under base conditions (which only consider field topographic features and effect of ridge height):

$$P_b = a(S_m - S_c)^b + P_{mb} \quad S_c < S_m \qquad (3.11)$$

$$P_b = c(S_c - S_m)^d + P_{mb} \quad S_c \geq S_m \qquad (3.12)$$

$$P_b = 1 \qquad S_c \geq S_e \qquad (3.13)$$

where P_b is the P_o value under base conditions; S_c is the local slope steepness; S_m and S_e are dividing points on the slope axis; P_{mb} is the minimum P value.

The three equations above describe the different sections of a "U" shaped curve, which describes the changing P_o value with slope. The coefficients a, b, c, d and the values of S_m , S_e , and P_{mb} vary with ridge height. Renard (1997) provided suggested values for these coefficients for different ridge heights.

(3.9) and (3.10) can be combined as:

$$P_{off-grade} = \frac{\iint_D [P_o + (1 - P_o)\left(\frac{S_f}{S_l}\right)^{\frac{1}{2}}] \sqrt{1 + \left(\frac{dz}{dx}\right)^2 + \left(\frac{dz}{dy}\right)^2}\, dx\, dy}{\iint_D \sqrt{1 + \left(\frac{dz}{dx}\right)^2 + \left(\frac{dz}{dy}\right)^2}\, dx\, dy} \qquad (3.14)$$

In this application, (3.14) is adopted as the model for the effect of off-grade contouring parallel paths farming on soil erosion.

3.3.4.2 Curved Path Cost

Curved paths pose challenges to the operation of the vehicle. For 3D terrain coverage path planning, curved paths are often required so that the paths can be nearly along the direction of contour lines in order to reduce soil erosion. When curved paths are needed, the whole set of parallel paths can be determined by a "seed curve" (fig. 3.3). It is easier when the paths on the convex side of the "seed curve" are generated, since the curvature decreases along this direction. However, on the concave side of the "seed curve", each subsequent path suffers from a higher turning curvature. The curvature keeps increasing along the subsequent paths until the vehicle is unable to make the designed turn. Skip areas occur in this situation (fig. 3.4). The skipped area between paths A and B in fig. 3.4 can be minimized by adopting the vehicle's minimum turning radius for path B. However, this would generate another sharp turning for the next path, C, leaving a new skipped area between paths B and C.

Similarly, the skipped areas would be generated between each pair of the following subsequent paths until the boundary of the field is reached. If remaining uncovered, these skipped areas would be a waste of land. Switch-back turns are sometimes used to cover such skipped areas in the turning corner to reduce the waste. However, switch back turns have high cost in time and high operation requirement. In other cases, extra travels are made particularly for the coverage of the skipped areas, but this would also cause more cost in time as well as overlapped coverage. It remains as future work to find out the best way of dealing with these skipped areas. In this application, the sum of the skipped areas resulted from the paths' high curvatures was calculated and included into the coverage cost function.

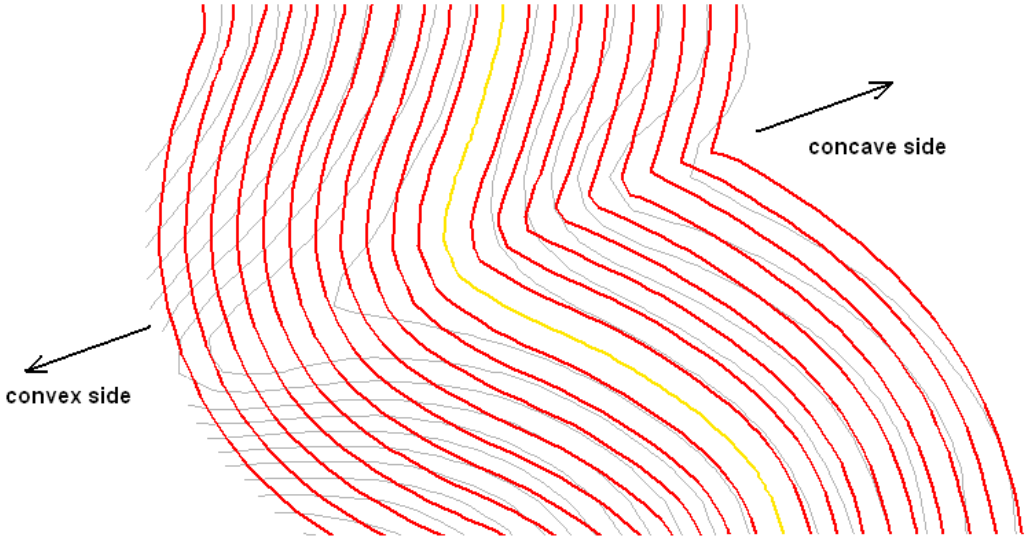

Figure 3.3. Parallel paths (red) can be determined by offsetting a "seed curve" (gold).

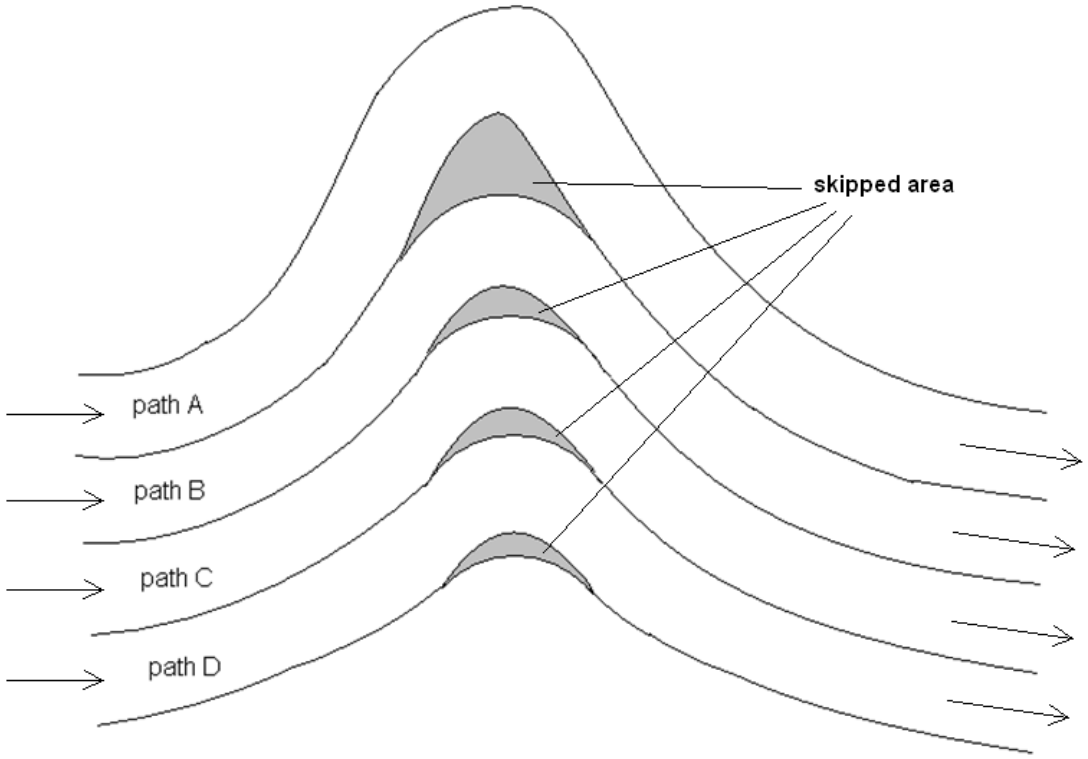

Figure 3.4. Skipped areas occur on the concave side of the “seed curve”.

The curvature of a curve is the rate of change of direction of the tangent line at one point with respect to the arc length (Rutter, 2000). In this project, the final output paths were in the form of polylines, and the curvature along the polyline is represented by the change of directions between each adjacent two edges with respect to the lengths of the edges (fig. 3.5). This curvature, or the change of direction, is limited by the minimum turning radius of the vehicle. The critical situation happens when the vehicle needs to turn with its minimum turning radius to drive through the three adjacent vertices along the polyline (section D-E-F in fig. 3.6). This maximum change of direction can be calculated as:

$$\Delta\theta_{max} = sin^{-1}\frac{d}{2r} \quad (3.15)$$

where d is the distance between the first and third vertices, and r is the vehicle’s minimum turning radius (15 feet was assumed in the tests). In this application, the path polylines keep high resolutions and d < 2r for all adjacent three vertices.

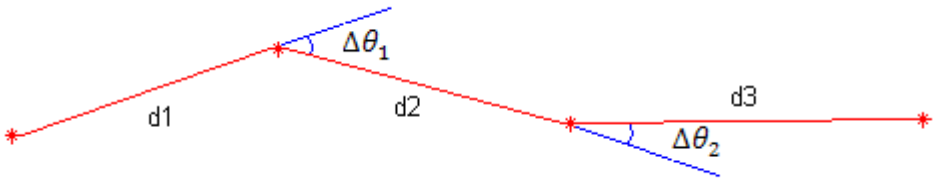

Figure 3.5. The curvature along the polyline is represented by the change of directions between each adjacent two edges with respect to the lengths of the edges.

For all the polyline paths in the result, the change of direction at each vertex along the polylines is subject to the limitation in (3.15). For any change of direction higher than the maximum value, the vertex at which the change happens needs to be adjusted. This adjustment may result in the situation in fig. 3.4 when skipped area happens between paths. Fig. 3.6 shows an example of a path polyline with high local curvature. It is assumed that in order to be exactly parallel from the last swath, the vehicle needs to travel along the route A-B-C-D-E-F-G-H-I. However, the arc D-E-F has a turning radius smaller than the vehicle's minimum turning radius. The best the vehicle can do is to keep turning with its minimum turning radius r along D-J-F. This adjustment (from E to J) results in a skipped area between D-E-F and D-J-F. When the polyline resolution is high (with low enough distances between neighboring vertices), the shaded area in fig. 3.6 can be calculated to approximate the skipped area from the adjustment. Curve fittings for the polyline vertices such as spline fittings are needed if the polyline resolution is low, so that the skipped area can be estimated more accurately. Assuming d, d1, d2 are the distances between DF, DE, EF, r is the vehicle's minimum turning radius, $\Delta\theta$ is the original change of direction at E, the skipped area can be calculated as:

$$\frac{d_1 d_2 \sin(\Delta\theta) - dr + d\left(r^2 - \frac{d^2}{4}\right)^{\frac{1}{2}}}{2} \quad (3.16)$$

In this application, all such skipped areas were summed together along all the generated paths for the approximation of the cost from the high curvatures of the paths.

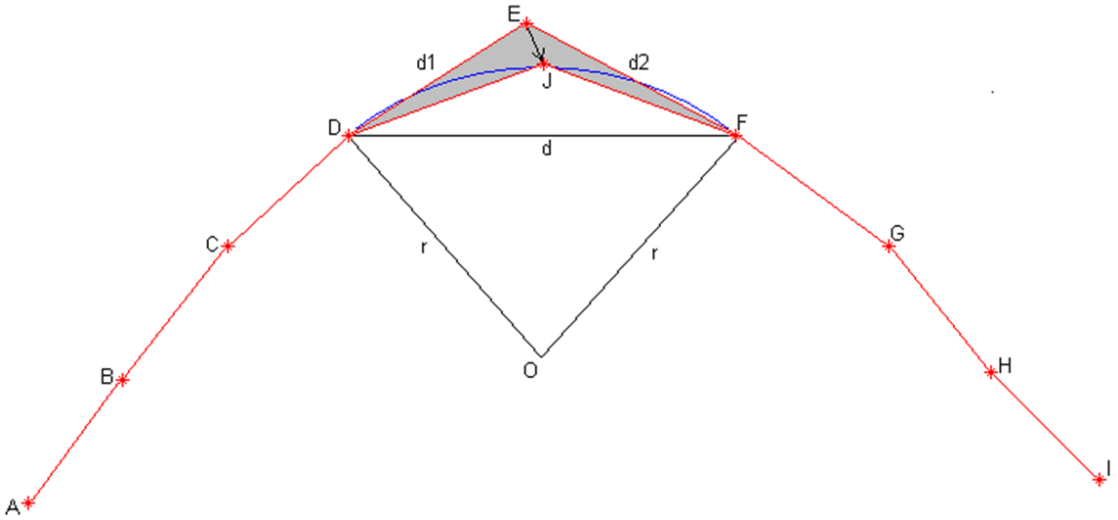

Figure 3.6. An example of a path polyline with high local curvature. The vehicle may not be able to make the sharp turning due to the restriction of its minimum turning radius, and skipped area (shaded) may be caused around the corner.

Other Types of Costs from the Curved Paths

There could be various other types of costs from the curved paths. Following is the discussion for some of them.

1) Operator Fatigue

When the vehicle is moving along a curve instead of a straight line, the operator has to pay close attention to always put the vehicle right on the designed path. Doing this for the coverage of thousands of acres could be a tiring task. Since the drawn implement turns a tighter corner than the tractor, the operator must "lead" on the turns to make the implement travel the correct path. “This is simply learned by experience, and it just doesn't ever seem to get easy”, said by an experienced farmer. Also, slopes cause a sideways drift down the hill. The side hill drift compounded with the different turning radius makes operation very difficult.

2) Uneven Rates

Most application machinery (planters, sprayers) determines the rate applied at one point on the tool bar and this rate is applied across the entire width of the implement (with GPS variable rate, this point is on top of the cab). However, the outer end of a fifty foot implement can be traveling much faster than the inside end on a tight curve. On sharp corners, the inside end will actually go backwards. The difference in application rates between the two ends may have negative effects on the yield. This cost from the over/under application should be included into the cost function too.

3) Inconsistent Row Spacing

It's more difficult to tow a planter on turns in terms of planting accuracy. This will lead to inconsistent row spacing or inefficient field coverage due to inaccurate planting path.

4) Lower Speed

Due to the increased difficulty of driving along a curved path, the operator often has to slow down, making the coverage task cost more time.

5) Influence to the GPS Auto-Guidance System

In terms of GPS Auto-Guidance System, when the receiver is on top of the cab on a corner, the drawn implement is not following the same path as the GPS on a curve. The implement position offset could be a severe problem in harvesting. Besides, this would contribute to the overlap and skipped areas between the adjacent swaths too.

6) Influence on the Implement

When an implement in contact with the soil travels along curved lines, there is a sideways drift. This drift is most noticeable on the inside half of the implement, especially on the very inside end. Nearly all implements are designed to travel in straight forward paths. They are less accurate (less efficient) in a skewed path. An obvious example would be a dual tool bar with opening coulters on the front bar and another tool on the back bar. When going along a curve, the front and back tools will not line up. An anhydrous bar working in damp conditions will encounter problems very quickly. The knife will plug because the residue is not cut in the middle of the path of the knife. Having to stop and unplug, or pull out of the field until it dries is very costly.

Each of the above costs varies with the type of operation, the field condition and the vehicle. Using Auto-Guidance equipped tractor can be helpful in reducing many of the costs. However, following curved paths is a more challenging task for current Auto-Guidance equipments too. Besides, different farmers may have different concerns about the curving path cost. For example, most farmers run combine at around 4 mph and they rarely slow down for curves. Some farmers may run combines at a higher speed up to 8 mph, and curves would slow these people down more dramatically. There is also a difference between gentle contour curves and sharp curves. The gentle curves would often pose no problems different than straight rows. As the curves tighten, the problems start and increase. However, it's difficult to provide a universal standard for the classification of gentle and sharp curves. Quantifying each of the costs above could be a new research topic and remains as future work.

3.3.4.3 Integration of Different Costs

As discussed above, headland turning cost, soil erosion cost and cost from the curvature of the paths are three mostly concerned cost categories. All the three costs were considered for the whole 3D planning cost function. The weighted average of these costs was adopted in this application. The weights should be determined by the operator according to his concern on the different categories of costs, or based on the economic impact of each cost category if there is a way to quantify each impact. These different categories of costs were measured in different ways and could not be simply added: the headland turning cost was in form of the time spent during the turnings, the support practice factor, P in the RUSLE equation, was used to indicate the soil erosion cost, and the summed skipped area from the sharp turnings was used to indicate the curving cost. The calculated cost values of each category were normalized before they were summed. As a summary, the final cost function of 3D planning was the weighted average of the normalized values of all the coverage cost categories.

3.3.5 "Seed Curve" Searching Algorithm

For each patch of terrain field, the final output of coverage path planning is a set of curved paths which are side by side to each other. The whole set of paths can be determined

by one “Seed Curve”: Once the “Seed Curve” is found, it can be offset sideways on the topographic surface for generating the subsequent paths, until the surface is covered completely. Therefore, the key for 3D terrain coverage path planning is to find the optimal “Seed Curve” which leads to the minimum coverage costs.

The searching space of any potential “Seed Curves” can be huge, making brutal search infeasible for the algorithm. For instance, if a curve is approximated with an 8-connected path in a gridded area, the computational complexity for the searching of a curve with length n will be $O(8^n)$. Therefore, heuristic methods are needed to reduce the searching space.

In practical farming, the field boundaries are most commonly used by farmers to guide the operation in order to eliminate number of headland turnings. Therefore, the field boundary edge segments are excellent candidates for seed curves. As discussed before, tillage and planting operations performed on the contour are very effective in reducing erosion. In order to reduce soil erosion cost, the paths need to be along or nearly along the contour directions on the slopes. As a result, the segments of contour lines within the field area are excellent candidates of seed curves too, since the sideways offsets of the contour line segments would most probably still be along the contour directions.

In this application, two categories of seed curve candidates were adopted for the search of the optimal “Seed Curve”: field edge segments and contour lines. The “seed curve” searching algorithm is illustrated in the following example with a triangle shaped terrain field with high slopes as an example. Fig. 3.7 and fig. 3.8 shows the satellite image and 3D surface plot of the field. The contour lines in and around the field is shown in fig. 3.9. As shown in fig. 3.7, the hypotenuse side of the triangle field is a small creek. The average slope on the field is 5.3 degrees, which makes the 3D path planning algorithm necessary.

Figure 3.7. Satellite image of an example field with high slopes.

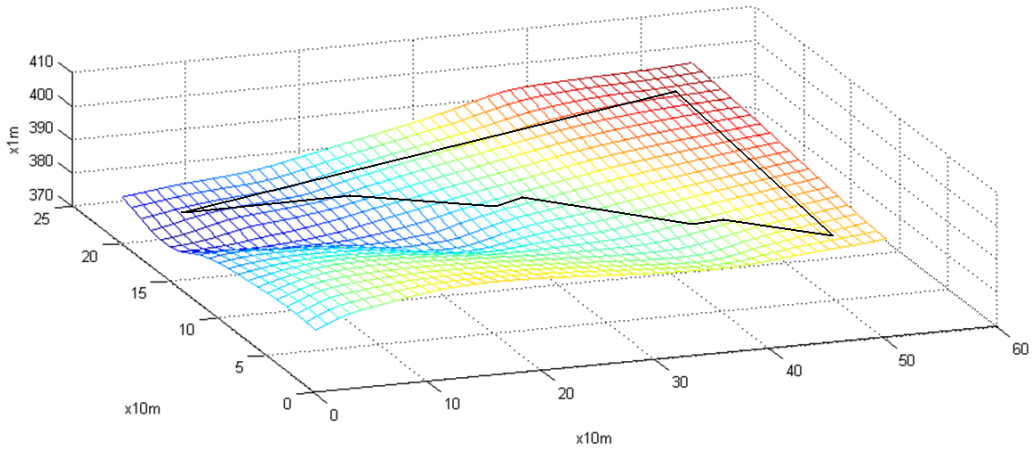

Figure 3.8. 3D Surface plot of the example field.

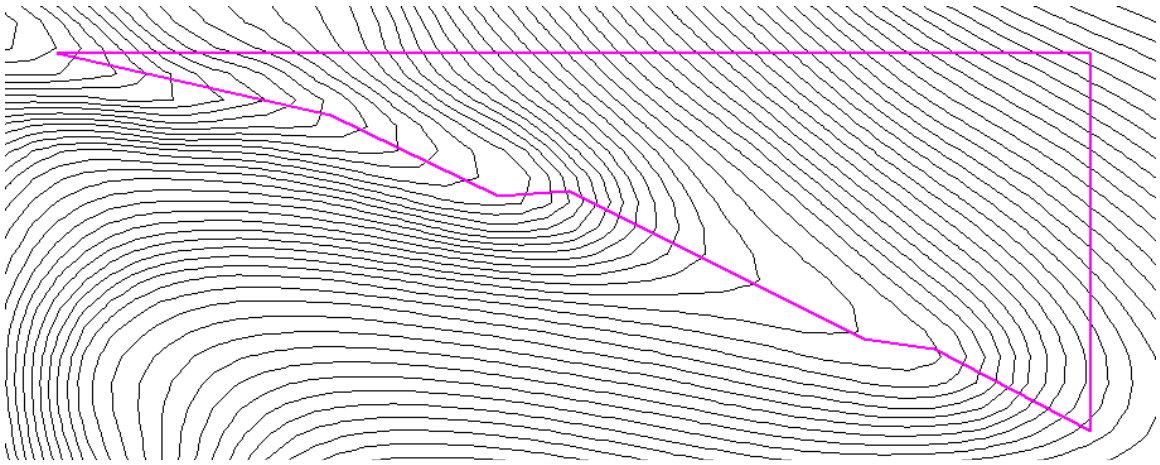

Figure 3.9. Contour lines in and around the example field.

First of all, a set of contour lines inside the field were found, as the gold curves shown in Fig. 3.10. These curves together with the three edges of the field make up the candidate set of the seed curves.

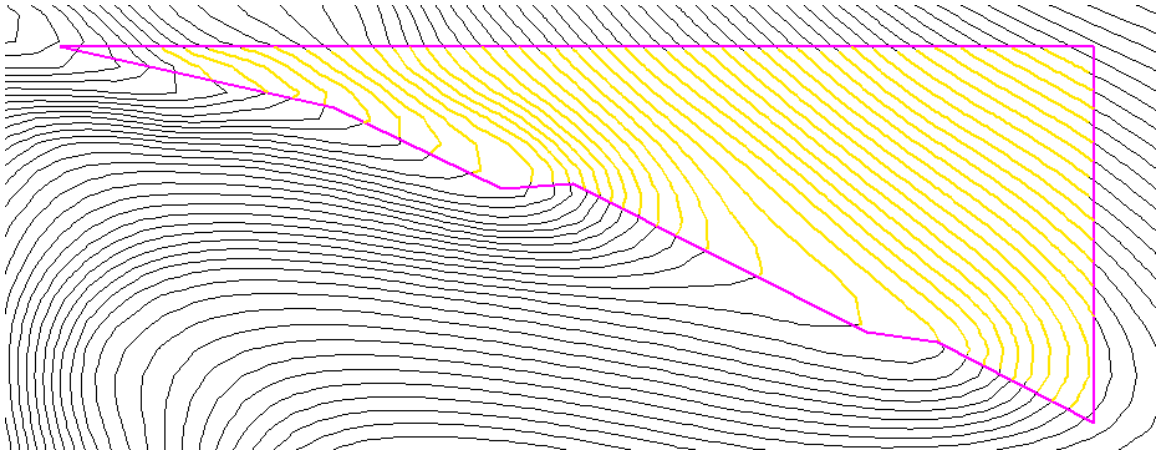

Figure 3.10. Contour lines within the example field with certain lengths are potential "Golden Seed Curves".

Next, for each of the seed curve candidates, the coverage paths are generated by offsetting the seed curve sideways, until the whole region is covered (fig. 3.11). The weighted average of the normalized costs of the resulted coverage pattern is calculated, which include headland turning cost, soil erosion cost and skipped area cost, as discussed before. Finally, the seed curve candidate leading to the lowest weighted average cost is adopted.

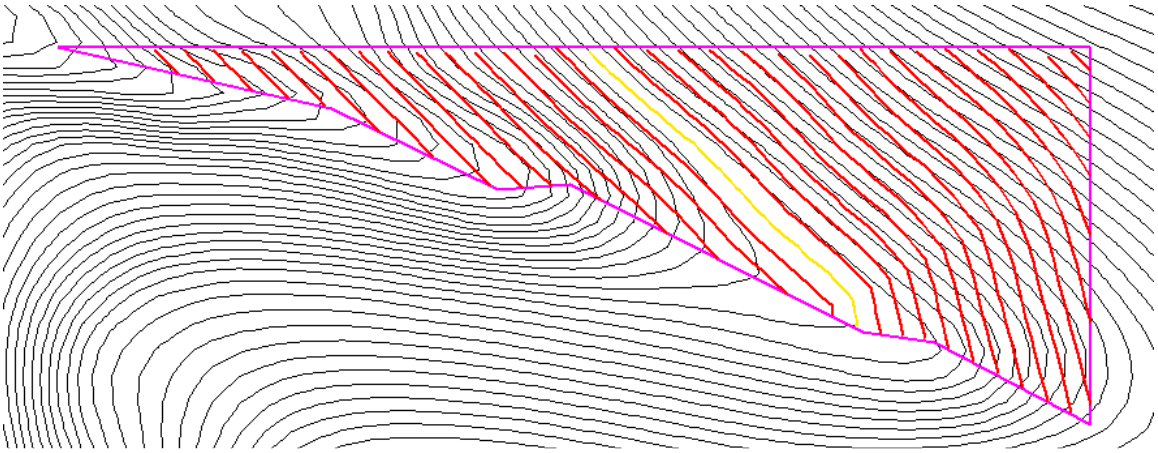

Figure 3.11. Example of expanding one of the potential “Seed Curves” (gold) and covering the field. The red lines are the generated paths from the seed curve.

3.4 Results

The 3D coverage path planning methods and algorithms have been implemented in MATLAB. The MATLAB programs take the DEM of a field as input, analyze the field terrain, compare all the potential covering schemes and finally provide the optimized path. All the elevation data used in this project was from the National Elevation Dataset (NED) of U.S. Geological Survey (USGS), with the planar resolution (distance between adjacent points) of 10 meters and altitude resolution of 1 meter (Gesch et al., 2007).

To help the understanding of how the 3D planning steps work, in 3.4.1 through 3.4.4, the application of each step on an example field is described separately. The whole 3D planning method has been applied to some practical terrain fields and generated the recommended coverage paths. These results together with the cost comparison summary are listed in 3.4.5.

3.4.1 3D Terrain Modeling Results

The B-Splines terrain model for one example field is shown in the following figures. Fig. 3.12 is the satellite image of the example field. This 400x250 square meters (24.7 acres) field example is located in east of Iowa. The maximum slope on this field is 25.9% and the average slope is 10.45%. In fig. 3.13 and fig. 3.14 are the 3D surface plot and contour view

of the field. In fig. 3.15a and fig. 3.15b are the fitting result by a 6th-degree polynomial and the fitting result by a 4th order B-Spline with uniform knot sequences, 5 grids/knot in both directions. The detailed fitting results of different models are listed in Table. 3.1.

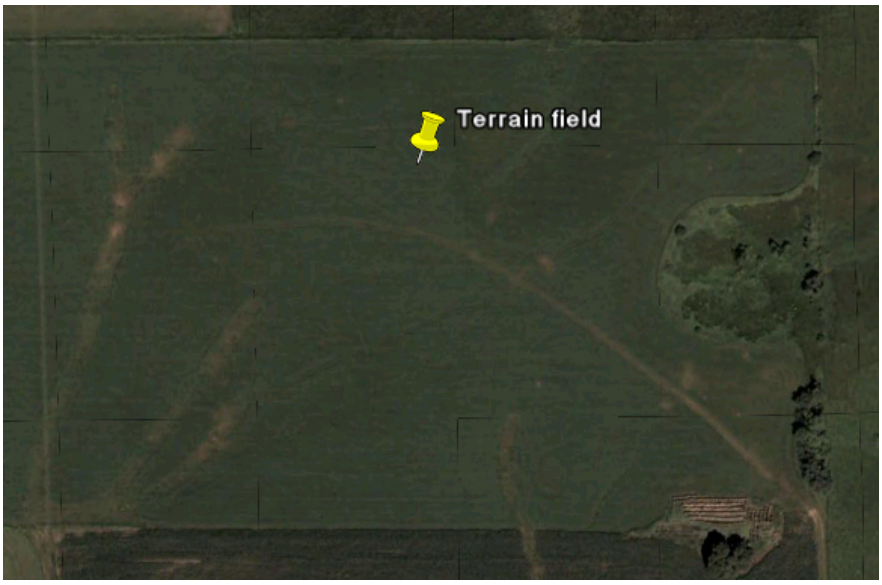

Figure 3.12. Satellite image of the 400x250 square meters (24.7 acres) field. The maximum slope in this field is 25.9% and the average slope is 10.45%.

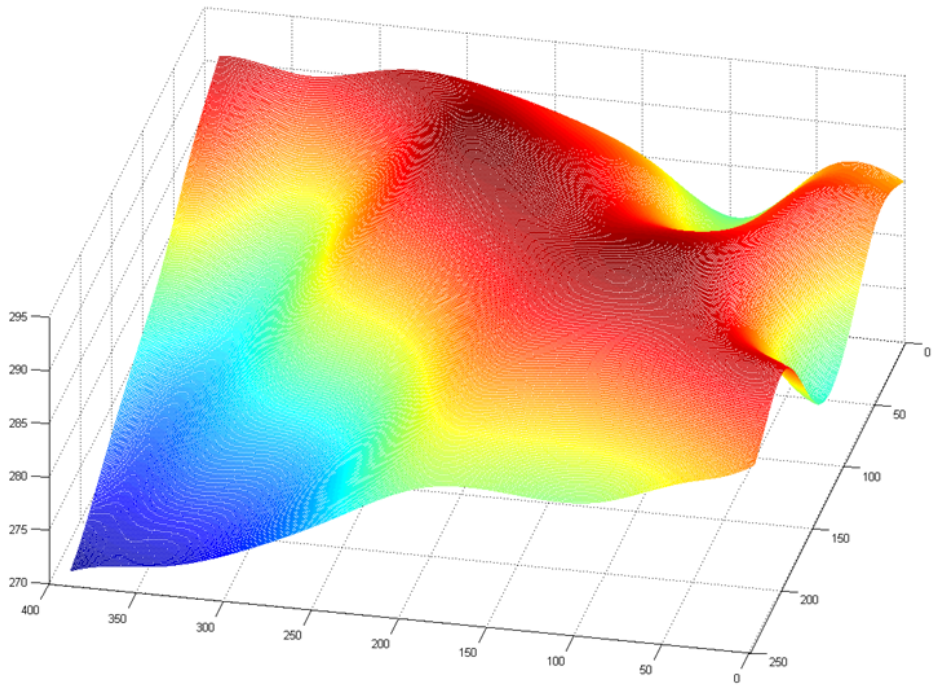

Figure 3.13. 3D surface plot of the DEM Data of the example field.

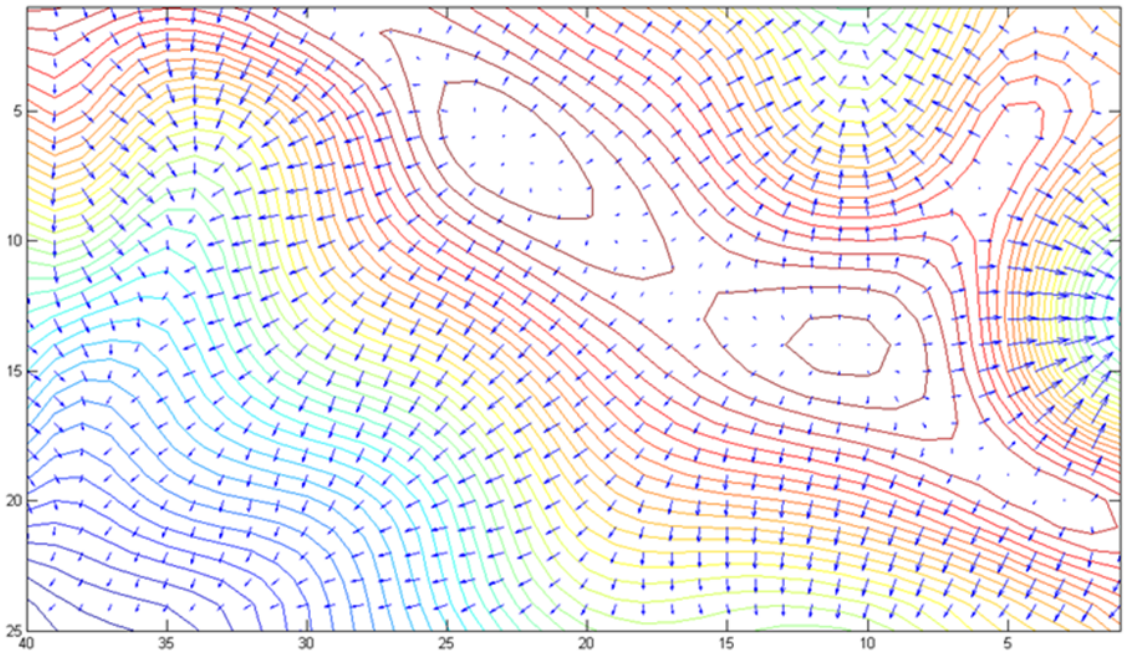

Figure 3.14. Contours and aspects on the example field, where the direction and length of the blue arrow vectors show the aspect directions and slope steepness, separately.

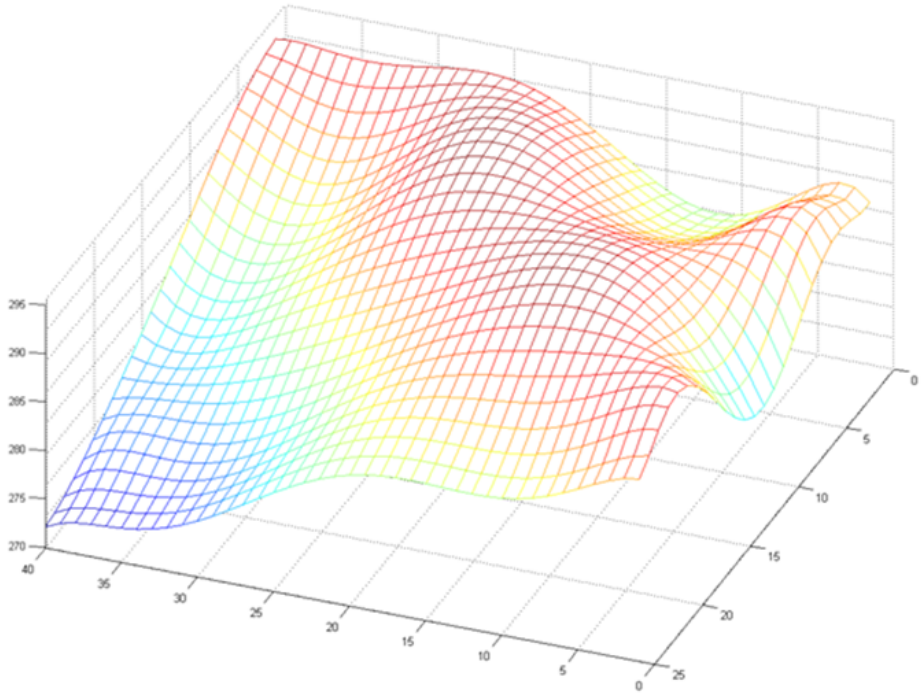

(a)

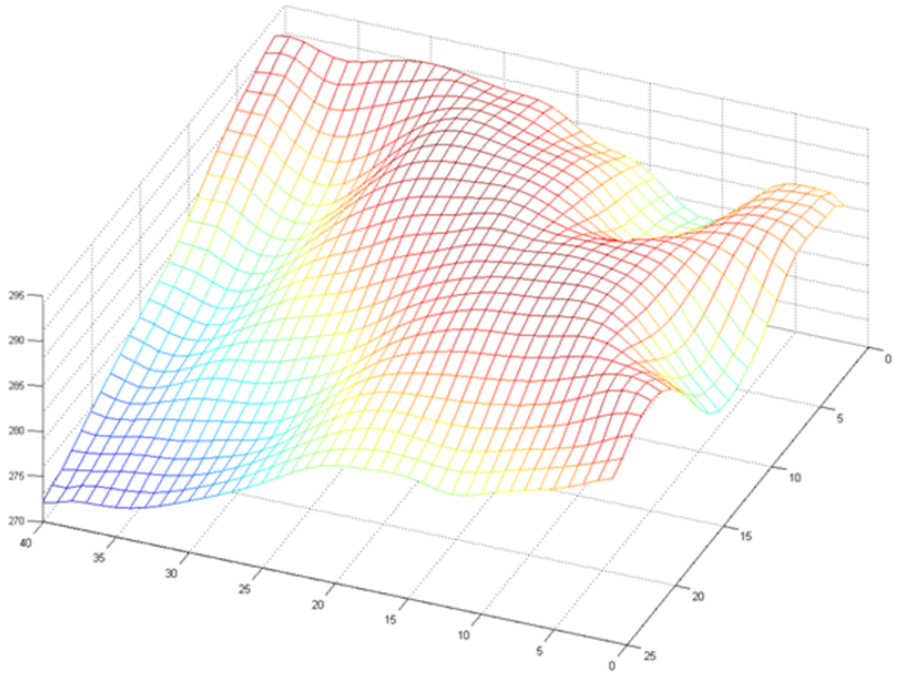

(b)

Figure 3.15. Fitting results: (a) Fitting result by a 6th-order polynomial; (b) Fitting result by a 4th order B-Splines with uniform knot sequences, 5 grids/knot in both directions.

According to Table 3.1, generally, B-Splines models outperformed polynomial models, except for the larger number of coefficients. The calculations on the terrain during the 3D planning were all based on the B-Splines models.

Table 3.1. DEM data fitting results of different models

Model	Number of Co-efficients	Max Elevation Error (m)	MSE (m^2)	R-Square
4th Polynomial	25	5.1152	1.1549	0.9604
5th Polynomial	36	2.9569	0.6860	0.9765
6th Polynomial	49	1.7871	0.2840	0.9903
4th B-Spline (5 grids/knot)	88	1.0398	0.0643	0.9978
4th B-Spline (4 grids/knot)	117	1.1358	0.0501	0.9983
4th B-Spline (3 grids/knot)	176	0.9437	0.0256	0.9991
4th B-Spline (2 grids/knot)	345	0.6600	0.0118	0.9996
5th B-Spline (5 grids/knot)	108	1.1917	0.0689	0.9976
5th B-Spline (4 grids/knot)	140	1.0251	0.0361	0.9988
5th B-Spline (3 grids/knot)	204	0.8187	0.0205	0.9993
5th B-Spline (2 grids/knot)	384	0.5094	0.0104	0.9996

3.4.2 Results of Analysis on Skips between Projected 2D Planning Results on 3D Terrain

For the same field example in fig. 3.12 and fig. 3.13, the skipped area between adjacent paths when projecting 2D planning result to 3D surface was calculated. Since this is a standard rectangular field with its north and south edges as the longer edges, in 2D planning, it would be optimal to cover it with straight parallel paths along these two edges (Fig. 3.16).

Figure 3.16. Result of 2D Coverage Path Planning for the field in Fig. 3.12.

If the 2D result shown in Fig. 3.16 is executed on the actual 3D terrain, there would be uncovered skips between neighboring paths, causing waste of farmland, as discussed before. The total skipped area can be calculated by equation (3.7). The resulted total skipped area on this field is 281.37 square meters, which is 0.28% of the total area of the field.

3.4.3 Terrain Decomposition Results

For the same field example in fig. 3.12 and fig. 3.13, the field terrain was decomposed based on the developed algorithm. After the first round of decomposition, the terrain was decomposed into 15 sub-regions. Slope stiffness was the only criterion used for the decomposition trail here. More criteria could be easily included based on the operator's request and the availability of field data. Two slope thresholds, 5% and 10%, divided the terrain into 3 classes represented by different colors in fig. 3.17.

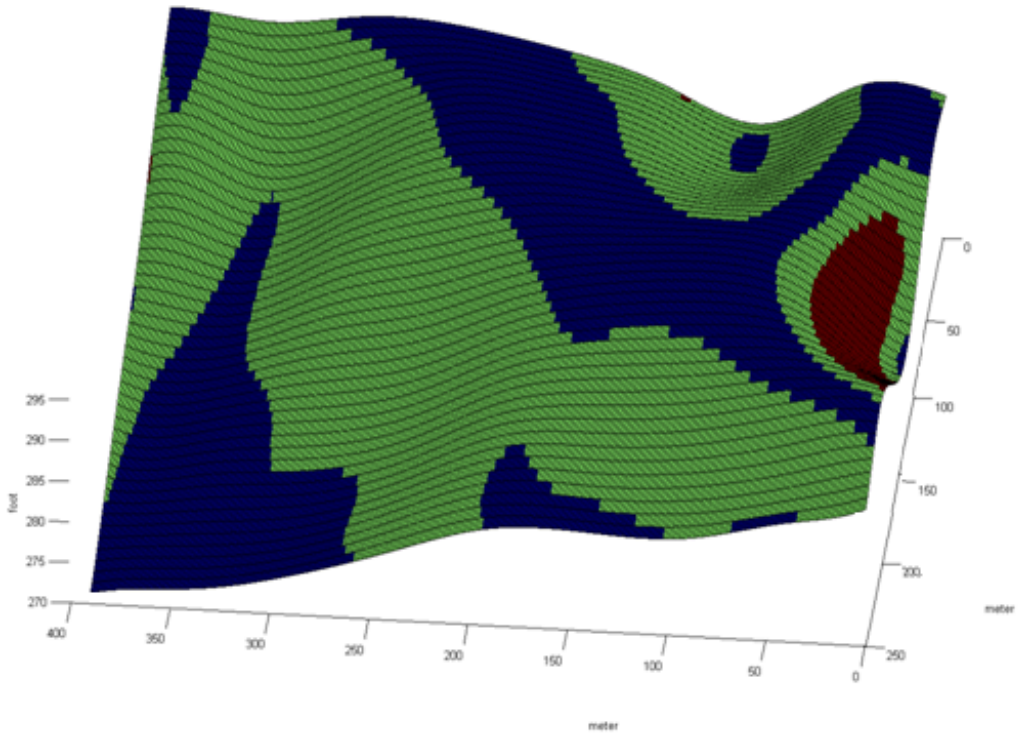

Figure 3.17. Result after the first round of decomposition with 15 sub-regions. Slope stiffness was the only criterion used for the decomposition. Two slope thresholds, 5% and 10%, divided the terrain into flat areas (blue), medium areas (green) and steep areas (red).

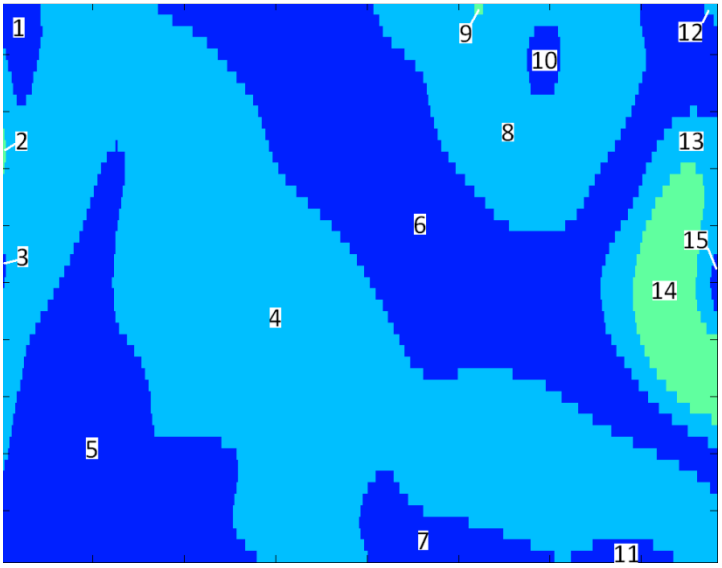

Figure 3.18. The first round of decomposition resulted in 15 sub-regions (labeled).

After combining the small area regions and those neighboring regions with complementary shapes, the field was composed with 3 sub-regions (fig. 3.19).

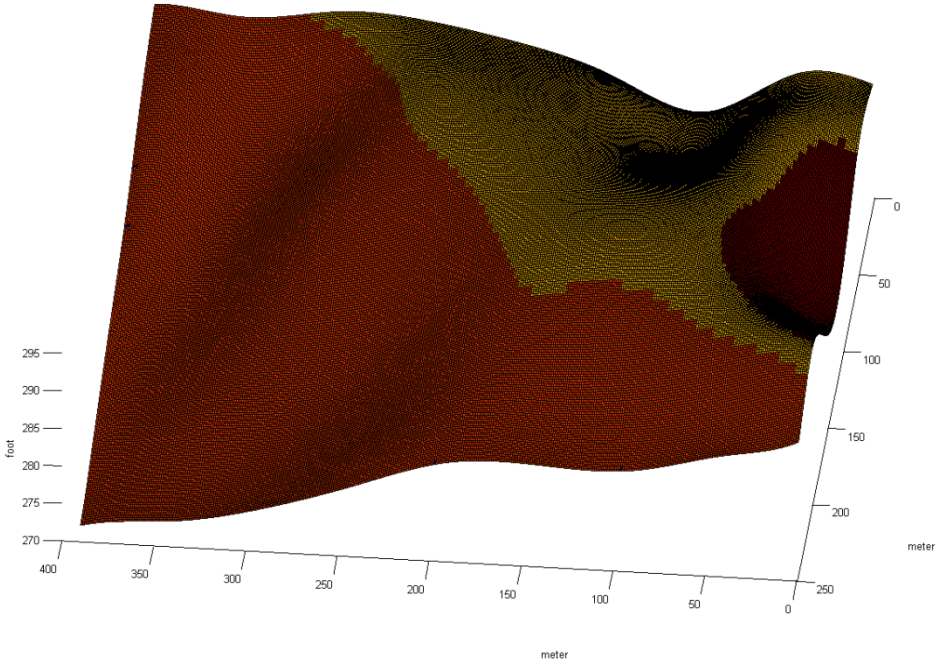

Figure 3.19. Decomposition result after recombination.

3.4.4 Soil Erosion Cost Results

Equation (3.14) has been used to calculate the P factor of the example terrain field in fig. 3.12 and fig. 3.13, on which the 2D planning result in fig. 3.16 was assumed to be projected and executed on the terrain. Assuming the ridge height was moderate (3 to 4 inches high), the P_o value of the field was calculated as 0.45, while the $P_{off-grade}$ was calculated as 0.85, which was about 1.9 times as P_o. This result indicated a significant effect of off-grade operation on soil erosion: the soil loss from the planned path pattern in fig. 3.16 was 90% higher than that from on-grade contouring farming. When the soil erosion is of concern, the soil loss must be incorporated into the cost function of the path planner. When necessary, 3D coverage planning algorithm should be adopted instead of the 2D planning, and on-grade contouring or nearly on-grade contouring should be adopted to prevent severe soil erosion.

3.4.5 Practical Experimental Results of 3D Terrain Optimal Coverage Path Planning

The whole 3D terrain optimal coverage path planning algorithm has been successfully applied to several practical farm fields with various topographical features. In the following, the experimental results for three terrain farm fields are provided and discussed.

3.4.5.1 Terrain Field Example 1

Fig. 3.20 is the satellite image of the first example field. This 60 acres farm field example is located in southwest of Iowa. The maximum slope on this field is 15.4 degrees and the average slope is 4.6 degrees. For a clearer view of the topography of this field, the 3D surface plot and contour view of the field are provided in fig. 3.21 and fig. 3.22.

Figure 3.20. Satellite image of the first example terrain field in southwest of Iowa. The maximum slope in this field is 15.4 degrees and the average slope is 4.6 degrees.

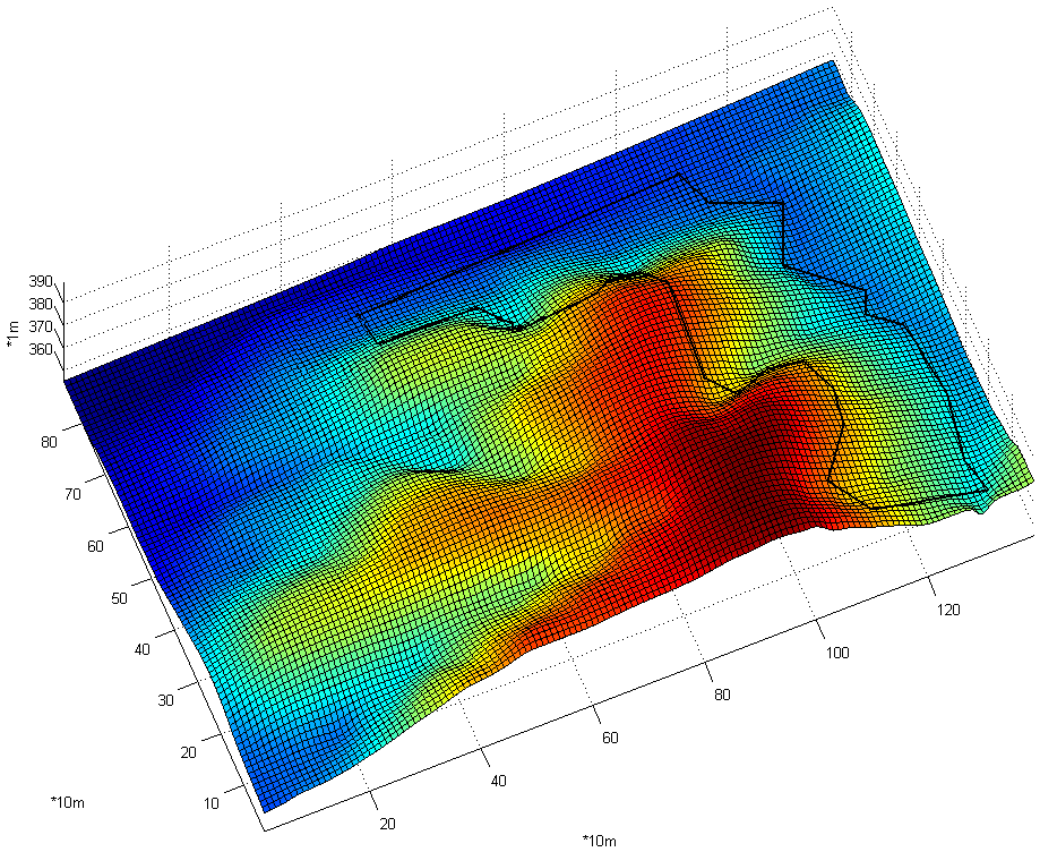

Figure 3.21. 3D surface plot of the DEM Data of the first example terrain field.

Figure 3.22. Contours view of the first example terrain field. Boundaries are plotted in black lines.

The slope data was calculated at each grid point of the field. Fig. 3.23 displays the slope data. The field can be classified into three classes, as shown in fig. 3.24. Slopes bellow 3% are defined as flat area (where 2D planning may be applicable), slopes between 3% and 5% are defined as medium area (either 2D or 3D planning may be applicable), and slopes above 5% are defined as steep area (where 3D planning may be applicable).

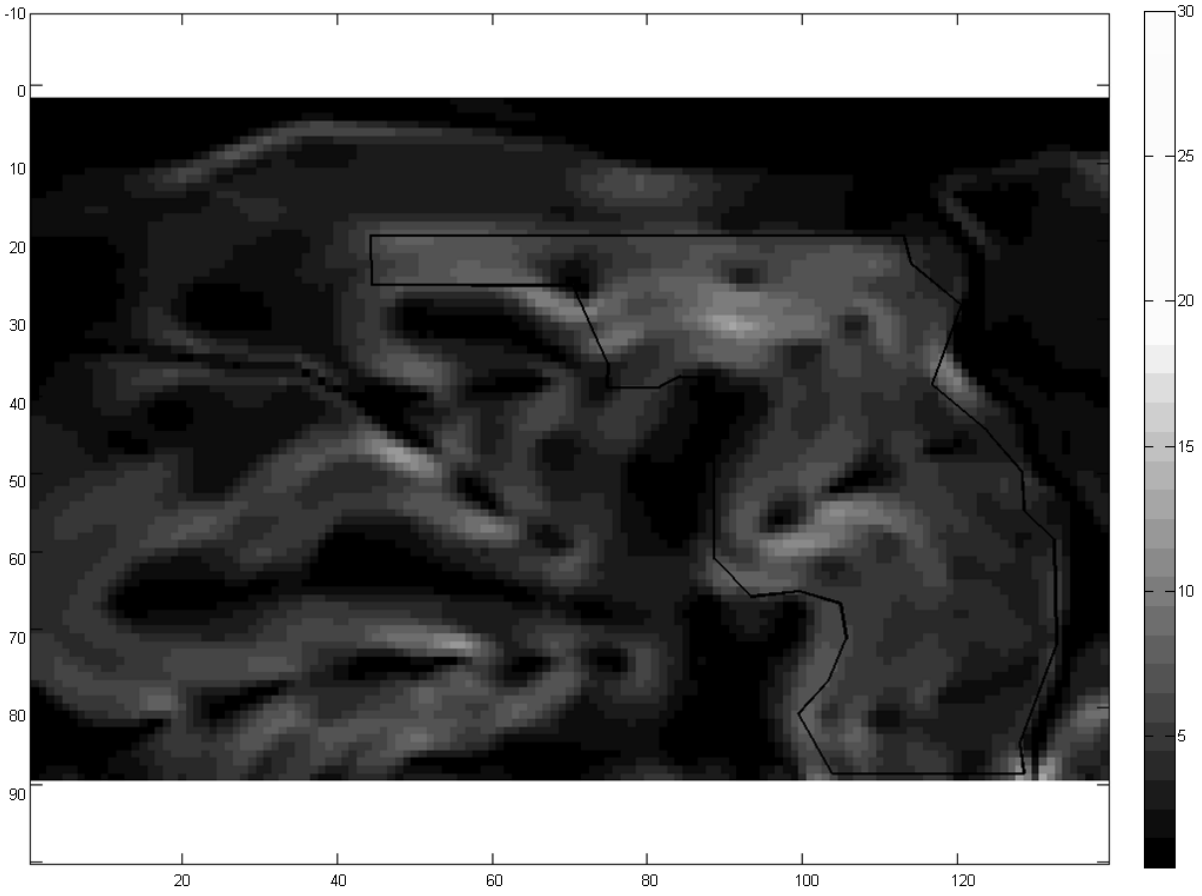

Figure 3.23. Slope map (in “%”) of the first example terrain field.

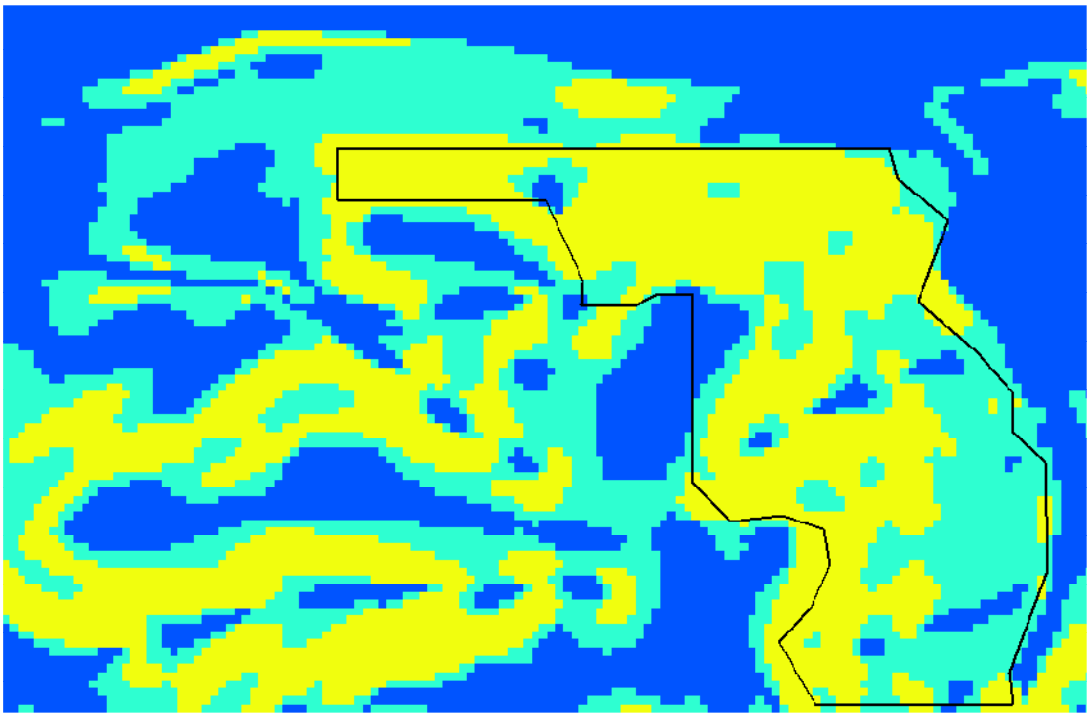

Figure 3.24. Decomposition result (before recombination) of the first example terrain field. The flat areas are in blue, the medium areas are in green, and the steep areas are in yellow.

Because of the high slope steepness in most of the field area, after re-combining the small area regions and those neighboring regions with complementary shapes, the 3D path planning algorithm was applied to the whole field without any subdivision.

During the experiment, the weights were first set as 1:1:0.5 between turning cost, erosion cost and skipped area cost. This setting of weights was suggested based on the balancing between the calculated costs of different cost categories. The searching among all the contour seed curve candidates resulted in the coverage solution in fig. 3.25, which had a lot of similarities with the farmer's practical solution (fig. 3.20).

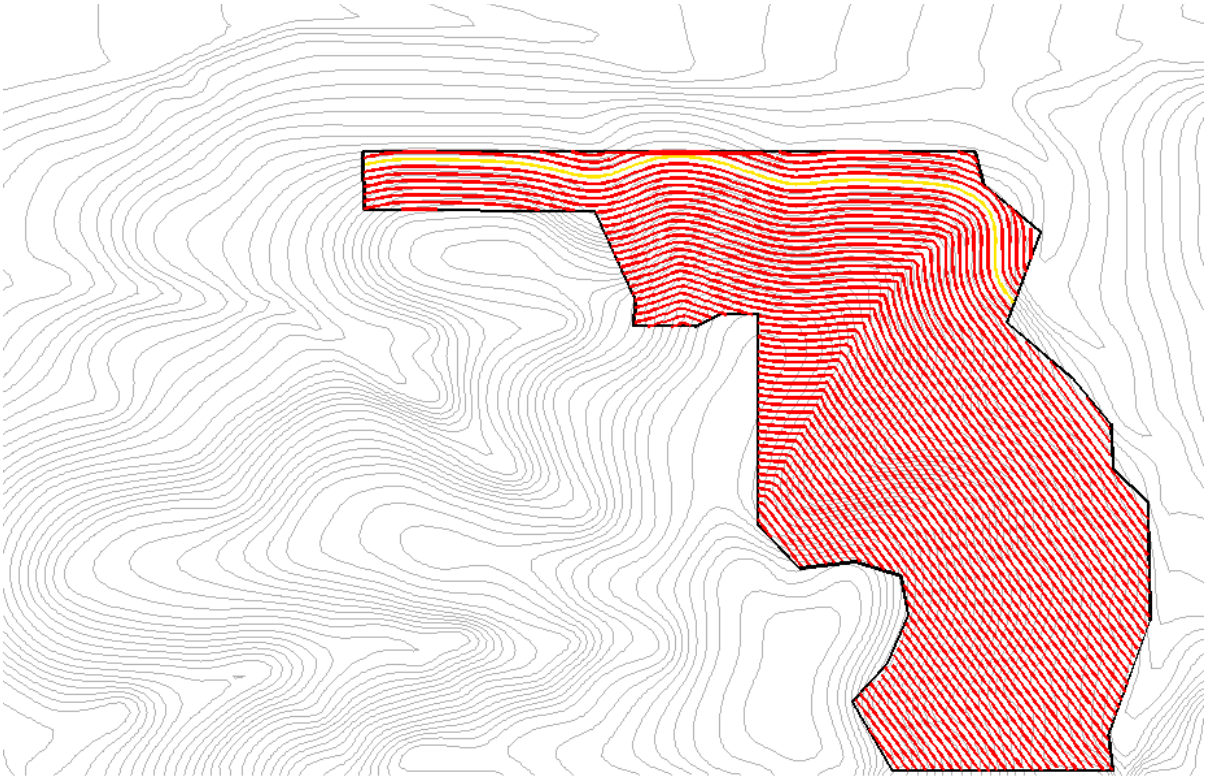

Figure 3.25. The recommended coverage solution for the first example field from the searching among all the contour seed curve candidates. The gold curve is the selected seed curve, which is one of the contour lines within the field area. The red curves are the corresponding paths. The weights were set as 1:1:0.5 between turning cost, erosion cost and skipped area cost for the search.

To be compared with the coverage solution in fig. 3.25, several of the other solutions were generated. First, the contour seed curve leading to the minimum soil erosion cost was adopted. In other words, the weights were set as 0:1:0 between turning cost, erosion cost and skipped area cost. This resulted in the coverage solution in fig. 3.26.

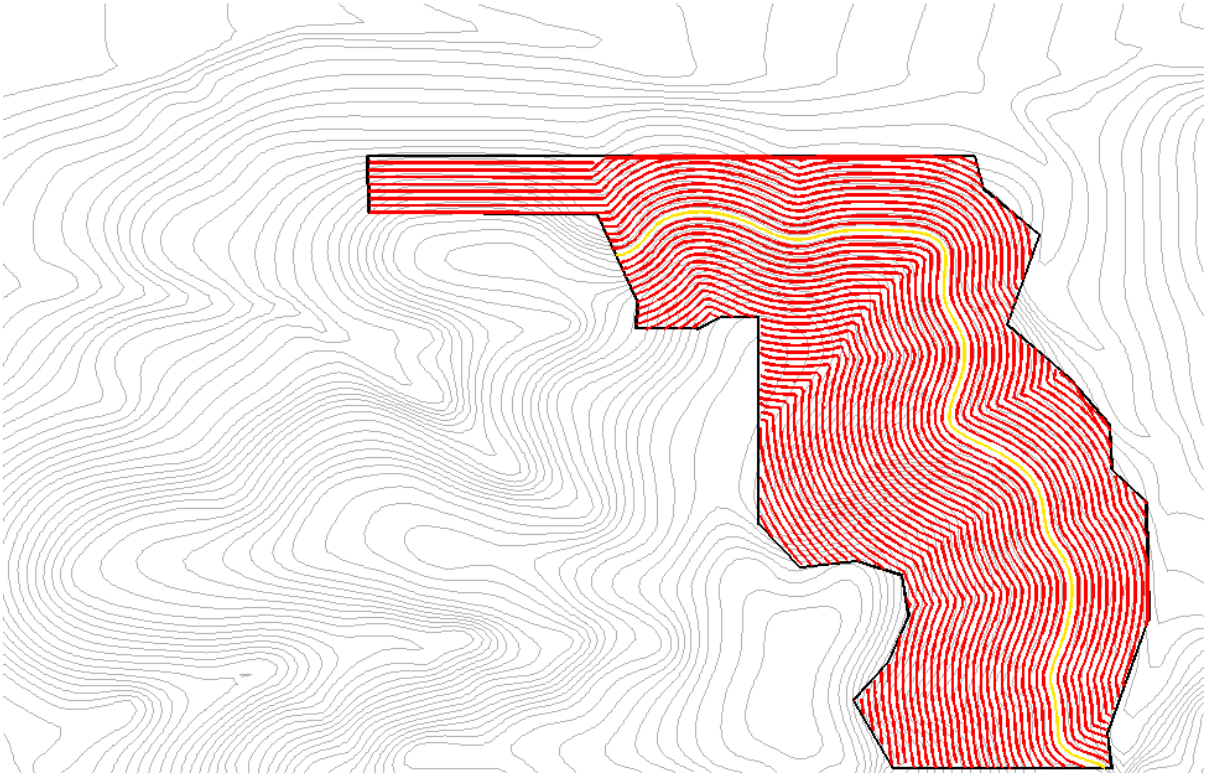

Figure 3.26. The coverage solution with minimum soil erosion cost for the first example field. The gold curve is the selected seed curve, which is one of the contour lines within the field area. The red curves are the corresponding paths. The weights were set as 0:1:0 between turning cost, erosion cost and skipped area cost for the search.

Besides the contour seed curves, three of the edges of the terrain field were adopted as the seed curve, separately. The resulted coverage solutions are shown in fig. 3.27, fig. 3.28, and fig. 3.29.

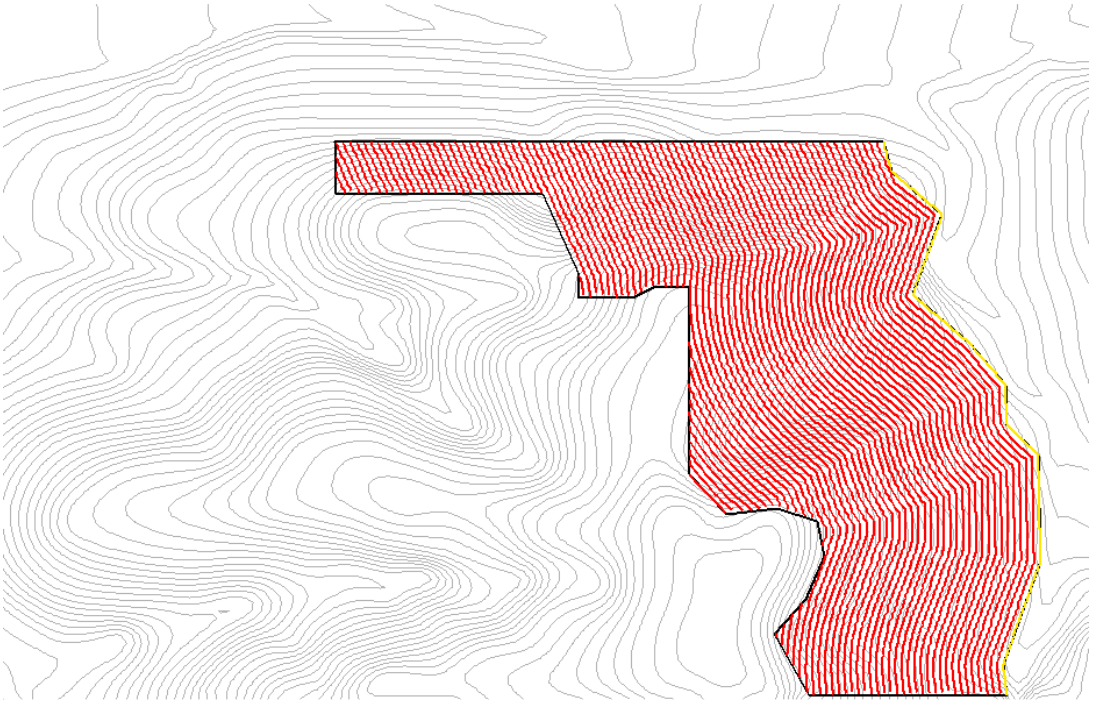

Figure 3.27. The coverage solution for the first example field with the east edge as the seed curve. The gold curve is the selected seed curve. The red curves are the paths.

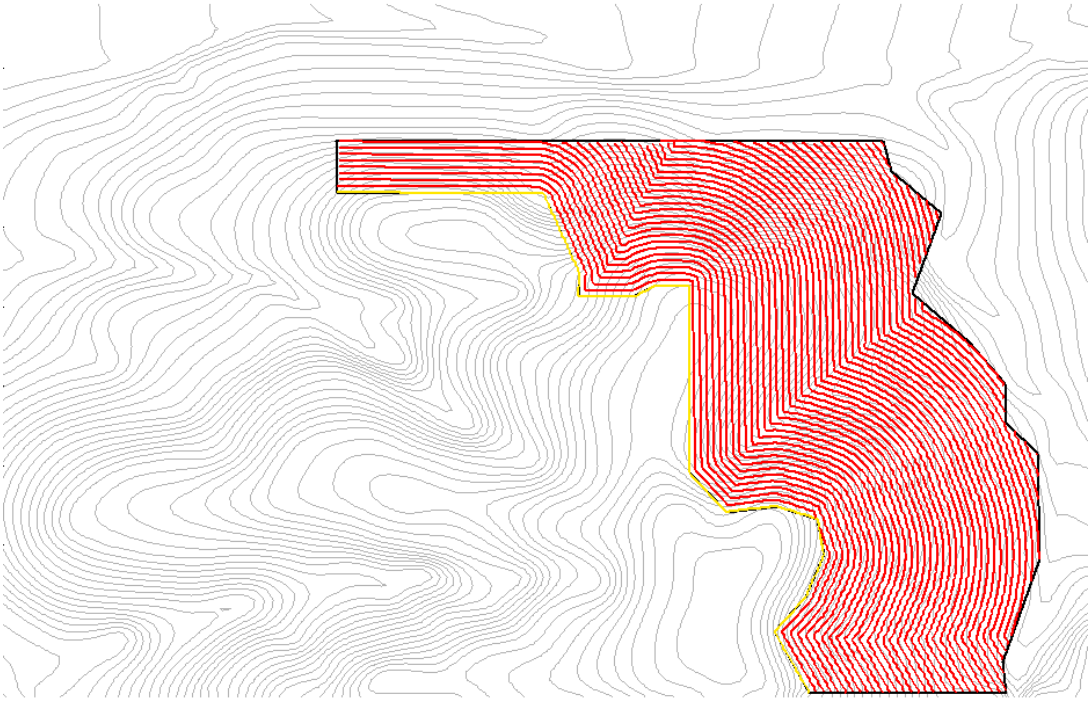

Figure 3.28. The coverage solution for the first example field with the west edge as the seed curve. The gold curve is the selected seed curve. The red curves are the paths.

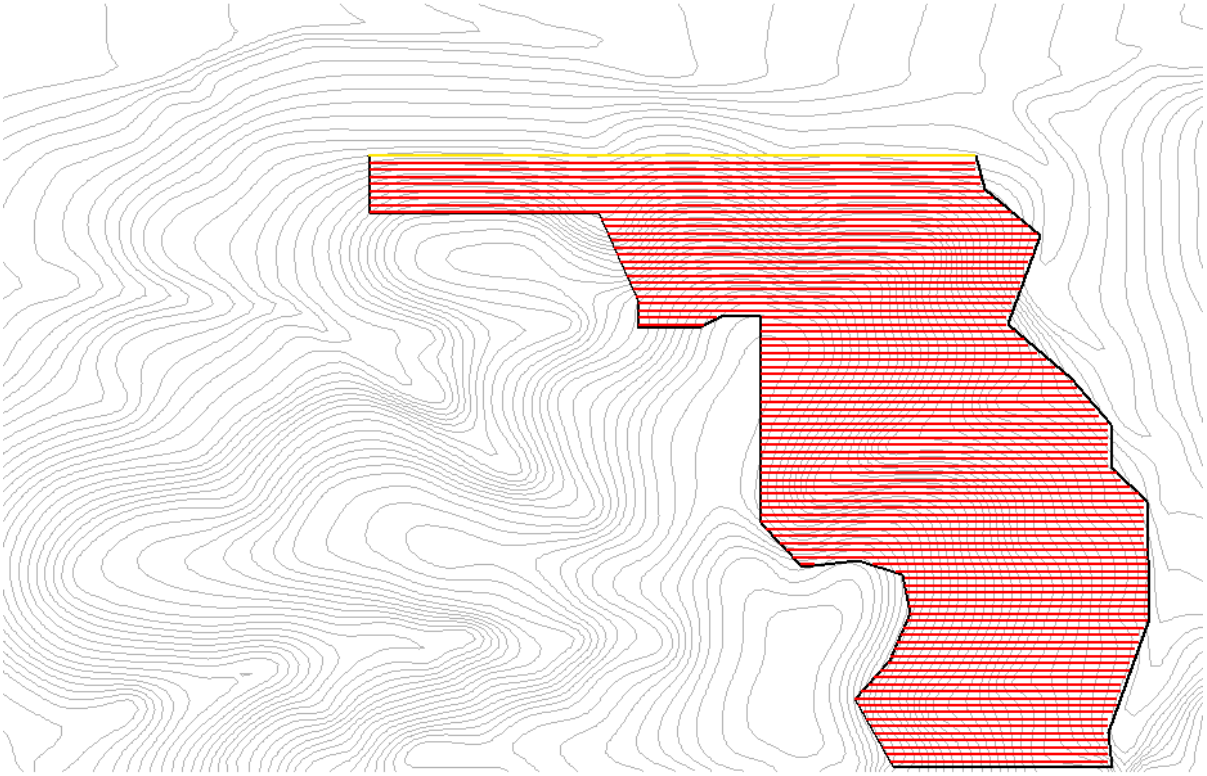

Figure 3.29. The coverage solution for the first example field with the north edge as the seed curve. The gold curve is the selected seed curve. The red curves are the paths.

Finally, to be compared with the 3D coverage planning results above, the 2D coverage planning result for this field was generated, as shown in fig. 3.30, which assumed the field is flat and ignored the elevation variances. The headland turning cost was the only concerned cost during the planning. The whole field is subdivided into two regions and different coverage directions were adopted for each region. After projecting the 2D planning result onto the 3D terrain surface, the resulted total skipped area on this field was 720 square meters, which was 0.30% of the total area of the field.

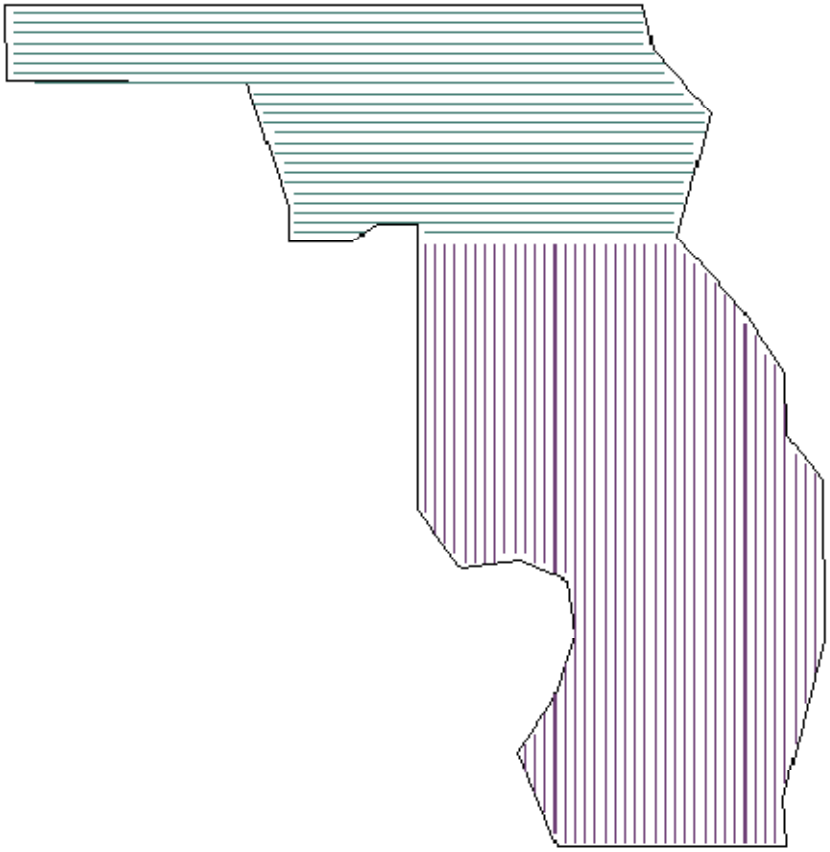

Figure 3.30. The 2D coverage planning result of the first example field. The whole field is subdivided into two regions and different coverage directions were adopted for each region.

The different categories of coverage costs as well as the weighted average of all the costs were calculated for all the six solutions above (both 3D and 2D solutions). The headland turning costs, erosion costs and skipped area costs of the six coverage solutions are compared in fig. 3.31 (the skipped area cost of the 2D planning solution was calculated differently based on the discussion in 3.3.2.2). The weighted averages of all the costs of the six coverage solutions are compared in fig. 3.32 (The weights were 1:1:0.5 between turning cost, erosion cost and skipped area cost). The 2D planning solution generated 16.6% higher headland turning cost, 8.7% higher erosion cost and 47.5% higher skipped area cost than the recommended 3D planning result. The final weighted average of all costs of the 2D solution was 18.1% higher than the recommended 3D solution.

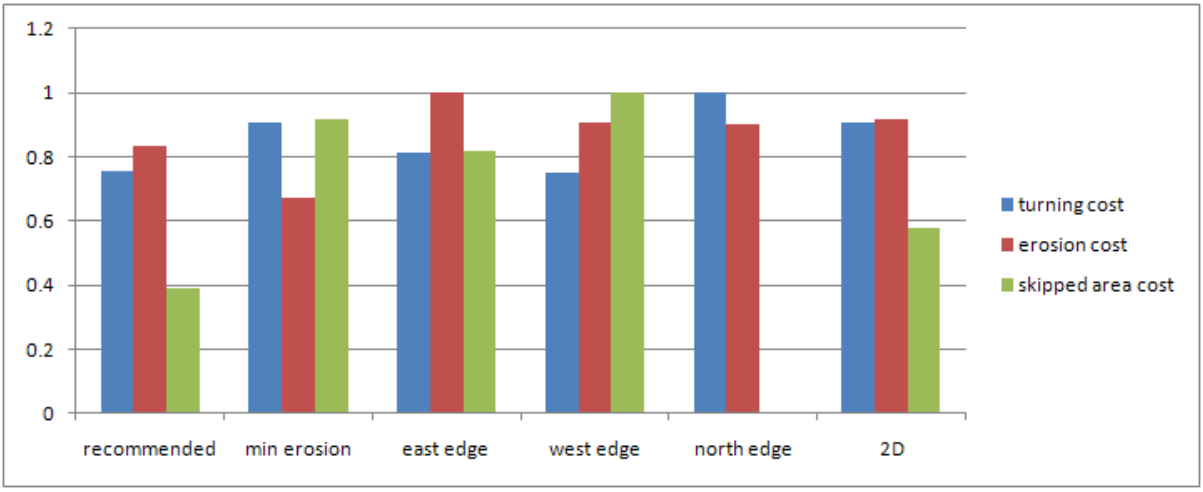

Figure 3.31. The turning costs, erosion costs and skipped area costs of the six coverage solutions for the first example field.

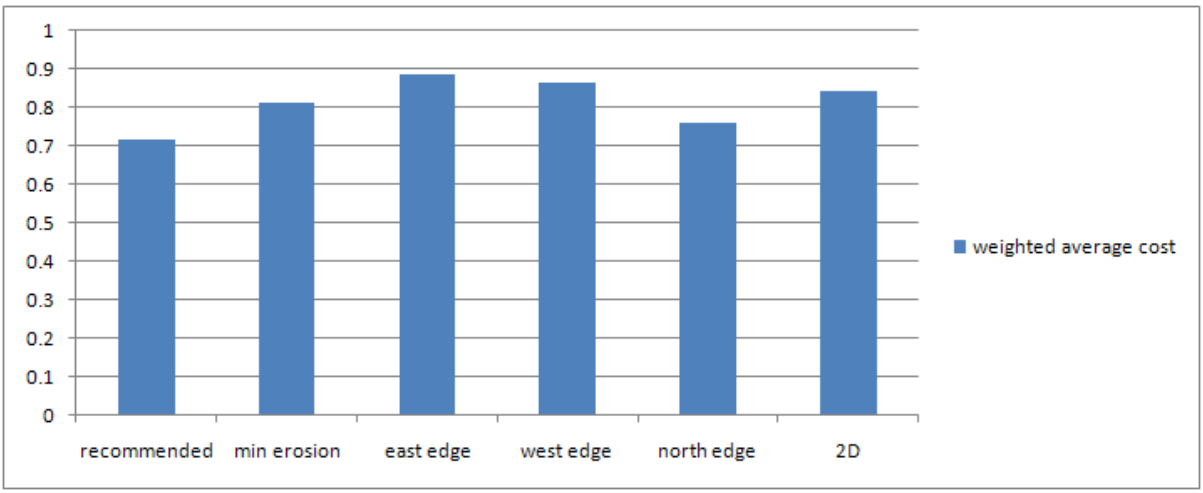

Figure 3.32. The weighted averages of all the costs of the six coverage solutions for the first example field. The weights were 1:1:0.5 between turning cost, erosion cost and skipped area cost.

3.4.5.2 Terrain Field Example 2

Fig. 3.33 is the satellite image of the second example field located in southwest of Iowa. This field has a triangle outside boundary and is of around 75 acres in area. The maximum slope on this field is 13.6% and the average slope is 3.9%. From the satellite image, terraces and water ways are visible inside the field. For a clearer view of the

topography of this field, the 3D surface plot and contour view of the field are provided in fig. 3.34 and fig. 3.35.

Figure 3.33. Satellite image of the second example terrain field in southwest of Iowa. The maximum slope in this field is 13.6% and the average slope is 3.9%.

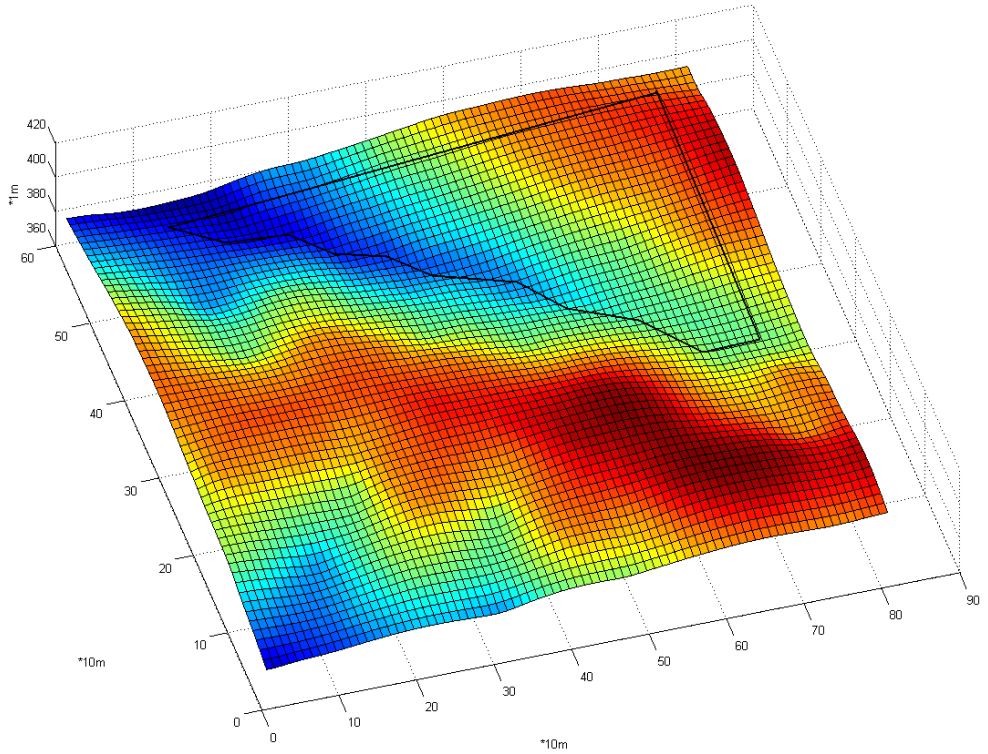

Figure 3.34. 3D surface plot of the DEM Data of the second example terrain field.

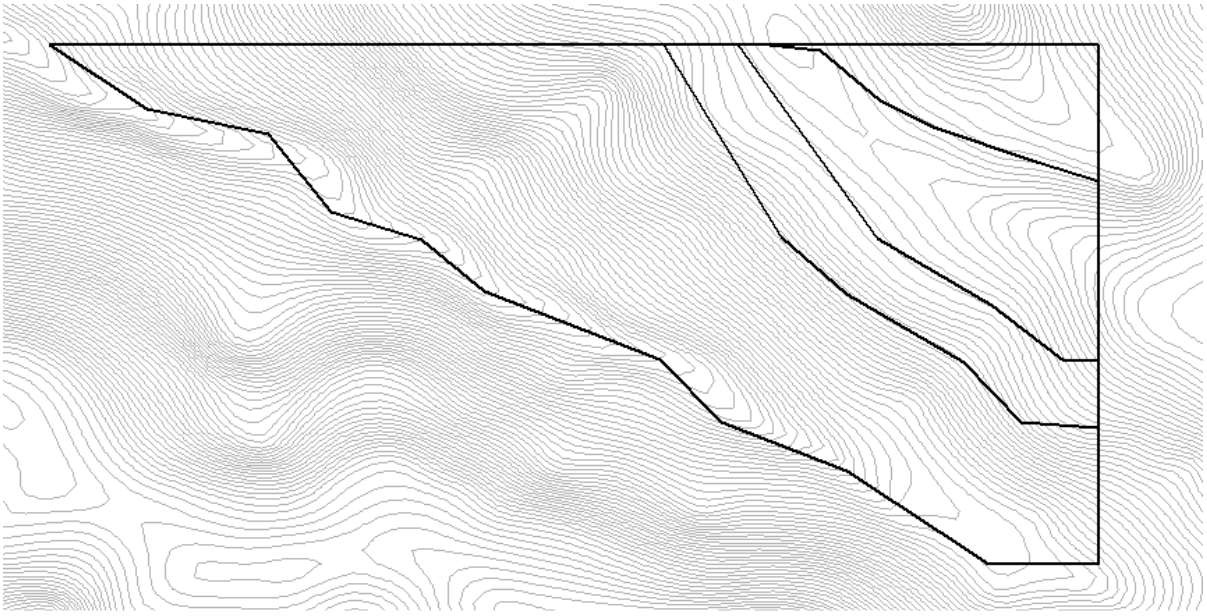

Figure 3.35. Contours view of the second example terrain field. Boundaries and terraces inside the field are plotted in black lines.

The slope data was calculated at each grid point of the field. Fig. 3.36 displays the slope data. If the slopes below 3% are defined as flat area, slopes between 3% and 5% are defined as medium area, and slopes above 5% are defined as steep area, the field can be classified into three classes, as shown in fig. 3.37.

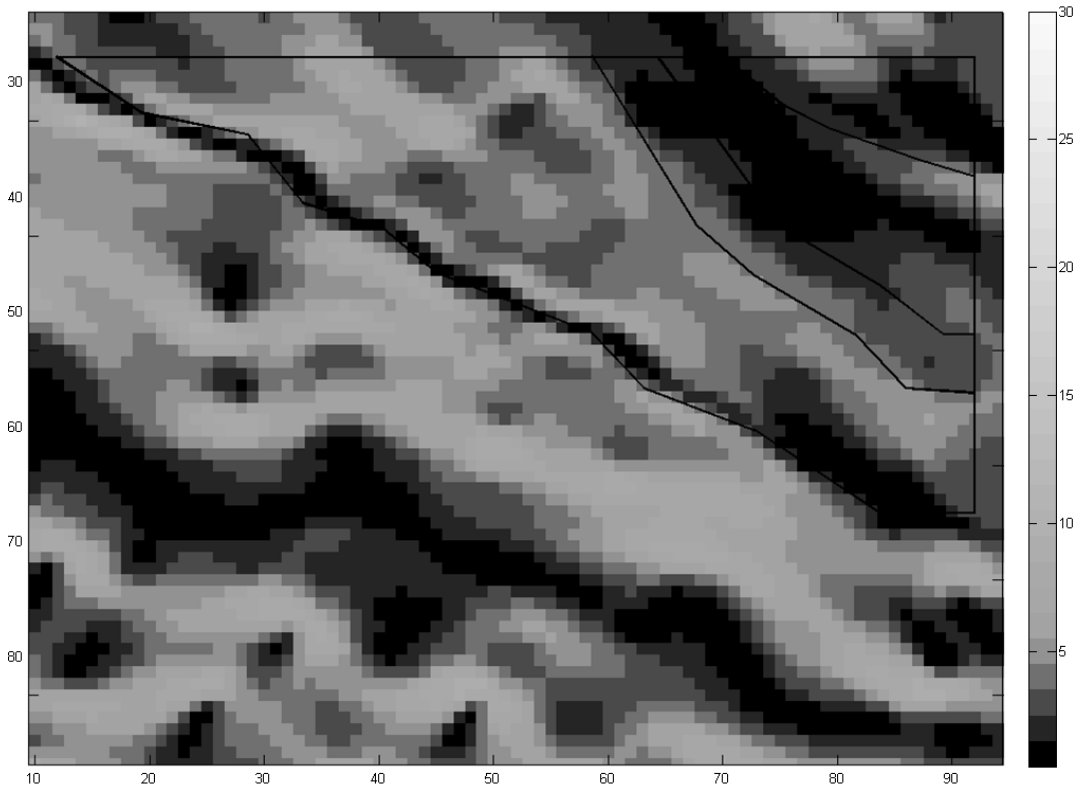

Figure 3.36. Slope map (in “%”) of the second example terrain field.

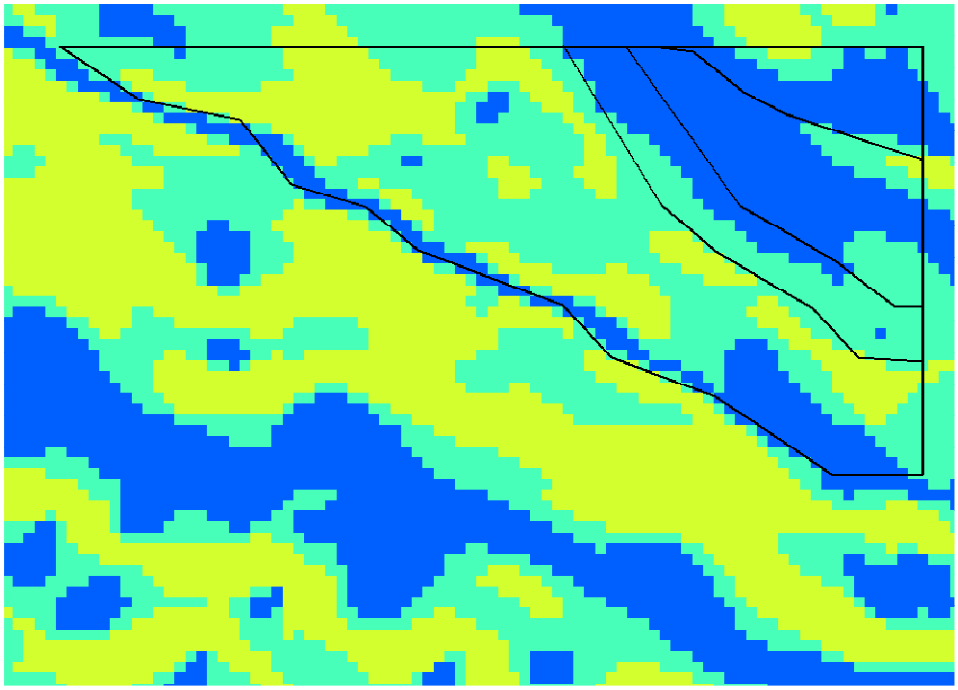

Figure 3.37. Decomposition result (before recombination) of the second example terrain field. The flat areas are in blue, the medium areas are in green, and the steep areas are in yellow.

Since the terraces already divided the field into four unconnected regions (fig. 3.38), the terrain decomposition was carried out in each of the four regions. After re-combining the small area regions and those neighboring regions with complementary shapes, the result indicated that without any further subdivision, the 2D path planning algorithm should be applied to regions 1 and 2, while 3D terrain path planning algorithm should be applied to regions 3 and 4.

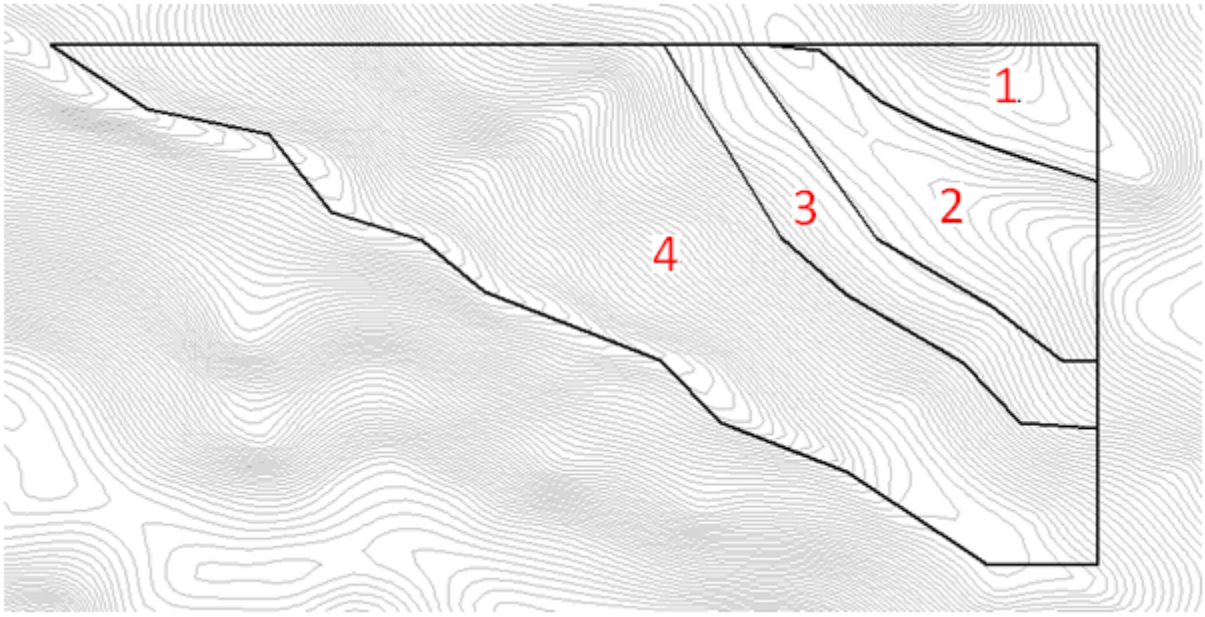

Figure 3.38. The terraces divided the field into four unconnected regions. Without any further subdivision, the 2D path planning algorithm should be applied to region 1 and 2, while 3D terrain path planning algorithm should be applied to region 3 and 4.

The 2D path planning results for regions 1 and 2 are displayed bellow. From the satellite image (fig. 3.33), there is another short segment of terrace within region 1, existing as an isolated obstacle inside the field. This terrace was input into the 2D path planning software as an obstacle within the field. After projecting the 2D planning results onto the 3D terrain surface, the resulted total skipped areas on these flat regions were small because of the low slopes: For region 1, the skipped area was only 6.1 square meters, which was 0.03% of the total area of the region. The total skipped area for region 2 was only 0.62 square meters, which was about 0.001% of the total area of the region.

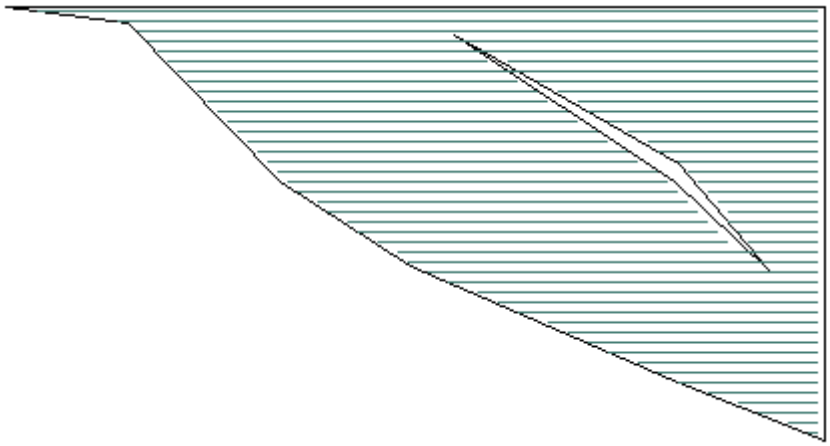

Figure 3.39. The 2D coverage planning result of region 1 in the second example field. The short segment of terrace within region 1 was input into the 2D path planning software as an obstacle within the field. No decomposition was suggested for region 1, and the resulted optimal coverage direction was along the north edge.

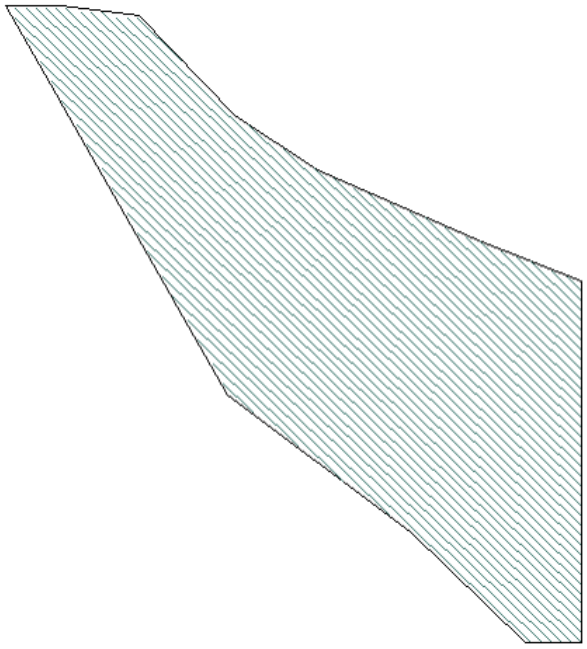

Figure 3.40. The 2D coverage planning result of region 2 in the second example field. No decomposition was suggested for region 2, and the resulted optimal coverage direction was along one of the southwest edge segments.

The 3D path planning results for regions 3 and 4 are displayed bellow. The weights were set as 1:1:0.5 between turning cost, erosion cost and skipped area cost.

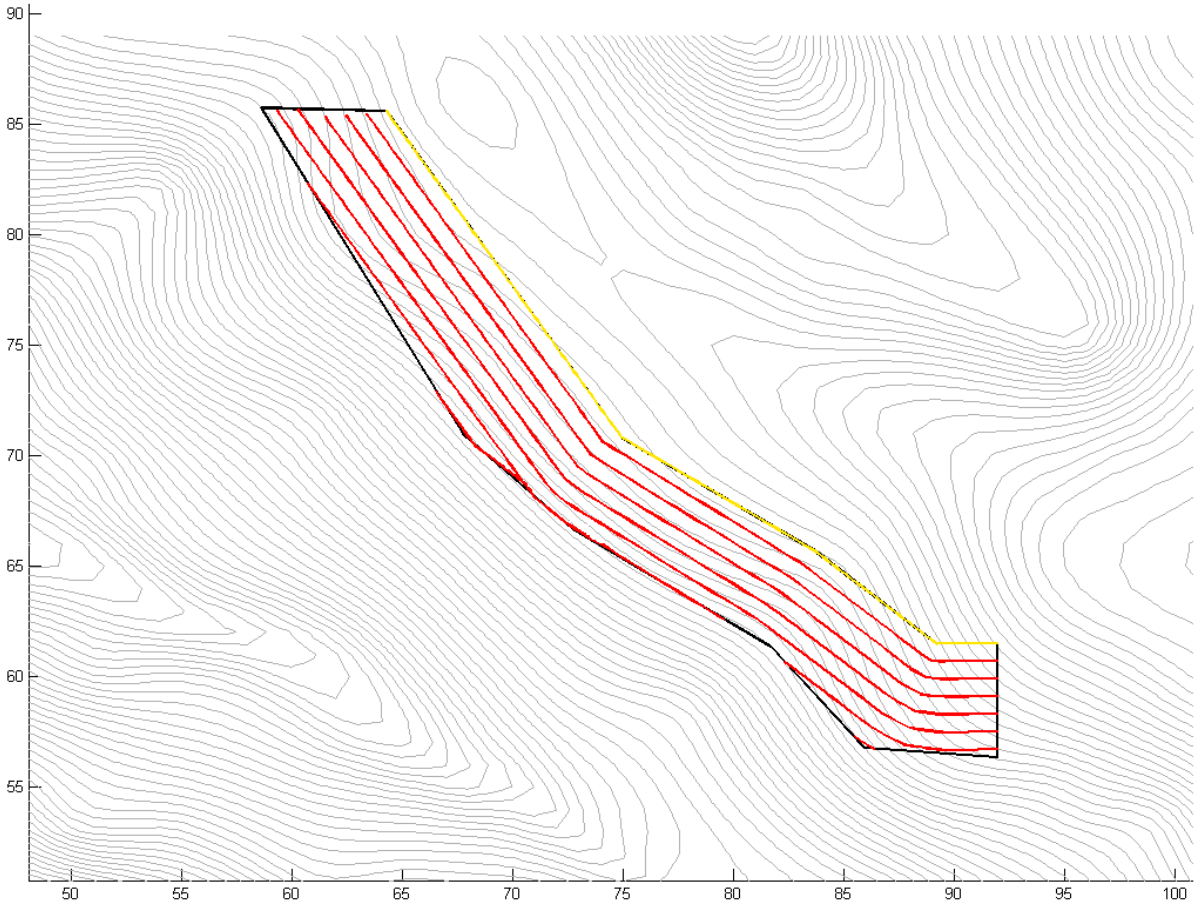

Figure 3.41. The recommended 3D coverage planning result for region 3 in the second example field. The gold curve is the selected seed curve. The red curves are the corresponding paths. The weights were set as 1:1:0.5 between turning cost, erosion cost and skipped area cost for the search.

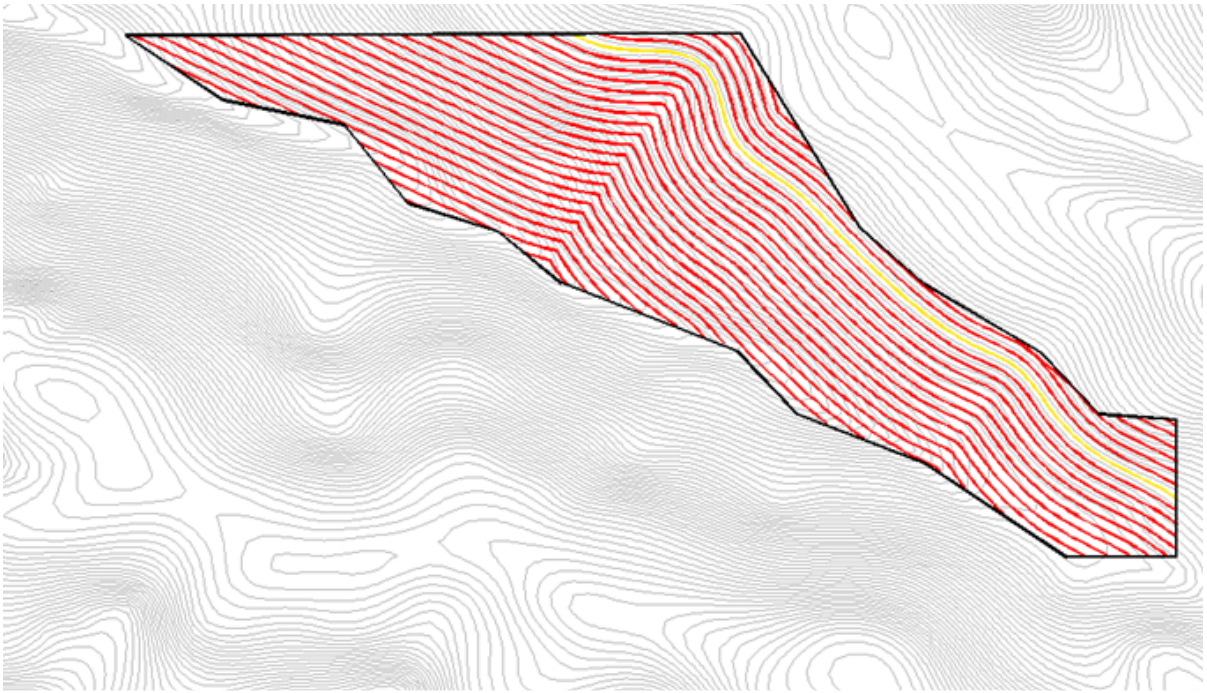

Figure 3.42. The recommended 3D coverage planning result for region 4 in the second example field. The gold curve is the selected seed curve, which is one of the contour lines within the field area. The red curves are the corresponding paths. The weights were set as 1:1:0.5 between turning cost, erosion cost and skipped area cost for the search.

To be compared with the coverage solution in fig. 3.42, several of the other solutions for region 4 in the second example field were generated. First, the contour seed curve leading to the minimum soil erosion cost was adopted. In other words, the weights were set as 0:1:0 between turning cost, erosion cost and skipped area cost. This resulted in the coverage solution in fig. 3.43. Besides the contour seed curves, three of the edges of region 4 in the second example field were adopted as the seed curve, separately. The resulted coverage solutions are shown in fig. 3.44, fig. 3.45, and fig. 3.46. Finally, to be compared with the 3D coverage planning results above, the 2D coverage planning result for region 4 in the second example field was generated, as shown in fig. 3.47, which assumed the field is flat and ignored the elevation variances. The headland turning cost was the only concerned cost during the planning. The whole field was subdivided into two regions and different coverage directions were adopted for each region. After projecting the 2D planning result onto 3D

terrain surface, the resulted total skipped area was 200 square meters, which was 0.11% of the total area of the region.

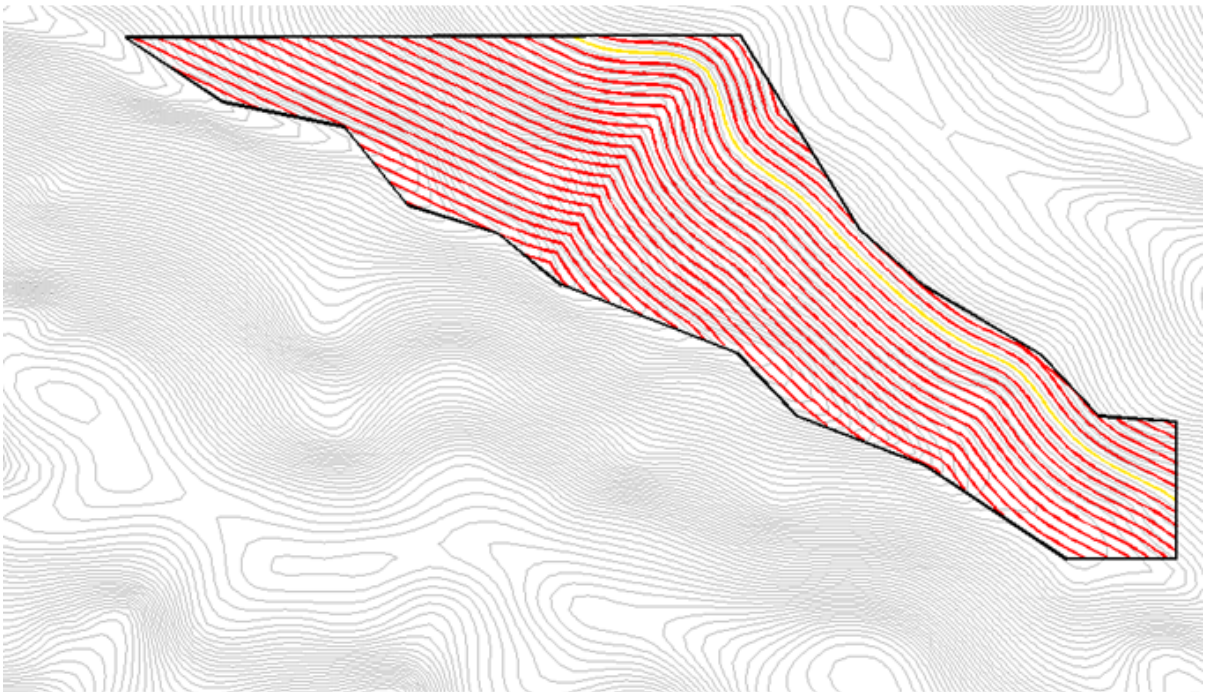

Figure 3.43. The coverage solution with minimum soil erosion cost for region 4 in the second example field. The gold curve is the selected seed curve, which is one of the contour lines within the field area. The red curves are the corresponding paths. The weights were set as 0:1:0 between turning cost, erosion cost and skipped area cost for the search.

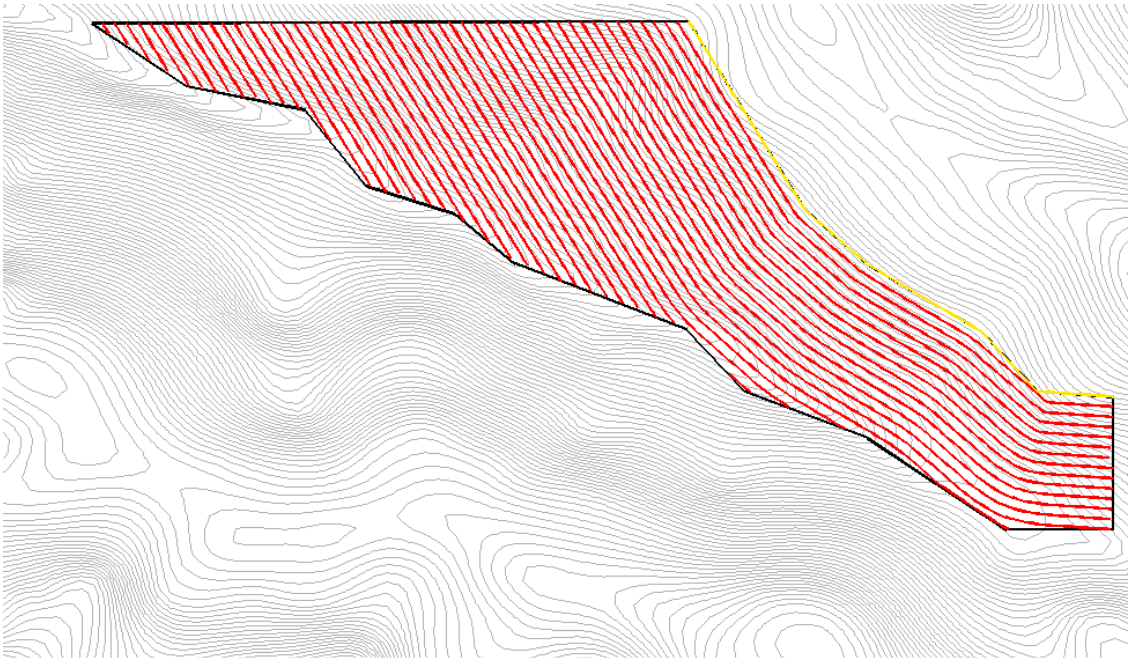

Figure 3.44. The coverage solution for region 4 in the second example field with the east edge as the seed curve. The gold curve is the selected seed curve. The red curves are the corresponding paths.

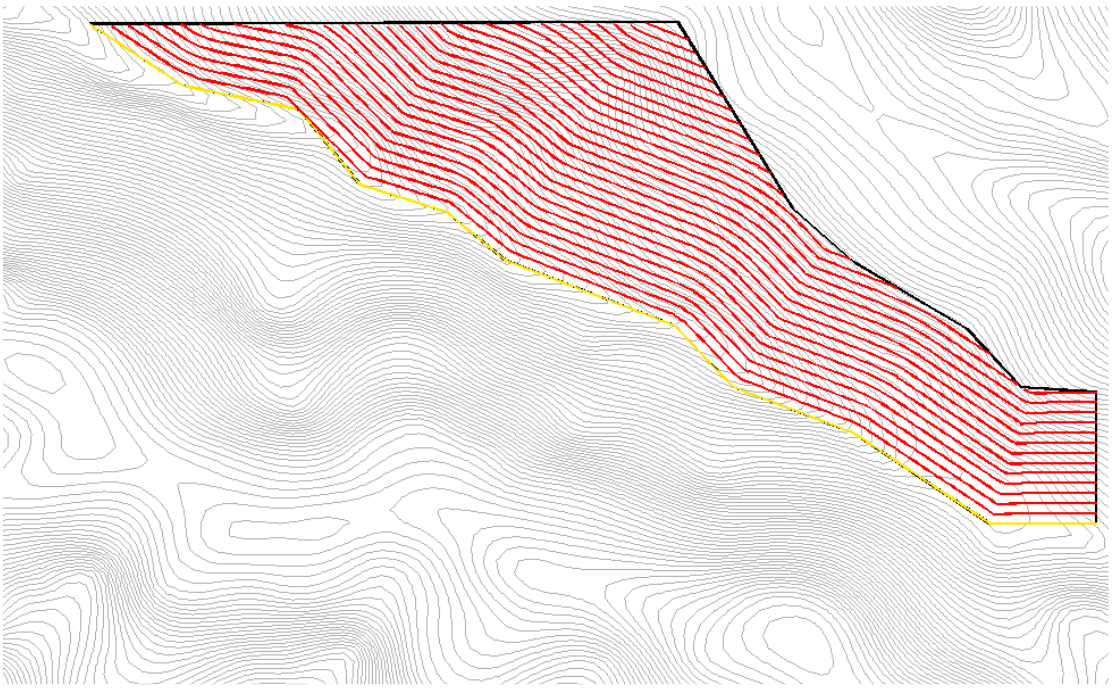

Figure 3.45. The coverage solution for region 4 in the second example field with the west edge as the seed curve. The gold curve is the selected seed curve. The red curves are the corresponding paths.

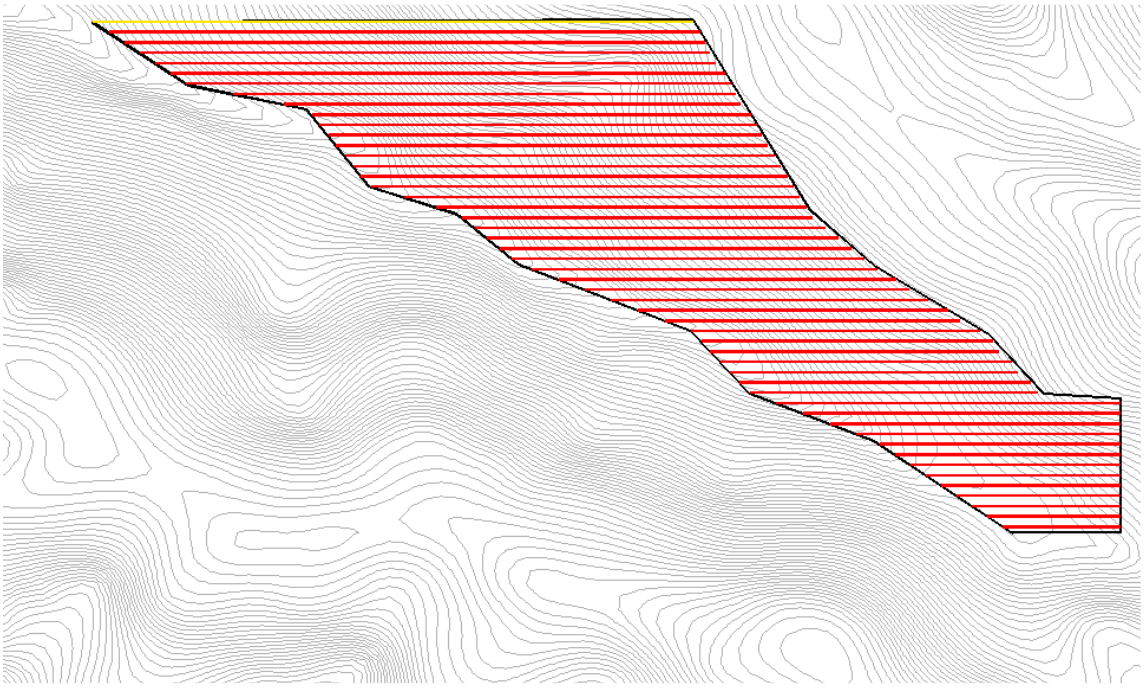

Figure 3.46. The coverage solution for region 4 in the second example field with the north edge as the seed curve. The gold curve is the selected seed curve. The red curves are the corresponding paths.

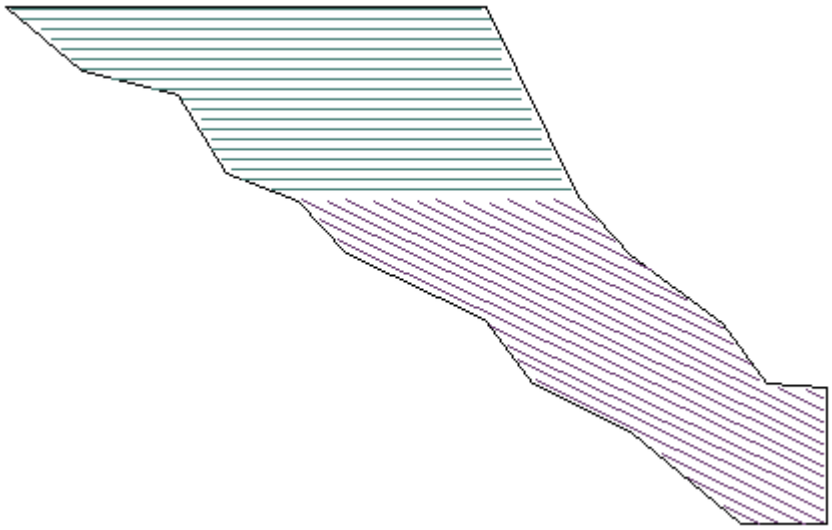

Figure 3.47. The 2D coverage planning result of the region 4 in the second example field. The whole field is subdivided into two regions and different coverage directions were adopted for each region.

The different categories of coverage costs as well as the weighted average of all the costs were calculated for all the five solutions above (both 3D and 2D solutions) of region 4 in the second example field. The headland turning costs, erosion costs and skipped area costs of the five coverage solutions are compared in fig. 3.48 (the skipped area cost of the 2D planning solution was calculated differently based on the discussion in 3.3.2.2). The weighted averages of all the costs of the five coverage solutions are compared in fig. 3.49 (The weights were 1:1:0.5 between turning cost, erosion cost and skipped area cost). The seed curve adopted by the recommended 3D planning result was not the optimal contour seed curve (fig. 3.42), but the west edge of the region (fig. 3.45). Though the optimal seed curve (west edge) generated higher soil erosion cost than the optimal contour seed curve, it saved on both the turning cost and skipped area cost.

The recommended 3D result saved 28.9% on headland turning cost, 6.8% on soil erosion cost, and 58.4% on skipped area cost compared with the 2D result. The weighted average of all coverage costs of the recommended 3D planning result (fig. 3.45) was 31.9% lower than the 2D planning result (fig. 3.47).

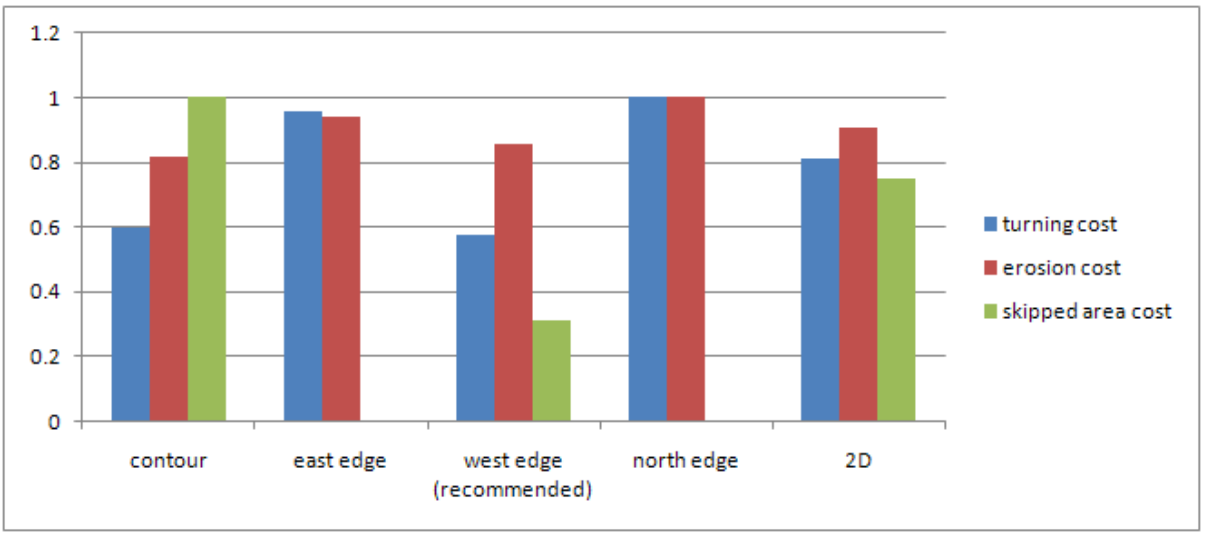

Figure 3.48. The turning costs, erosion costs and skipped area costs of the five coverage solutions for region 4 in the second example field.

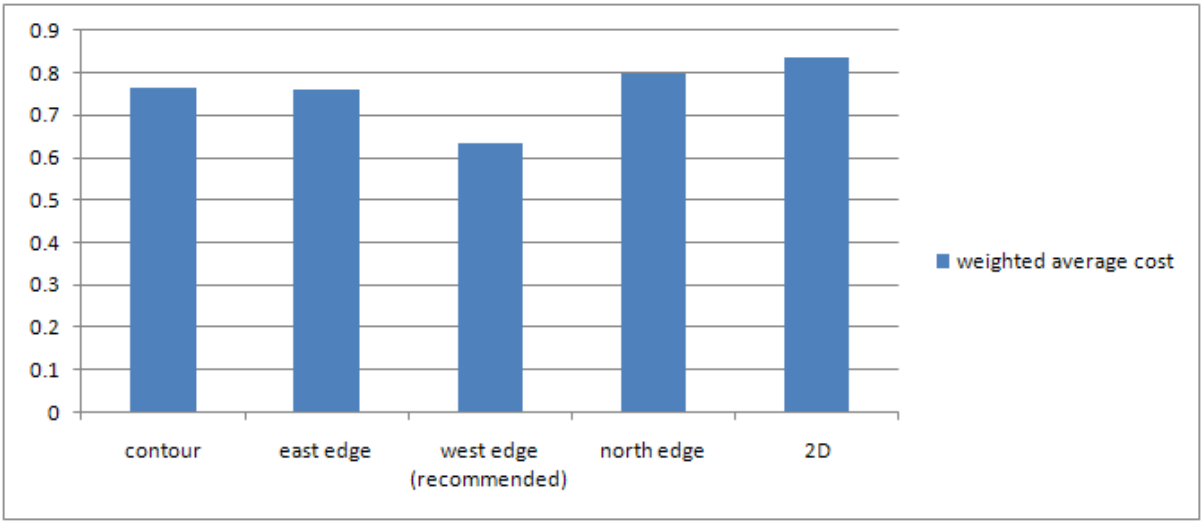

Figure 3.49. The weighted averages of all the costs of the five coverage solutions for region 4 in the second example field. The weights were 1:1:0.5 between turning cost, erosion cost and skipped area cost.

The final result of the whole second example field was the combined recommended solutions for the four regions (Fig. 3.50).

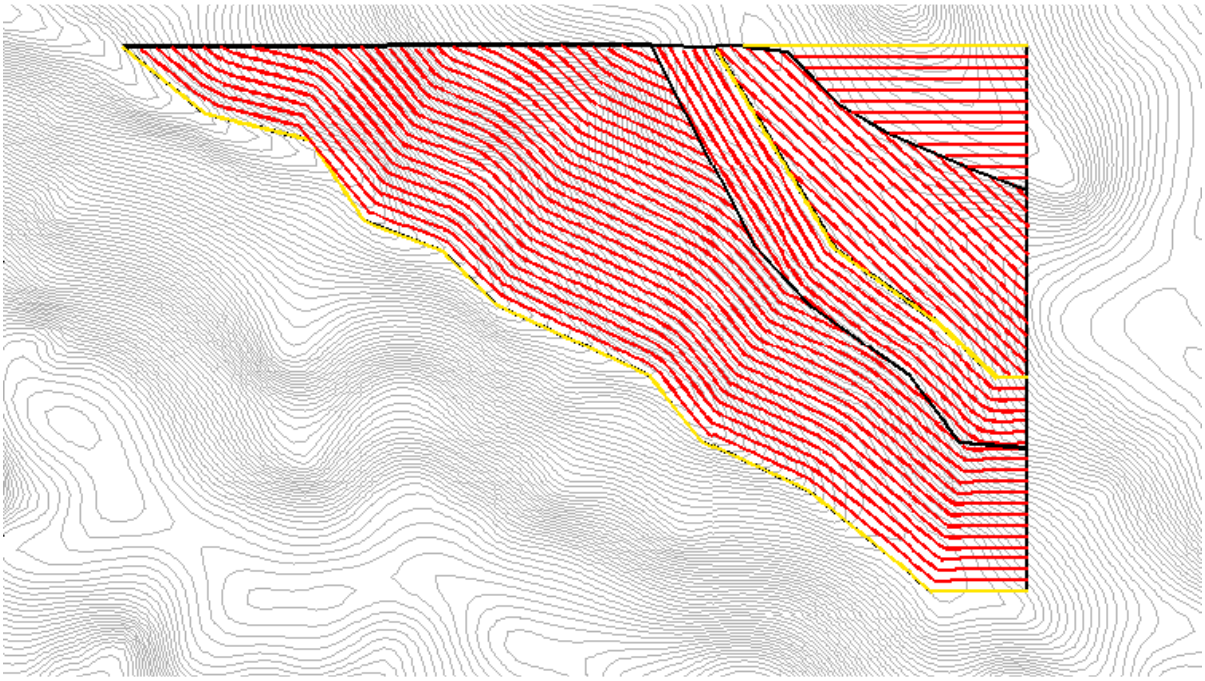

Figure 3.50. The result of the whole second example field. The gold curves are the selected seed curves. The red curves are the corresponding paths.

3.4.5.3 Terrain Field Example 3

Fig. 3.51 is the satellite image of the third example field. This 120 acres farm field is also located in southwest of Iowa. The maximum slope on this field is 16.5% and the average slope is 3.1%. From the satellite image, terraces, creek and water ways are visible inside the field. For a clearer view of the topography of this field, the 3D surface plot and contour view of the field are provided in fig. 3.52 and fig. 3.53.

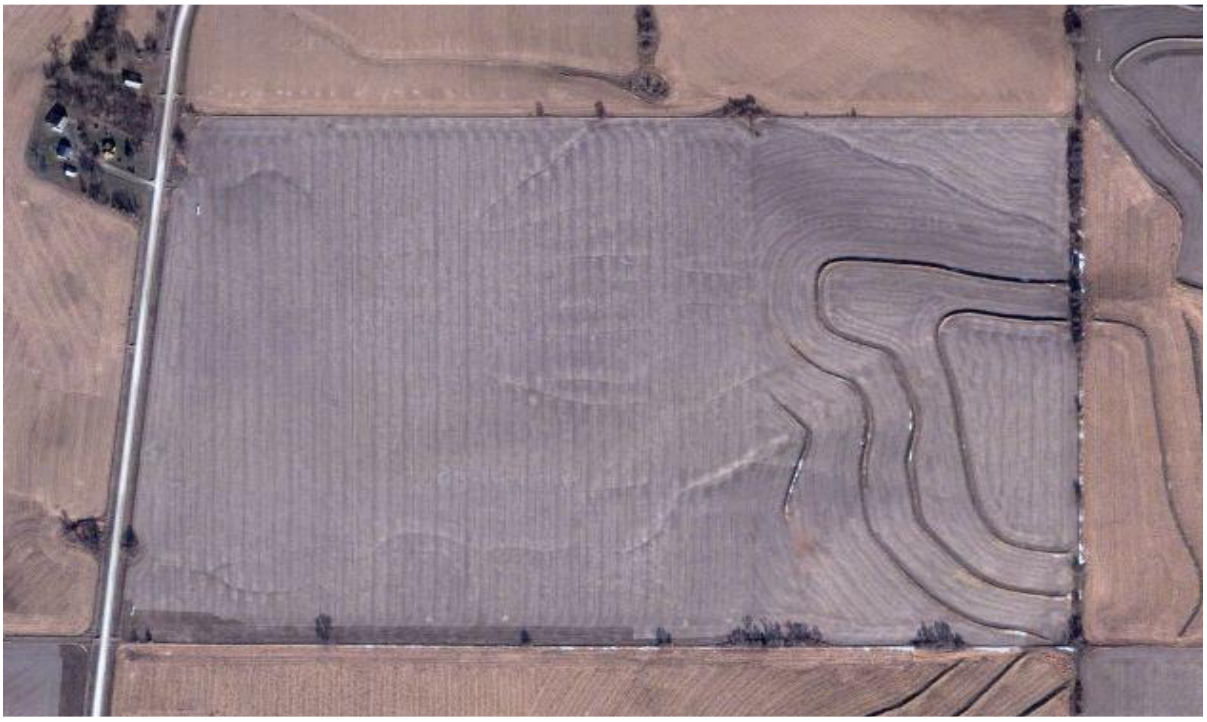

Figure 3.51. Satellite image of the third example terrain field in southwest of Iowa. The maximum slope in this field is 16.5% and the average slope is 3.1%.

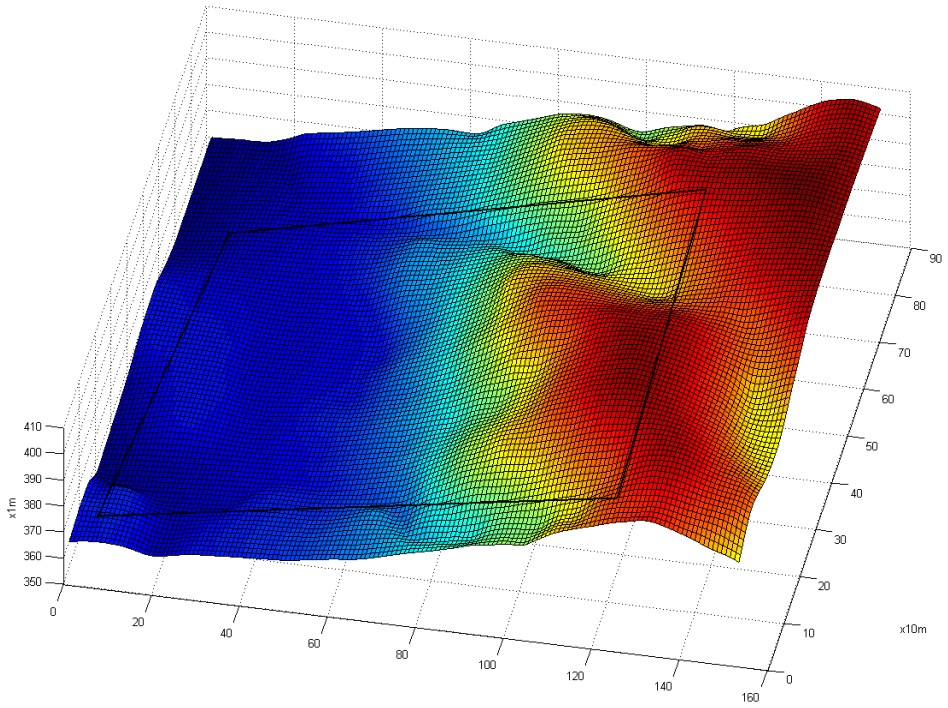

Figure 3.52. 3D surface plot of the DEM Data of the third example terrain field.

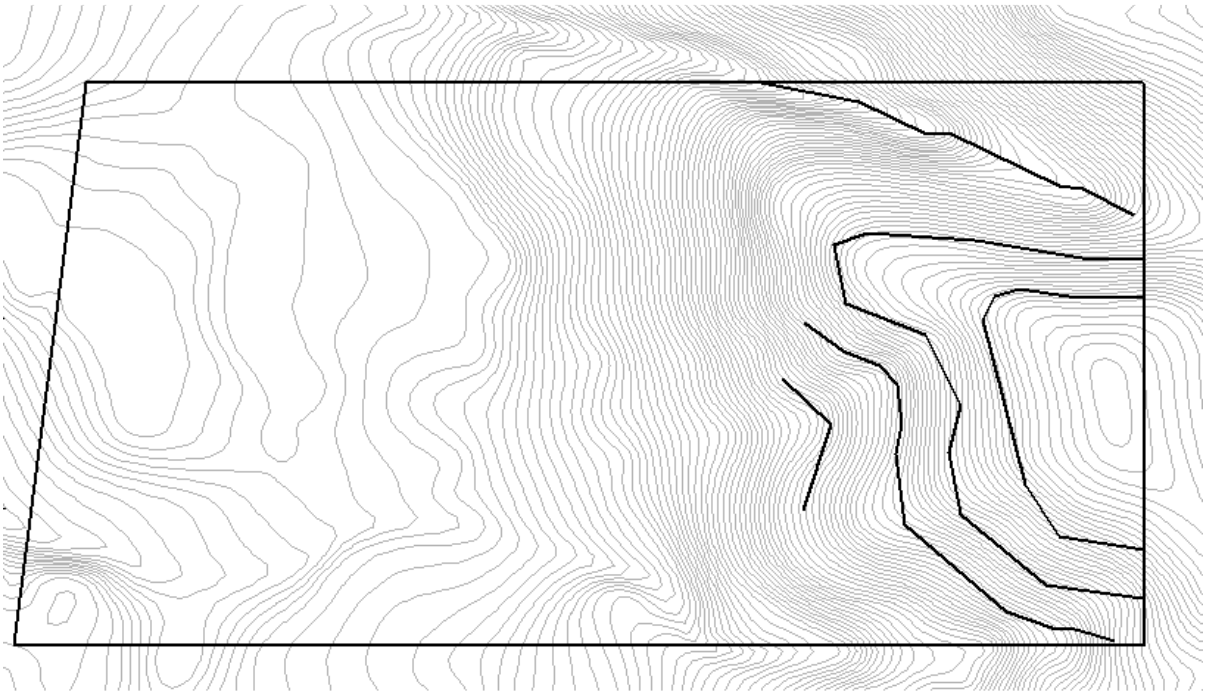

Figure 3.53. Contours view of the third example terrain field. Boundaries and terraces inside the field are plotted in black lines.

The slope data was calculated at each grid point of the field. Fig. 3.54 displays the slope data. If the slopes bellow 3% is defined as flat area, slopes between 3% and 5% is defined as medium area, and slopes above 5% is defined as steep area, the field can be classified into three classes, as shown in fig. 3.55.

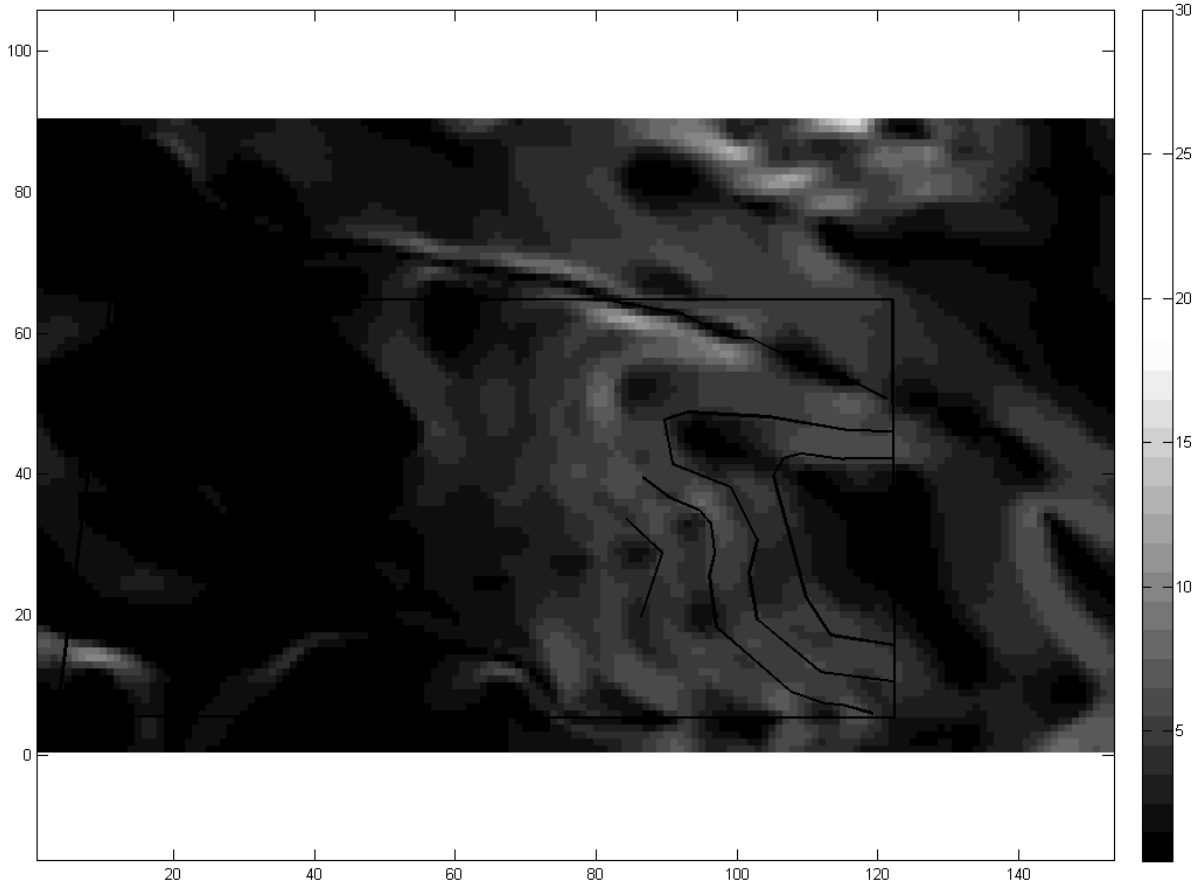

Figure 3.54. Slope map (in “%”) of the third example terrain field.

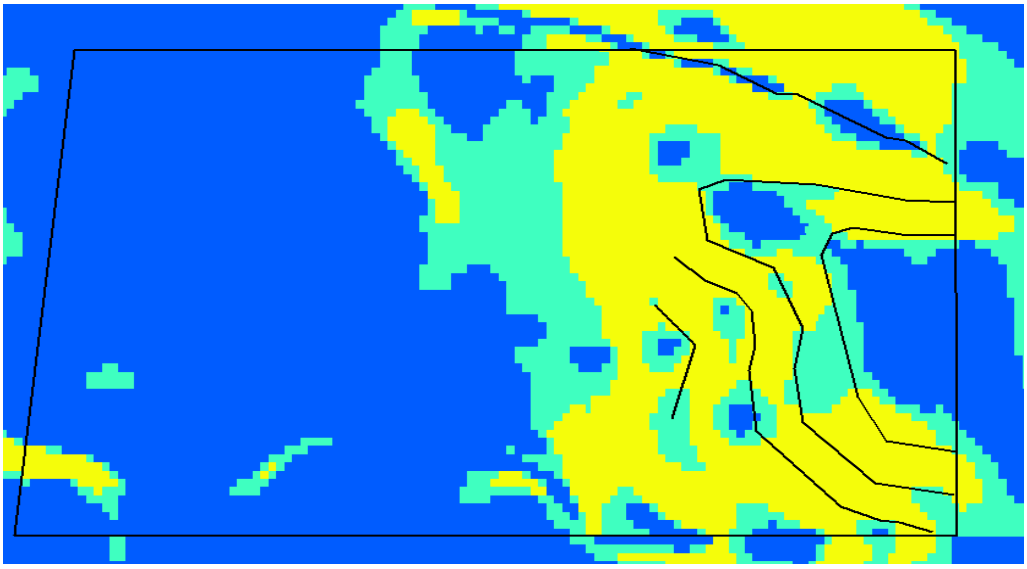

Figure 3.55. Decomposition result (before recombination) of the third example terrain field. The flat areas are in blue, the medium areas are in green, and the steep areas are in yellow.

Since the terraces and the river already divided the field into five unconnected regions (fig. 3.51), the terrain decomposition was carried out in each of the five regions. After re-combining the small area regions and those neighboring regions with complementary shapes, the result indicated that only the most west region was divided into two areas (fig. 3.56). The 2D path planning algorithm should be applied to regions 1, 2, 3, while 3D terrain path planning algorithm should be applied to regions 4, 5, 6.

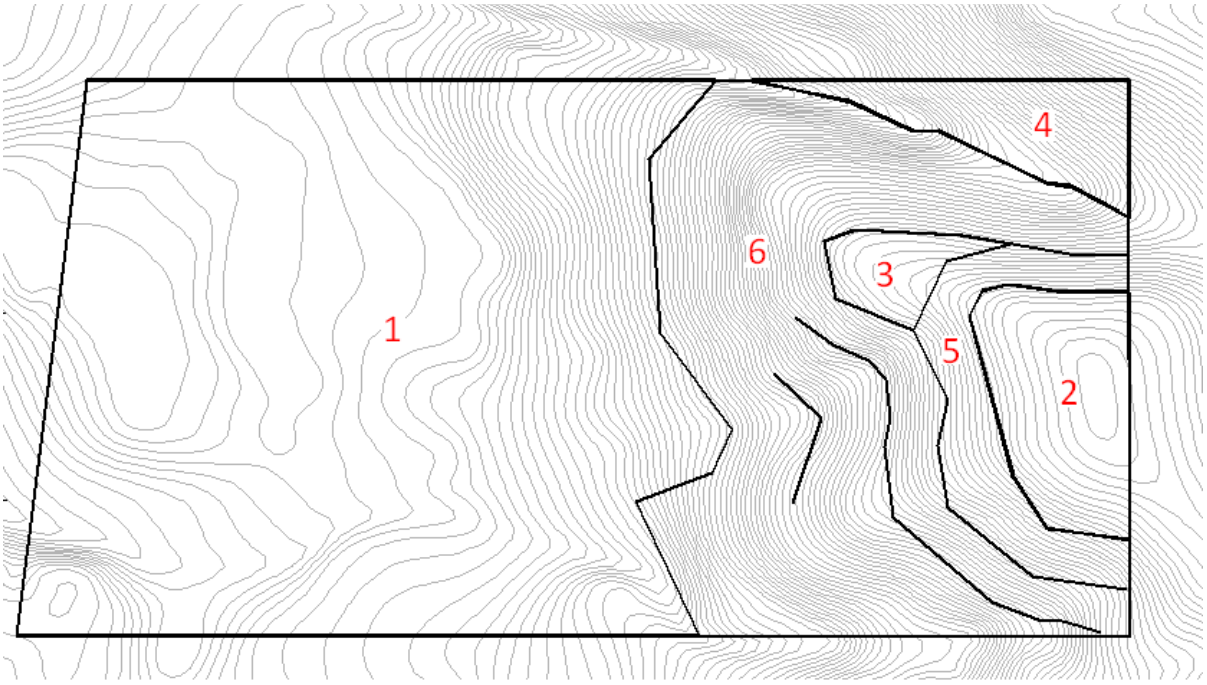

Figure 3.56. The terraces and the river divided the field into five unconnected regions. Further decomposition resulted in six regions. The 2D path planning algorithm was applied to region 1, 2, 3, while 3D terrain path planning algorithm was applied to region 4, 5, 6.

The 2D path planning results for regions 1, 2, 3 are displayed bellow in fig. 3.57. No decomposition was suggested for any of the three flat regions. Each of the resulted optimal coverage direction was along one of the edge segments.

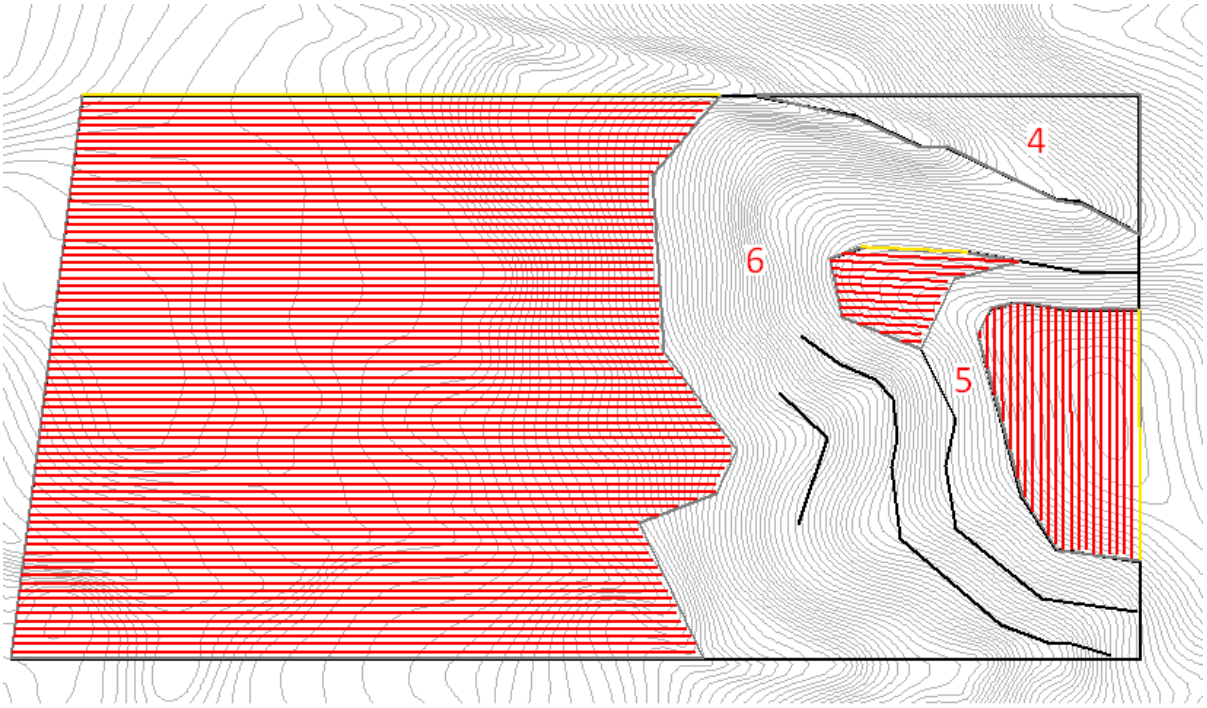

Figure 3.57. The 2D coverage planning result of region 1, 2, 3 in the third example field. The red curves are the paths. No decomposition was suggested for any of the three regions. Each of the resulted optimal coverage direction was along one of the edge segments (plotted as gold lines).

The 3D path planning algorithm was applied to the remaining three regions. The planning result for region 4 is displayed in fig. 3.58.

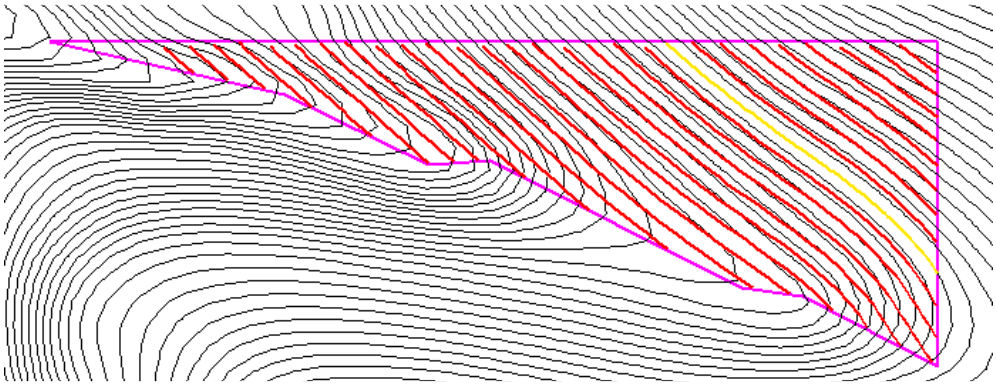

Figure 3.58. The recommended 3D coverage planning result for region 4 in the third example field. The gold curve is the selected seed curve, which is one of the contour lines within the field area. The red curves are the corresponding paths. The weights were set as 1:1:0.5 between turning cost, erosion cost and skipped area cost.

To be compared with the coverage solution in fig. 3.58, several of the other solutions were generated for region 4 in the third example field. First, the contour seed curve leading to the minimum soil erosion cost was adopted. In other words, the weights were set as 0:1:0 between turning cost, erosion cost and skipped area cost. This resulted in the coverage solution in fig. 3.59.

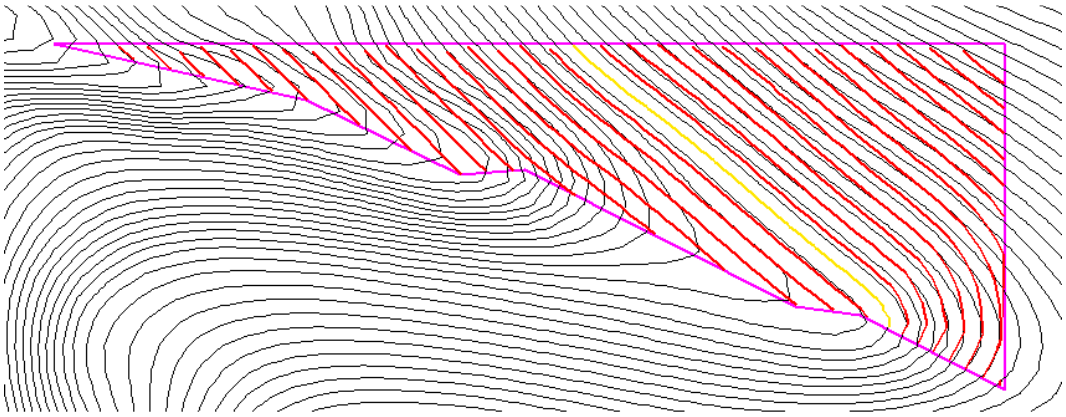

Figure 3.59. The coverage solution with minimum soil erosion cost for region 4 in the third example field. The gold curve is the selected seed curve, which is one of the contour lines within the field area. The red curves are the corresponding paths. The weights were set as 0:1:0 between turning cost, erosion cost and skipped area cost for the search.

Besides the contour seed curves, three of the edges of region 4 in the third example field were adopted as the seed curve, separately. The resulted coverage solutions are shown in fig. 3.60, fig. 3.61, and fig. 3.62.

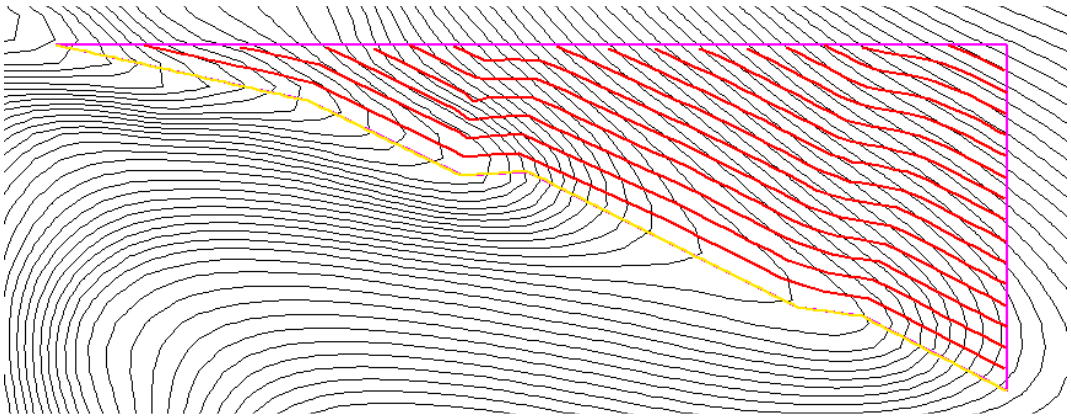

Figure 3.60. The coverage solution for region 4 in the third example field with the southwest edge as the seed curve. The gold curve is the selected seed curve. The red curves are the corresponding paths.

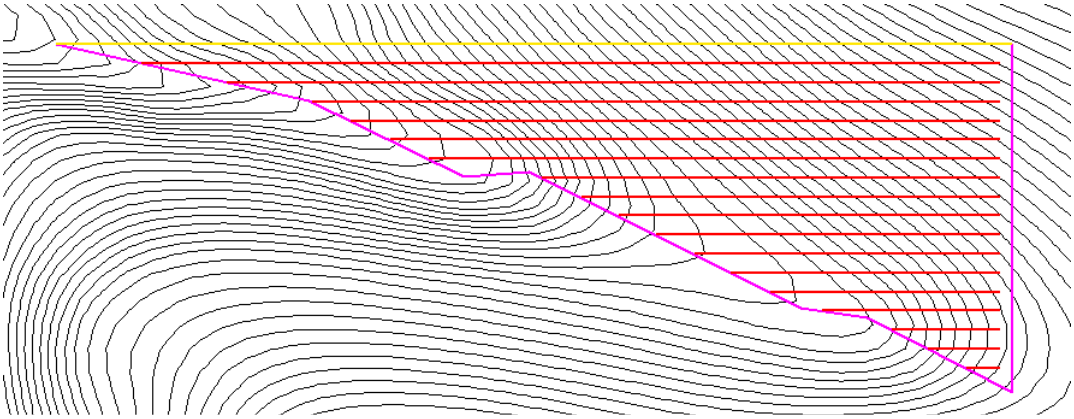

Figure 3.61. The coverage solution for region 4 in the third example field with the north edge as the seed curve. The gold curve is the selected seed curve. The red curves are the corresponding paths.

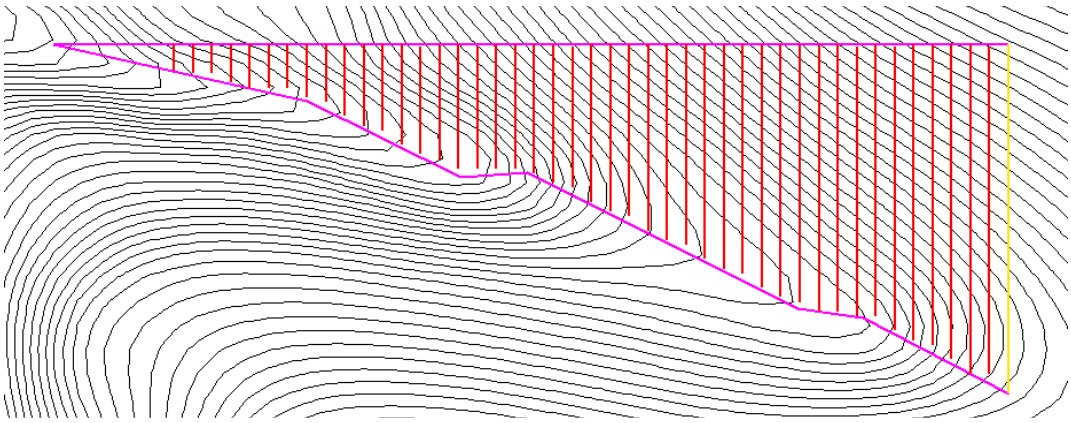

Figure 3.62. The coverage solution for region 4 in the third example field with the east edge as the seed curve. The gold curve is the selected seed curve. The red curves are the corresponding paths.

Finally, to be compared with the 3D coverage planning results above, the 2D coverage planning result for region 4 in the third example field was generated, which assumed the field is flat and ignored the elevation variances. The headland turning cost was the only concerned cost during the planning. The 2D path planning result generated nearly the same result as in fig. 3.61 (except that the paths were offset on the 2D plane surface instead of the 3D slope surface): the north edge was adopted as the optimal coverage direction. After projecting the 2D planning result onto the 3D terrain surface, the resulted total skipped area was 70 square meters, which was 0.24% of the total area of the region.

The different categories of coverage costs as well as the weighted average of all the costs were calculated for all the six solutions above (both 3D and 2D solutions) for region 4 in the third example field. The headland turning costs, erosion costs and skipped area costs of the six coverage solutions are compared in fig. 3.63 (the skipped area cost of 2D planning solution was calculated differently based on the discussion in 3.3.2.2). The weighted averages of all the costs of the six coverage solutions are compared in fig. 3.64 (The weights were 1:1:0.5 between turning cost, erosion cost and skipped area cost). The two contour seed curves (fig. 3.58 and fig. 3.59) generated the best coverage results: their weighted averages of all coverage costs were 36.1% and 35.8% lower than the 2D planning result (fig. 3.61),

separately. Compared with the 2D planning result, the recommended 3D planning result generated 36.0% higher headland turning cost, 69.5% lower soil erosion cost and there was no skipped area cost for the recommended 3D solution.

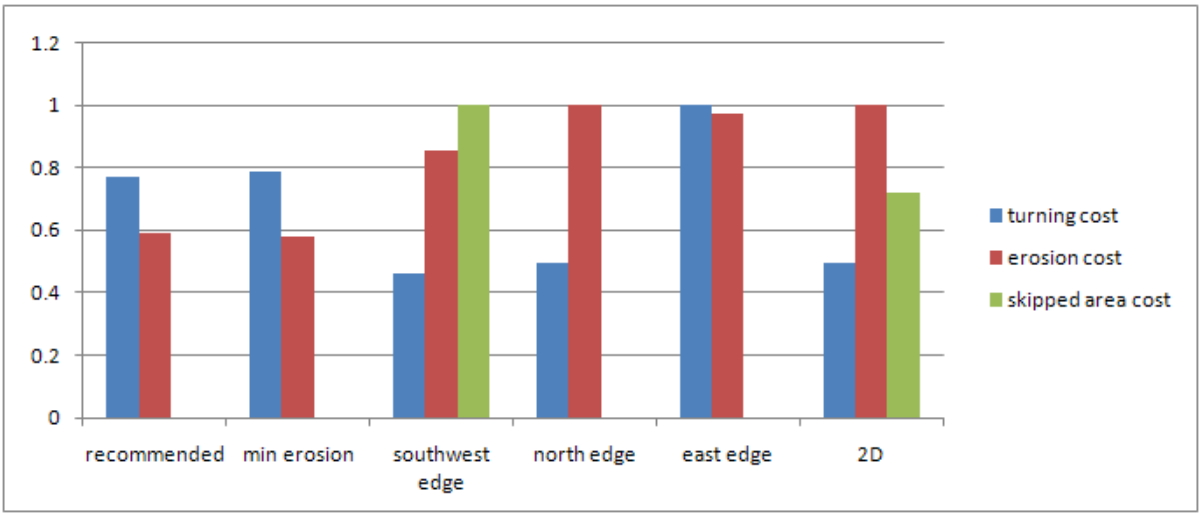

Figure 3.63. The turning costs, erosion costs and skipped area costs of the six coverage solutions for region 4 in the third example field.

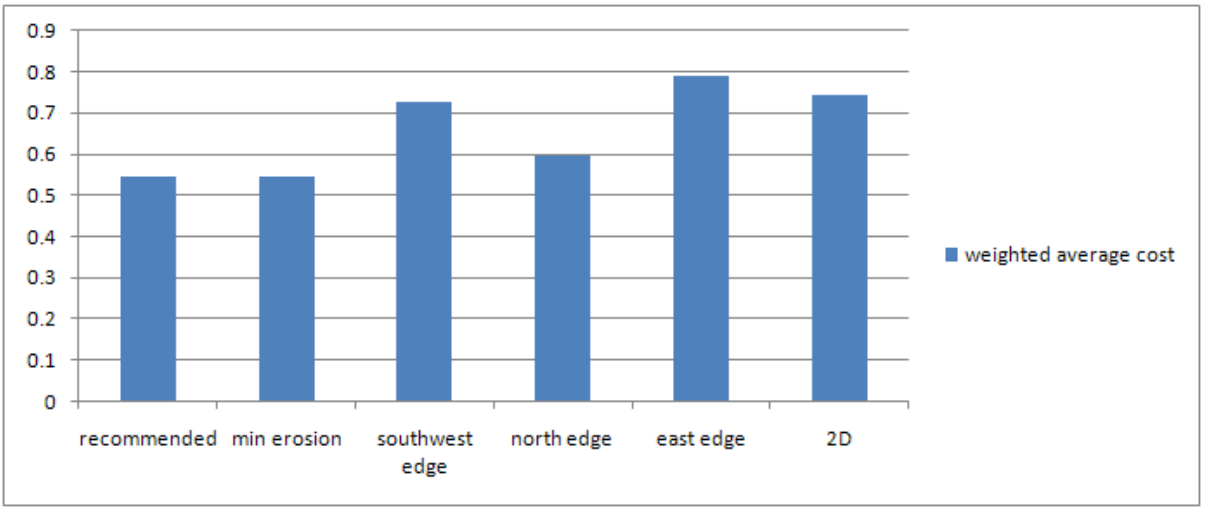

Figure 3.64. The weighted averages of all the costs of the six coverage solutions for region 4 in the third example field. The weights were 1:1:0.5 between turning cost, erosion cost and skipped area cost.

Similarly, the 3D planning algorithm was applied to region 5 and 6. The result of the whole third example field was the combined recommended solutions for all the six regions (Fig. 3.65).

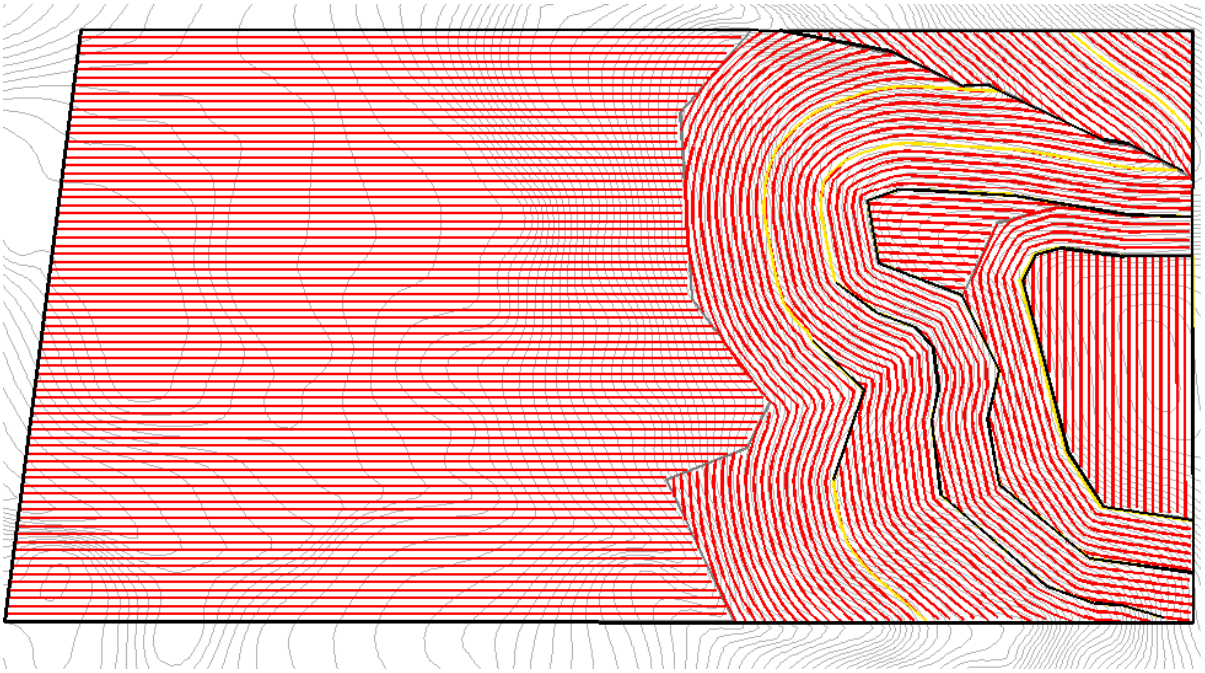

Figure 3.65. The result of the whole third example field. The gold curves are the selected seed curves. The red curves are the corresponding paths.

As shown in fig. 3.65, the zigzag boundary between region1 and region 6 resulted in unnecessary headland turning costs. The result can be further improved by replacing this boundary with the last path in region 6. The improved result is displayed in fig. 3.66 and the 3D surface plot of the improved result is displayed in fig. 3.67.

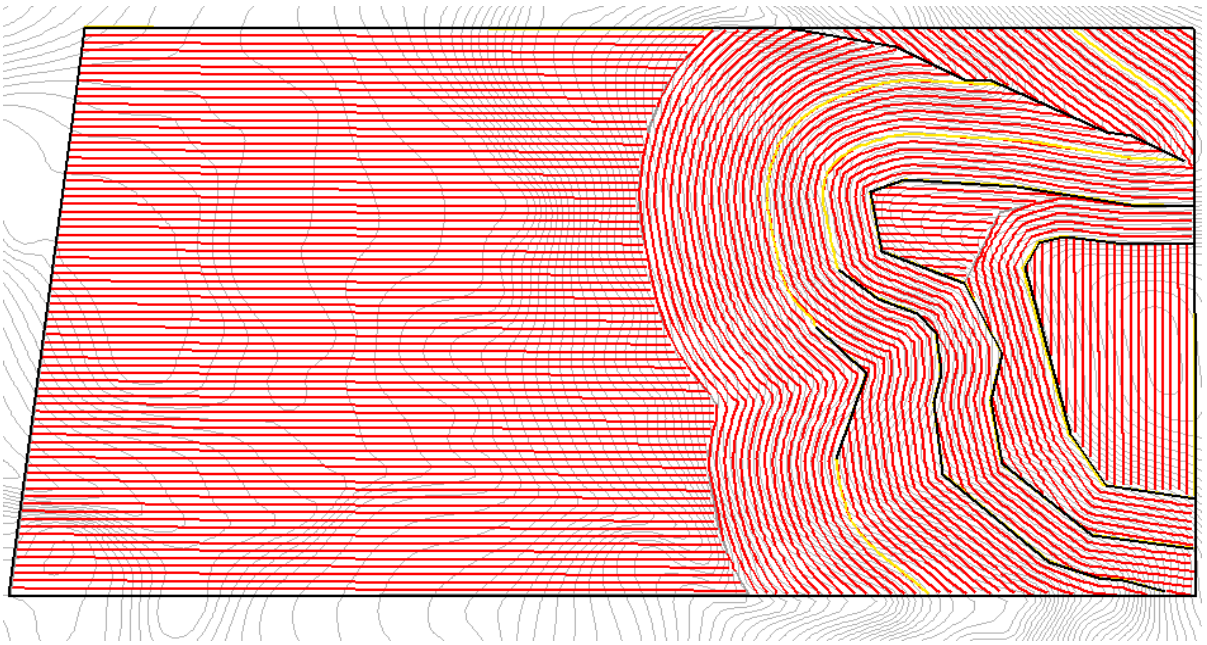

Figure 3.66. The improved result of the whole third example field. The gold curves are the selected seed curves. The red curves are the corresponding paths.

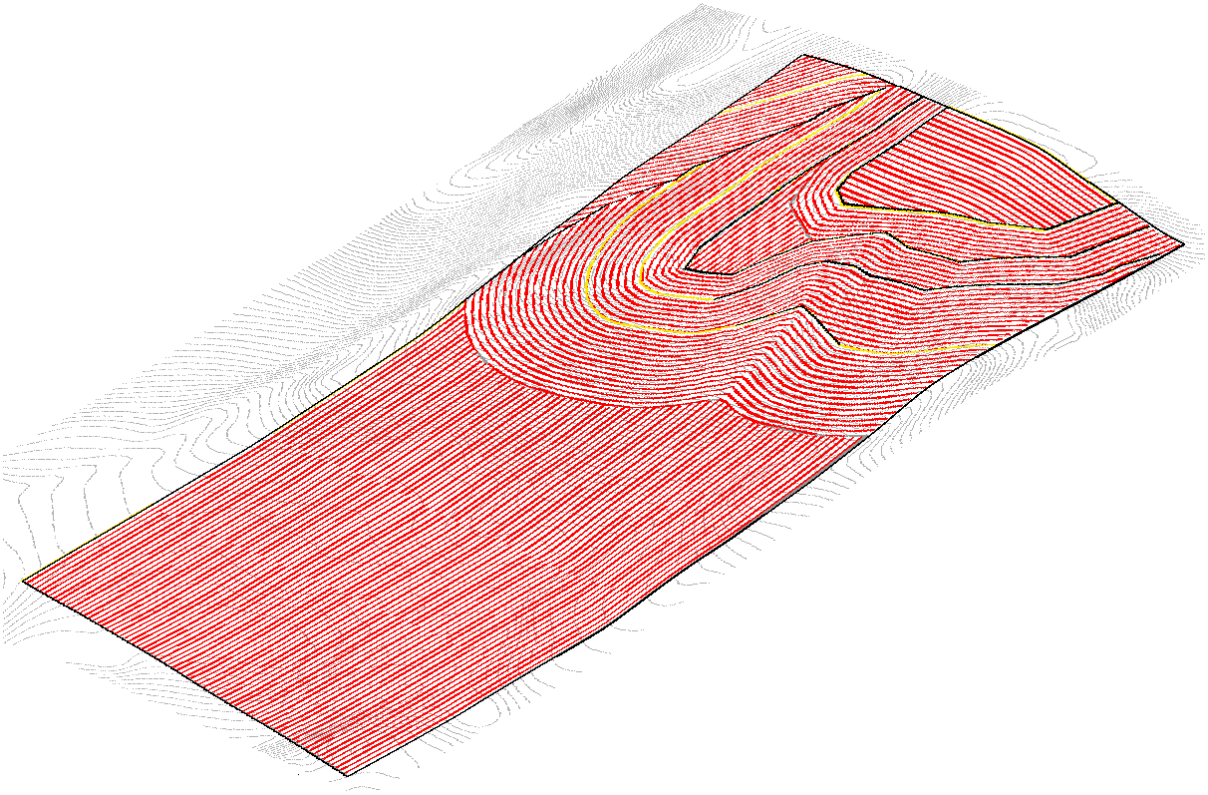

Figure 3.67. The 3D surface plot of the path planning result of the whole third example field. The gold curves are the selected seed curves. The red curves are the corresponding paths.

3.4.5.4 Cost Comparison Summary

The comparison between the coverage costs of 3D and 2D planning is summarized in table 3.2. The weights are 1:1:0.5 between headland turning cost, erosion cost and skipped area cost for the summed costs.

Table 3.2. Coverage costs comparison between 3D and 2D planning results.

Field Name	3D Planning's Saving on Turning Cost	3D Planning's Saving on Erosion Cost	3D Planning's Saving on skipped area Cost	3D Planning's Saving on Summed Cost
First Example Terrain Field	16.6%	8.7%	47.5%	18.1%
Second Example Terrain Field Region 3	14.1%	19.0%	100%	12.0%
Second Example Terrain Field Region 4	28.9%	6.8%	58.4%	31.9%
Third Example Terrain Field Region 4	-36.0%	69.5%	100%	36.1%
Third Example Terrain Field Region 5	27.9%	19.4%	100%	11.8%
Average	10.3%	24.7%	81.2%	22.0%

3.5 Conclusion

An analytical 3D terrain model with B-Splines was developed for representing 3D terrain for field coverage planning purpose. Based on the test result with one terrain field example in Iowa, for the 4th order B-Spline model with 5 grids/knot, the terrain was represented with only 1.79 times of coefficients as the 6th polynomial model, but with much better fitting effects: The maximum elevation error of the B-spline model was 57% of the polynomial model, the mean square error was only 22% of the polynomial model, and the R-square increased from 0.9903 to 0.9978. Terrain topography has impacts on operational patterns, including the impact on speed limit, skipped area between adjacent paths when projecting 2D planning result to 3D terrain, soil erosion impact and so on. The analysis of these impacts was provided and the methods for quantifying these impacts were derived. The terrain decomposition and classification methods were developed. With these methods, the terrain field could be divided into sub-regions with similar field attributes and comparatively

smooth boundaries. The divide-and-conquer strategy could then be applied in the 3D terrain coverage planning, and the most appropriate path planning strategy (such as 2D planning or 3D planning algorithms) could be applied to each region so as to achieve the minimum coverage cost. The analysis of different categories of coverage costs on 3D terrain has been provided. Methods have been developed for quantifying soil erosion cost and curving path cost corresponding to a particular coverage solution. The “Seed Curve” searching algorithm was developed and implemented. This searching algorithm has been successfully applied to several practical farm fields with various topography. The new 3D planning algorithm has shown its superiority on 3D terrain fields compared with the 2D planning algorithm. On the tested terrain fields, on average the 3D planning algorithm saved 10.3% on headland turning cost, 24.7% on soil erosion cost, 81.2% on skipped area cost, and 22.0% on the weighted sum of different costs (the weights were 1:1:0.5 between turning cost, erosion cost and skipped area cost). Especially, in one of the regions, the 3D planning algorithm generated one result with only 30.5% of the soil erosion from the 2D planning result. It can also be observed that the skipped area resulted from the sharp turning curvature in 3D planning result is generally much smaller than the skipped area between paths when projecting 2D planning result to 3D surface.

Due to the advanced 2D optimal decomposition algorithm, some of the final weighted average costs of the 2D solutions were nearly the same as the recommended 3D solutions (even lower in some cases). Currently, the decomposition algorithm in 3D planning is only aimed at classifying the terrain into flat areas and slope areas, so the proper planning method can be applied to each sub-region. It is expected that a more advanced decomposition algorithm for 3D terrain field would further optimize the 3D coverage solution. The summed skipped area at the sharp turning corners along the curved paths was adopted as the estimate of the “curving cost”. However, to have a more accurate estimate of the curving cost, each of the different costs discussed at the end of section 3.3.4.2 needs to be investigated for different field operations. In the current algorithm, field edge segments and contour lines are the only two categories of seed curve candidates. In order to make sure of the global optimal coverage solution, the searching space needs to be enlarged to incorporate more candidates. These improvements are left as future work.

3.6 References

Atkar, P. N., Greenfield, A., Conner, D. C., Choset, H. and Rizzi, A. A., 2005. Hierarchical Segmentation of Surfaces Embedded in R3 for Auto-Body Painting. In Proceedings of the 2005 IEEE International Conference on Robotics and Automation Barcelona, Spain, April 2005. Page: 574-579.

Aziz, A. S., Steward, L. B., Tang, L. and Karkee, M., 2009. Utilizing repeated GPS surveys from field operations for development of agricultural field DEMs. Transactions of the ASABE ASABE. Vol. 52(4):1057-1067.

Berrut, J. P. and Trefethen, L. N., 2004. Barycentric Lagrange interpolation, SIAM Review 46, 501–517, doi: 10.1137/S0036144502417715, ISSN 1095-7200

Cheng, F. and Goshtasby, A., 1989. A Parallel B-Spline Surface Fitting Algorithm. ACM Transactions on Graphics, 8(1).

Dillon, C., Gandonou, M. J., Koostra, B., Stombaugh, T. and Mueller, T., 2006. Evaluating the Economic Impact of Field Area Measurements. Poster and abstract presented at the 8th International Conference on Precision Agriculture, July 23-26, Minneapolis, MN.

Forsey, D. R. and Bartels, R. H., 1995. Surface Fitting with Hierarchical Splines. ACM Transactions on Graphics, Vol. 14, No. 2.

Fulton, W., 1974. Algebraic Curves. Mathematics Lecture Note Series. p. 112. ISBN 0-8053-3081-4. W.A. Benjamin.

Gesch, D.B., 2007. The National Elevation Dataset, in Maune, D., ed., Digital Elevation Model Technologies and Applications: The DEM Users Manual, 2nd Edition: Bethesda, Maryland, American Society for Photogrammetry and Remote Sensing, p. 99-118.

Gray, A., 1997. Modern Differential Geometry of Curves and Surfaces with Mathematica, 2nd ed. Boca Raton, FL: CRC Press.

Jia, Y., Mi, L. and Tian, J., 2006. Surface Patch Reconstruction via Curve Sampling. Proceedings of the 2006 IEEE International Conference on Robotics and Automation, Orlando, Florida.

Keren, D., Cooper, D. and Subrahmonia, J., 1994. Describing Complicated Objects by Implicit Polynomials. IEEE Transactions on Pattern Analysis and Machines Intelligence, Vol. 16, No. 1.

Kim, T. and Sarma, S., 2003. Optimal Sweeping Paths on a 2-Manifold: A New Class of Optimization Problems Defined by Path Structures. IEEE Transactions on Robotics and Automation, 19(4):613–636, August 2003.

Koostra, B.K., Stombaugh, T., Mueller, G. T. and Shearer, A. S., 2006. Evaluating the Effect of Terrain on Field Area Measurements. ASABE Paper No. 061045, St. Joseph, MI: ASABE.

Renard K. G., 1997. Predicting Soil Rrosion by Water : a Guide to Conservation Planning with the Revised Universal Soil Loss Equation (RUSLE). Agriculture Handbook, USDA, Agricultural Research Service, Vol. 703.

Rutter, J. W., 2000. Geometry of Curves. Chapman & Hall/CRC.

Schwab O. G., Fangmeier, D.D. and Elliot, J. W, 1993. Soil and Water Management Systems, Wiley, New York.

Sheng, W., Chen, H., Xi, N., Chen, Y. and Song, M., 2003. Surface Partitioning in Automated CAD-Guided Tool Planning for Additive Manufacturing. In IEEE/RSJ Int'l. Conf. on Intelligent Robots and Systems, volume 2, pages 2072–2077, Las Vegas,USA, 2003.

Stombaugh, T., Koostra, K. B., Dillon, R. C., Mueller, G. T. and Pike, C. A., 2009. Implications of Topography on Field Coverage When Using GPS-Based Guidance. University of Kentucky.

USDA, 1992. National Resources Inventory. Washington, D.C.: USDA National Resources Conservation Service. Available at: http://www.nrcs.usda.gov/technical/NRI/.

Van Doren, A. C., Stauffer, S. R. and Kidder, H. E, 1950. Effect of Contour Farming on Soil Loss and Runoff, Soil Sci. Soc. Am. Proc. 15 (1950), pp. 413–417.

Vincze, M., Pichler, A. and Biegelbauer, G., 2003. Detection of Classes of Features for Automated Robot Programming. In IEEE Int'l. Conf. on Robotics and Automation, volume 1, pages 151–156, Taipei, Taiwan, September 2003.

Wendt, G., 1998. Guidelines for the Use of the Revised Universal Soil Loss Equation (RUSLE) Version 1.06 on Mined Lands, Construction Sites, and Reclaimed Lands. Peabody Western Coal Company.

CHAPTER 4. GENERAL CONCLUSIONS

4.1 Conclusions

The optimal field coverage path planning algorithms have been successfully proposed and implemented for both 2D planar field and 3D terrain field. Both coverage path planning problems were carefully modeled and formulated as optimization problems. The various costs for the coverage operations were investigated and the coverage cost functions for 2D and 3D fields have been defined. The searching algorithms for finding the optimal decomposition and path pattern have been developed. The effectiveness of the developed coverage path planners have been evaluated with various field examples.

The search mechanism of the 2D planar path planning algorithm was guided by a customized cost function that was concerned with the cost of different types of angled turns in the headland. Field examples with complexity ranging from a simple convex shape to an irregular polygonal shape that has multiple obstacles within its interior were tested with the algorithm. For each field, the optimal decomposition was reported and the optimal boustrophedon coverage direction was found out. For all tested fields with no more than 20 vertices and 5 interior obstacles, the program found optimal coverage solutions within 60 seconds on a computer with a 3.20GHz Pentium(R) 4 CPU and 1.50 GB of RAM. The OPP's results were compared with the results of former researchers or farmers' practical solutions. The results have depicted that in the most extreme cases, OPP saved up to 16% in number of turns and 15% in headland turning cost. There were no cases where OPP outputted worse solutions than farmers' solutions in terms of headland turning cost. These results indicated that the OPP algorithm was effective in improving the field equipment efficiency on planar fields by producing optimal field decomposition and coverage path direction in each sub-region.

The terrain topography's impacts on operational patterns have been incorporated into the new 3D terrain path planner. The "Seed Curve" searching algorithm was successfully developed and applied to several practical farm fields with various topographical features. Each terrain field was divided into sub-regions with similar field attributes and comparatively smooth boundaries. The recommended terrain surface coverage paths were found out for

each sub-region. The new 3D planning algorithm has shown its superiority on 3D terrain fields compared with the 2D planning algorithm. On the tested terrain fields, on average the 3D planning algorithm saved 10.3% on headland turning cost, 24.7% on soil erosion cost, 81.2% on skipped area cost, and 22.0% on the weighted sum of different costs (the weights were 1:1:0.5 between turning cost, erosion cost and skipped area cost). Especially, in one of the regions, the 3D planning algorithm generated one result with only 30.5% of the soil erosion from the 2D planning result. It can also be observed that the skipped area resulted from the sharp turning curvature in 3D planning result is generally much smaller than the skipped area between paths when projecting 2D planning result to 3D surface.

4.2 Recommendations

There are multiple ways the optimal coverage path planning algorithms can be further improved:

1) In the current solutions of the OPP algorithm the paths are all in the form of straight lines. For some fields with curved boundaries, adopting curved paths may further improve the operation efficiency.

2) Besides the turning cost, other costs such as headland open-up cost need to be included for 2D path planning. In fig. 2.2, overlap coverage cost occurs when the vehicle is travelling from A to B and from D to E. This cost need to be quantified and included into the cost function in the future too.

3) The integrated curvature along the curved paths has been adopted as the estimate of the “curving cost”. However, to have a more accurate estimate of the curving cost, each of the different costs discussed in section 3.3.4.2 needs to be investigated for different field operations.

4) The current decomposition algorithm in 3D planning is only aimed at classifying the terrain into flat areas and slope areas, so the proper planning method can be applied to each sub-region. It’s expected that a more advanced decomposition algorithm for 3D terrain field would further optimize the 3D coverage solution (as in the 2D case). This improvement is left as future work.

5) Heuristic methods have been used to reduce the searching space of the “Seed Curve” searching algorithm. In the current algorithm, field edge segments and contour lines are the only two categories of seed curve candidates. In order to make sure of the global optimal coverage solution, the searching space needs to be enlarged to incorporate more candidates. For instance, there are often zigzag contour lines inside the field. Adopting these lines as seed curves may results in high curving costs. Sharp turnings may even be generated on the paths on the concave side of the contour. Adopting smoothened contour lines as seed curves has a potential to further reduce the coverage cost. As the searching space grows, more advanced searching algorithms will be necessary too.

6) There are various other problems in optimal path planning, such as how to incorporate the loading and unloading locations into the algorithm and how to coordinate between the vehicles when there are multiple vehicles in the field. Solving these problems remains as the future work.

7) After the optimal coverage path is determined, the next phase is motion planning of the vehicle. A preliminary analysis of speed control on slope was carried out for calculating the maximum speed of the vehicle moving on the slope so that no roll over would occur. However more details need to be investigated in the vehicle’s motion planning. The optimal motion planning for the vehicle moving along the determined path is another way to further optimize the infield operations.

ACKNOWLEDGEMENTS

I started doing the research on optimal farm field coverage path planning since 2005 without much former knowledge available on this topic. During the four years, exciting progresses have been made on the research project. The path planning algorithms for both 2D planar and 3D terrain fields have been in good shape now. These achievements cannot be made without the help and support from many people.

First of all, I would like to express my greatest thanks to my major advisor, Dr. Lie Tang. He helped me in selecting this interesting and challenging research topic and provided his guidance throughout the whole project. His knowledge, experience and creativity have always been great help for me every time when I encountered any difficulty. He contributed many valuable ideas in this research and his way of thinking has always been inspiring to me. Dr. Tang is not only a great academic advisor, but also a nice friend. During the last four years, he and his family have always been giving me all kinds of care and help for my life here in Ames, which greatly helped me to finish my research work. I've been feeling very fortunate to be a student of Dr. Tang, who's made the last four years a pleasant experience and good memory in my life.

I also want to give my special thanks to my POS committee members and other faculty members in our department. Especially, Dr. Stuart Birrell has given me very helpful guidance on field operation cost analysis. Dr. Matthew Darr has provided his valuable data files with field boundary and farmer's practical coverage path information. Dr. Matthew Helmers is an expert in farm field soil and water conservation who's provided precious help for my research with his knowledge in this area. Dr. Yan-Bin Jia taught me two valuable courses in Computer Science and provided very useful suggestions to my research. The key searching algorithm in 3D planning was inspired by a paper referred to me by Dr. Jia. Dr. Brian Steward has always been concerned with my path planning research and has constantly given me encouragements during various phases of this research. He also spent a large amount of time helping reviewing several of my research papers, which greatly helped me in improving my technical writing skills.

The later part of the research project was sponsored by John Deere Company. I would like to thank Dr. Shufeng Han who introduced and proposed our research to his department. The John Deere partners have been providing many valuable ideas and suggestions during our monthly discussions on the project. I want to say “thank you” to these partners: Troy Johnson, David Johnson, Jeffery Puhalla, Jim Beck, and Stewart Moorehead.

I also would like to thank my lab colleagues: Marcel van der Veeken, Lav Khot, Kazunobu Hayashi, Xuyong Tu, Yong Chen, Shuxin Du, Akarsh Nakarmi, Simon Nielsen and others. They have provided help in my research in various ways and also accompanied me during the long hours working in the Agricultural Automation and Robotics Lab in the department.

Finally, I want to give my special thanks to my family. I want to dedicate my dissertation to my parents, who have always been supporting me to reach any goal I decided to pursue in my life. Their love has always been, and will still be my power to keep moving forward. The dissertation is also dedicated to my dear wonderful wife, Xiaomin Qian, who’s given me enormous love and support. Last summer, Xiaomin brought me the greatest gift in my life, my little son Eric, who is pretty healthy and growing happily with us now. His cuteness has reduced a lot of pressure from me during the dissertation writing process.